

8-2020

A SCREEN FOR PEPTIDES TARGETING CHEMORESISTANT METASTATIC TRIPLE-NEGATIVE BREAST CANCER

Shraddha Subramanian

Follow this and additional works at: https://digitalcommons.library.tmc.edu/utgsbs_dissertations

 Part of the [Medicine and Health Sciences Commons](#)

Recommended Citation

Subramanian, Shraddha, "A SCREEN FOR PEPTIDES TARGETING CHEMORESISTANT METASTATIC TRIPLE-NEGATIVE BREAST CANCER" (2020). *The University of Texas MD Anderson Cancer Center UTHealth Graduate School of Biomedical Sciences Dissertations and Theses (Open Access)*. 1024. https://digitalcommons.library.tmc.edu/utgsbs_dissertations/1024

This Thesis (MS) is brought to you for free and open access by the The University of Texas MD Anderson Cancer Center UTHealth Graduate School of Biomedical Sciences at DigitalCommons@TMC. It has been accepted for inclusion in The University of Texas MD Anderson Cancer Center UTHealth Graduate School of Biomedical Sciences Dissertations and Theses (Open Access) by an authorized administrator of DigitalCommons@TMC. For more information, please contact digitalcommons@library.tmc.edu.

**A SCREEN FOR PEPTIDES TARGETING CHEMORESISTANT METASTATIC
TRIPLE-NEGATIVE BREAST CANCER**


By

Shraddha Subramanian, B.E

APPROVED:



Mikhail G. Kolonin, Ph.D.
Advisory Professor



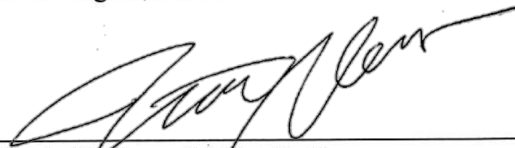
Sendurai A. Mani, Ph.D.



Gheath Al-Atrash, D.O., Ph.D.



Wenliang Li, Ph.D.



Naoto T. Ueno, M.D., Ph.D.

APPROVED:

Dean, The University of Texas MD Anderson Cancer Center UTHealth Graduate School of
Biomedical Sciences

**A SCREEN FOR PEPTIDES TARGETING MORE RESISTANT METASTATIC
TRIPLE-NEGATIVE BREAST CANCER**

A

THESIS

Presented to the Faculty of

The University of Texas

MD Anderson Cancer Center UTHealth

Graduate School of Biomedical Sciences

in Partial Fulfillment

of the Requirements

for the Degree of

MASTER OF SCIENCE

By

Shraddha Subramanian, B.E

Houston, Texas

August 2020

Dedicated to my family, who continue to stand by my side through thick and thin.

ACKNOWLEDGEMENTS

I would like to express my deepest gratitude to my supervisor, Dr. Mikhail G. Kolonin, for encouraging me to pursue this project. Dr. Kolonin's systematic approach, insightful comments, and patience have been instrumental in my evolution into an effective researcher. This work would not have materialized without the support of my advisory committee members: Dr. Sendurai A. Mani, Dr. Gheath Al-Atrash, Dr. Naoto T. Ueno, and Dr. Wenliang Li. Together, they provided constructive criticism and valuable inputs that steered this project forward.

I would also like to thank the members of the Kolonin lab: Dr. Alexes C. Daquinag, Dr. Zhanguo Gao, and Cale Fussell for fostering an invigorating research environment that stimulated original thinking and initiative. A huge thank you to Dr. Robiya Joseph (Mani lab) and Dr. Bahran Fekry (Mahan lab) for helping me set up and image the spontaneous lung metastasis mouse model. I would also like to acknowledge Dr. Ville Meretoja (UTHealth Flow Cytometry Core) and Dr. Zhengmei Mao (UTHealth Histology Core) for their extensive technical support and guidance.

I am thankful to Dr. Michael R. Blackburn, Dr. Michelle C. Barton, Dr. Eric C. Swindell, Dr. Kelly A. Moore, and the other members of the GSBS community for deeming me a worthy addition to their esteemed institution. My three-year stint at GSBS has given me the chance to spread my wings and experience cutting edge research that has brought me a step closer to my goal of becoming a cancer biologist.

I would like to thank my friends: Dhvani, Vidhi, Sumedha, Akash, Tanvi, Mayuri, Meghana, and Kumaresh for being a guiding light on this arduous yet transformative endeavor. I would like to extend my deepest appreciation to my family. To my sister Smriti, for celebrating my successes harder than I did. To my aunt Kirthika, for motivating me to chase after my American dream. To my grandparents, for their unerring faith in me. Lastly to my loving parents, for raising me up to more than I can be.

A SCREEN FOR PEPTIDES TARGETING CHEMORESISTANT METASTATIC TRIPLE-NEGATIVE BREAST CANCER

Shraddha Subramanian, B.E

Advisory Professor: Mikhail G. Kolonin, Ph.D.

Cancer metastasis is the principal cause of most cancer-associated morbidities. While radiotherapy, hormone therapy, and novel therapeutic strategies, including immunotherapy, have shown promise in inhibiting tumor growth, chemotherapy remains the mainstay in the clinical management of metastatic progression. This is often the case in triple-negative breast cancer (TNBC), an aggressive breast cancer subtype where tumorigenesis is independent of HER-2, progesterone, or estrogen receptor expression. Despite improving TNBC prognosis, recent studies report that after chemotherapy administration, TNBC drug-tolerant tumor cell survival, relapse, and metastatic dissemination may be promoted. Overcoming drug resistance exhibited by metastatic tumor cells is a challenge owing to the lack of specific biomarkers and the absence of drugs available to selectively target them. The development of such therapeutics would be pivotal for cancer medicine, as they would enable targeted ablation of the mortality-responsible tumor cell population with minimal off-side effects.

Our studies indicate that in TNBC mouse models, the chemotherapeutic agent cisplatin exacerbates spontaneous metastases to the lung. In this project, we have aimed to develop novel compounds that specifically target chemoresistant cancer metastases. It is based on the hypothesis that metastatic cancer cells express unique cell surface receptors that can be targeted. To test this hypothesis, we performed a combinatorial phage-displayed peptide library screen to isolate phage-displayed cyclic peptides that mimic the natural ligands of novel receptors expressed by chemoresistant metastatic TNBC tumor cells. These peptides were termed Breast Lung Metastasis Peptides (BLMPs), owing to their pulmonary metastases-specific tropism. Two lead BLMPs were

validated in murine cancer models *in vivo* and *in vitro*. We demonstrate that BLMP homing to pulmonary metastases was independent of chemotherapy administration. Our findings suggest that the BLMPs localized predominantly along the invasive edges of the pulmonary metastases. Immunofluorescence assays suggest that the two lead BLMPs are selective for tumor cells exhibiting a mesenchymal phenotype. BLAST sequence analysis of the two lead BLMP peptides reveals that they bear homology with biological ligands of receptors implicated in EMT activation and metastatic progression. To explore the therapeutic potential of these metastatic tumor cell-specific peptides, the BLMPs were modified to generate hunter-killer peptides (HK-BLMPs) that induce apoptosis upon internalization into targeted cancer cells. We demonstrated that one of the HK-BLMP peptides selectively kills cancer cells and shows potential in decreasing metastatic burden in a murine model of spontaneous TNBC metastasis.

TABLE OF CONTENTS

Dedication.....	iii
Acknowledgements.....	iv
Abstract.....	v
Table of Contents.....	vii
List of Figures.....	xi
List of Tables.....	xiii
Chapter 1: Introduction.....	1
1. Breast Cancer.....	2
1.1 Epidemiology.....	2
1.2 Breast Cancer Subtyping.....	2
2. Metastatic Breast Cancer.....	5
3. Epithelial to Mesenchymal Transition and Cancer Metastasis.....	6
4. Treatment Modalities of Triple-Negative Breast Cancer.....	8
4.1 Surgery.....	8
4.2 Chemotherapy.....	8
4.3 Novel Potential Therapies.....	12
5. Mechanisms of Triple-Negative Breast Cancer Chemoresistance.....	15
5.1 ATP-Binding Cassette Transporters.....	16
5.2 Mutations in DNA Replication and Mismatch Repair Enzymes.....	16
5.3 Tumor Dormancy.....	17
5.4 Epithelial to Mesenchymal Transition.....	17
5.5 Cancer Stem Cells.....	18
5.6 Hypoxia.....	18
5.7 Cell-Signaling Pathways.....	19

5.8 Receptor Tyrosine Kinases.....	21
6. Tumor-Targeting Peptides.....	21
6.1 Phage Display Screening for the Isolation of Tumor-Targeting Peptides.....	22
6.2 Tumor-Targeting Peptides Specific to the Tumor Microenvironment.....	23
6.3 Tumor-Targeting Peptides Specific to Overexpressed Tumor Receptors.....	27
6.4 Design of Tumor Specific Hunter-Killer Peptides.....	29
Chapter 2: Statement of Objective.....	31
1. Knowledge Gap.....	32
2. Hypothesis.....	32
3. Aims and Experimental Approach.....	32
4. Graphical Abstract.....	33
Chapter 3: Materials and Methods.....	34
1. Cell Lines and Cell Culture.....	35
2. Murine Model of Experimental Lung Metastasis.....	35
3. Orthotopic Murine Model of Spontaneous Lung Metastasis.....	36
4. Non-Invasive Bioluminescence Imaging to Monitor Metastatic Progression <i>In Vivo</i>	37
5. <i>In-situ</i> Lung Perfusion and Fixation.....	37
6. Enumerating Pulmonary Metastasis in Mice.....	38
7. <i>In Vivo</i> Phage-Peptide Library Bio-panning for Lung Metastases Targeting Peptides....	38
7.1 Round 1 of <i>In Vivo</i> Phage-Displayed Peptide Library Bio-panning.....	38
7.2 Lung Tissue Digestion for Cell Isolation	39
7.3 FACS Recovery of Pulmonary Metastatic 4T1-Luc+mCherry+ Tumor Cells.....	40
7.4 Recovery of Phage-Displayed Peptides from Metastatic Tumor Cells.....	40
7.5 Enrichment of Peptides in Rounds 2 and 3 of <i>In Vivo</i> Bio-panning.....	40
7.6 PCR, DNA Sequencing and Insert Analysis.....	41

8. <i>In Vitro</i> Phage-Displayed Peptide Homing Validation.....	42
8.1 Phage-Displayed Peptide Internalization Assay.....	42
8.2 Phage-Displayed Peptide Internalization Validation by Immunofluorescence.....	43
9. <i>In Vivo</i> Phage-Displayed Peptide Validation.....	43
10. Design and Synthesis of Hunter-Killer Peptides.....	44
11. Biotin-labeled HK-BLMP Internalization Assay <i>In Vitro</i>	45
12. <i>In Vitro</i> Assay for Cell Viability.....	46
12.1 Validation of Cell Viability by Trypan-Blue staining.....	46
12.2 Validation of Apoptosis Induction by Cleaved-Caspase 3 Staining.....	46
13. <i>In Vivo</i> Metastasis Ablation Study with HK-BLMP8.....	47
14. Statistical Analysis.....	47
Chapter 4: Results.....	48
1. Cisplatin treatment elicits no tumor response but exacerbates metastatic burden.....	49
2. A screen for phage-displayed breast lung metastasis homing peptides.....	53
3. Nine novel breast lung metastasis homing phage-peptides were identified through <i>in vivo</i> screening of chemoresistant TNBC pulmonary metastases.....	57
4. All BLMP clones bind specifically to murine cancer cell lines <i>in vitro</i>	59
5. Both BLMP7 and BLMP8 demonstrate pulmonary metastases-specific tropism in a spontaneous TNBC metastasis model.....	63
6. Only BLMP8 demonstrates pulmonary metastases-specific tropism in an experimental melanoma metastasis model.....	73
7. BLMP7 and BLMP8 home to mesenchymal tumor cells in lung metastases.....	79
8. Phage-displayed BLMP7 and BLMP8 do not home to epithelial tumor cells <i>in vitro</i>	86
9. Biotin-labeled HK-BLMP7 and HK-BLMP8 bind specifically to cancer cell lines <i>in vitro</i>	89

10. Biotin-labeled HK-BLMP8 does not home to epithelial tumor cells <i>in vitro</i>	92
11. HK-BLMP8 induces cell death in murine cancer cell lines <i>in vitro</i>	94
12. HK-BLMP8 administration induces a modest reduction in 4T1 pulmonary metastatic burden but does not improve overall survival.....	98
Chapter 5: Discussions.....	104
Chapter 6: Conclusions and Future Directions.....	112
Chapter 7: Bibliography.....	115
Vita.....	145

LIST OF FIGURES

Figure Number	Title	Page Number
1.	Chemoresistance promotes metastatic recurrence	15
2.	A diagrammatic representation of M13 bacteriophage	23
3.	Schematic depiction of study	32
4.	Cisplatin treatment elicits no tumor response but exacerbates metastatic burden	52
5.	An <i>in vivo</i> phage-displayed peptide library screen for peptides homing to cisplatin resistant metastatic tumor cells	56
6.	Summary of top BLMP clones enriched over three rounds of <i>in vivo</i> phage-displayed peptide library bio-panning	58
7.	Validation of phage-displayed BLMP clone specificity to cancer cells <i>in vitro</i>	61
8.	BLMP7 and BLMP8 home to pulmonary metastases in the 4T1 TNBC mouse model	69
9.	Absence of BLMP7 and BLMP8 homing in metastases free mice	72
10.	BLMP8 homes to pulmonary metastases in the B16F10 melanoma mouse model	78
11.	BLMP7 and BLMP8 do not home to E-cadherin positive tumor cells	82
12.	BLMP7 and BLMP8 home to N-cadherin positive tumor cells	85
13.	BLMP7 and BLMP8 home to tumor cells expressing reduced levels of E-cadherin	88

14.	Validation of biotin-labeled HK-BLMP7 (B-BLMP7) and biotin-labeled HK-BLMP8 (B-BLMP8) homing specificity to cancer cells <i>in vitro</i>	91
15.	B-BLMP8 homes to tumor cells expressing reduced levels of E-cadherin	93
16.	HK-BLMP7 and HK-BLMP8 induce apoptosis in cell culture	96
17.	HK-BLMP8 induces cleaved caspase-3 mediated apoptosis in murine cancer cell lines <i>in vitro</i>	97
18.	HK-BLMP8 administration reduces metastatic burden but does not improve overall survival <i>in vivo</i>	103

LIST OF TABLES

Table Number	Title	Page Number
1.	Breast cancer subtyping	3

Chapter 1: Introduction

1. Breast Cancer

1.1 Epidemiology

The occurrence of breast cancer is heavily skewed by gender. Roughly 1 in 8 women have a lifetime risk of developing breast cancer, which is orders of magnitude higher than the corresponding risk in men - around 1 in 1000 (1). Nearly 25% of cancer diagnoses in women worldwide fall under the category of breast cancer (2), placing this disease second on the list of common causes of cancer death in women (3). Among women in the US, around 41,760 deaths were expected in 2019 from a projected 316,700 cases (4). Old age is the next major risk factor associated with breast cancer followed by factors like race, ethnicity, obesity, alcohol consumption, physical inactivity, early onset of menstruation, and late/no pregnancy. Advances in screening techniques, effective treatment, and early detection have contributed to a significant decrease in the death rate due to breast cancer (by about 40%) over the past 30 years (4). Although these advancements merit praise, there has been no respite in the incidence of breast cancer, which continues to be on the rise. This necessitates a more comprehensive strategy to counter the disease while providing treatment that is both efficient and reliable.

1.2 Breast Cancer Subtyping

Building a systematic strategy for treating breast cancer requires an appropriate classification of its heterogeneity. Initial attempts used the presence or absence of estrogen receptors (ER), progesterone receptors (PR), and human epidermal growth factor receptor 2 (HER-2) to develop subtypes (5). Techniques like gene expression profiling are still gaining traction and require better standardization and cost-effectiveness before they can be used as a rubric for classification (6). From a clinical perspective, breast cancer continues to be subtyped on a molecular basis governed by the presence or absence of the receptors mentioned above. The

four resulting categories are Luminal A, Luminal B, HER-2, and TNBC. Their general relation with the three receptors is shown in Table 1.

	ER	PR	Her-2
Luminal A	+	+	-
Luminal B	+	+	+/-
Her-2	-	-	+
TNBC	-	-	-

Table 1: Breast cancer subtyping: Classification based on hormone receptor expression

1.2.1 Luminal A

The presence of both estrogen and progesterone receptors, along with the absence of HER-2, characterizes the Luminal A subtype. This is the most commonly occurring subtype, and it exhibits a slow proliferation rate, which can be inferred through low Ki67 staining. Patients with Luminal A breast cancer generally receive the most favorable prognosis (7). Treatment for this subtype is typically contingent on the menopausal status of the patient and their estrogen source (8). The effectiveness of hormone therapy against Luminal A reduces the recurrence rate and increases the chance for survival (9, 10). Mutations in *PIK3CA*, *MAP3K1*, *GATA3*, and *TP53* genes are common in Luminal A.

1.2.2 Luminal B

This subtype's characteristics differ from Luminal A in one key feature - higher proliferation rates observable through greater Ki67 staining. Like Luminal A, they express

estrogen and progesterone receptors, but they may be HER-2 positive or negative. Diagnosis of this subtype often occurs at a young age, and the large tumor size associated with Luminal B typically results in poor prognosis. The survival rate for Luminal B patients is second only to Luminal A (10). The genes *PIK3CA*, *GATA3*, and *TP53* are commonly mutated in Luminal B.

1.2.3 HER-2

As suggested by the name, this subtype has high expression levels of HER-2 and typically lacks both ER and PR expression. Patients with HER-2 breast cancer are diagnosed at an even younger age compared to the two Luminal subtypes. Targeted therapies against HER-2 have gathered pace in recent years (10, 11). These advances are improving the bleak prognosis that usually accompanies HER-2 breast cancer. The commonly mutated genes in this subtype are *TP53*, *PIK3CA*, and *MUC16*. These are accompanied by a higher expression of tyrosine kinases like fibroblast growth factor receptor (FGFR) and epidermal growth factor receptor (EGFR).

1.2.4 TNBC

TNBCs represent a subtype of breast cancers that lack the expression of ER, PR, or HER-2 genes. It is commonly observed in young patients and accounts for over 15% of newly diagnosed breast cancer cases (12). At the time of diagnosis, most TNBCs are found to have progressed to an advanced stage due to the higher grade, larger size, and lymph node involvement presented by TNBC tumors (13). An additional level of complexity observed to accompany TNBCs is intra-tumoral and inter-patient heterogeneity (14). Although all TNBC tumors present a similar gene expression profile, their mutation burden is often non-uniform. No two TNBC tumors have the same mutations, which accounts for the high inter-patient heterogeneity encountered clinically. Moreover, the genetic composition of TNBC tumors and thus, their prognosis varies from patient to patient. TNBCs harbor mutations in vital tumor suppressors such

as p53 and BRCA (15). Several critical signaling pathways, including the phosphatidylinositol 3-kinase and protein kinase B (PI3K-AKT) pathway, mitogen-activated protein kinase (MAPK), nuclear factor kappa light chain enhancer of activated B cells (NF- κ B) pathway, and wingless and int-1 (Wnt) pathway, are often dysregulated in this cancer subtype (16). To gain more insight into the intra-tumoral diversity exhibited by TNBCs, a classification based on gene expression profiles was performed in 386 TNBC tumors (13). This clustering revealed six new TNBC subtypes namely basal, mesenchymal, mesenchymal stem-like (MSL), immunomodulatory (IM), luminal androgen receptor (LAR), basal-like 1 (BL1), and basal-like 2 (BL2), each characterized by a unique gene and pathway signature (13). For instance, the LAR subtype showed enrichment in metabolic pathways and androgen receptor signaling, while the BL1 subtype exhibited enrichment in DNA replication and cell cycle pathways (13). Another seminal study that analyzed the RNA and DNA profiles of 198 TNBC tumors classified them into four distinct molecular subtypes: a) Luminal androgen receptor (LAR) subtype with up-regulated cell surface mucin expression, b) Mesenchymal (MES) subtype overexpressing platelet-derived growth factor receptor (PDGFR) and c-kit growth factor receptors, c) Basal-like immune-suppressed (BLIS) subtype expressing the immune-suppressing molecule V-set domain-containing T-cell activation inhibitor (V-VTCN1) and lastly, d) Basal-like immune activated (BLIS) subtype which expresses signal transducer and activator of transcription-3 (STAT-3) molecules and cytokines (17).

2. Metastatic Breast Cancer

Metastasis is a convoluted biological phenomenon. It involves cancer cell dissociation from the primary tumor, invasion of surrounding connective tissue, intravasation into host vasculature, and entry into circulation. Upon survival in circulation, the tumor cells disseminate to secondary sites harboring a permissible tumor microenvironment (TME). Here, they extravasate and form micro-metastases, establish a favorable metastatic niche, and eventually

proliferate into macro-metastases (18). The ability to complete each stage of the metastatic cascade dictates the metastatic potential of the tumor cells.

Although localized primary tumors are the source of malignancy burden, it is the metastases that attribute to over 90% of all cancer-associated morbidity and mortality (19). Owing to the genetic instability of metastatic tumors, their treatment is a daunting challenge. In addition to a unique immunophenotypic profile, TNBCs possess several aggressive clinicopathological features such as young age of onset and large tumor size (20). These factors promote the development of distant metastases in several organs, including the lung, brain, and liver.

A large cohort study of over 1600 women with invasive breast cancer reported that the TNBC patient subgroup reflected tumors that were more aggressive and grew rapidly (21). These observations were further corroborated by Liedtke and colleagues, who revealed that TNBC patients had higher recurrence rates when compared to their hormone-sensitive counterparts (22).

Further, these tumors often resemble basal-like breast cancers, which are identified as poor prognosis subgroups with respect to relapse-free survival and overall survival (OS) (23). The gene expression profile of most basal-like tumors consists of a myriad of candidate genes that might contribute to their aggressive phenotype. Since TNBCs and basal-like cancers are believed to reflect a higher level of genetic instability, it might explain their propensity towards metastatic progression. Thus, to improve metastatic TNBC (mTNBC) patient outcomes, it is crucial to gain insight into the cellular and molecular mechanisms that govern metastatic dissemination (24).

3. Epithelial to Mesenchymal Transition and Breast Cancer Metastasis

Epithelial to mesenchymal transition (EMT) is a latent developmental program implicated in wound healing and tissue regeneration (25). EMT is accompanied by a loss of apicobasal cell polarity, disruption of adherens junctions, and cytoskeletal reorganization by which cells acquire a mesenchymal and migratory phenotype (26). In cancer, a hijacked EMT

program endows metastasis favoring characteristics upon the cancer cells (27). An armamentarium of cell surface markers, cytoskeletal organization proteins, transcription factors, microRNAs, ligands, and growth factors work in unison to choreograph this intricate process (28). The reverse process, termed mesenchymal to epithelial transition (MET), is also highly regulated during development (28, 29). Distant metastases resemble the molecular subtype of their primary tumor, and several studies have proved that the disseminated cancer cells are often epithelial (30, 31). The term ‘plasticity’ describes the ability of cells to transition seamlessly between the epithelial and mesenchymal phenotypes. While the migratory and invasive features of cancer cells initiate the metastatic cascade, its completion is contingent upon the plasticity between EMT/MET (32).

EMT is primarily induced through alterations in gene expression, that enables cells to acquire mesenchymal properties. During EMT, cells demonstrate epithelial cadherin (E-cadherin) repression and neural cadherin (N-cadherin) up-regulation simultaneously (33). The cadherin switch, a prominent EMT hallmark, is observed regardless of cell type or EMT-inducing factor (34). The Snail family of transcription factors induces the mesenchymal phenotype through the epigenetic inhibition of E-cadherin. Snail is also responsible for turning on the expression of mesenchymal markers such as N-cadherin, collagen, fibronectin, matrix metalloproteases (MMPs), Twist, and zinc finger e-box binding homeobox-1 (ZEB-1) (34). EMT can also be triggered by hypoxia and other extracellular stimuli, including tumor necrosis factor-alpha (TNF- α), transforming growth factor-beta (TGF- β), EGF, FGF, and PDGF, to name a few. Signal transduction pathways, including Wnt, Notch, NF- κ B, MAPK, and PI3K pathways, are also reported to coordinate the EMT program (35). The transcriptional factors and the hallmarks of EMT are often associated with a malignant phenotype in breast cancer patients. The high expression of Slug and Twist was demonstrated to closely correlate with poor prognosis in breast

cancer patients (36, 37). Further, Jeong and colleagues underscored that EMT was related to a high histological grade and the triple-negative phenotype (38).

4. Treatment Modalities of Triple-Negative Breast Cancer

Patients with TNBC fail to respond to hormone-based therapy due to the absence of ER, PR, and HER-2 target receptor expression. Thus, surgery and chemotherapy, individually or in combination, continue to remain viable treatment modalities in clinical TNBC management. However, recent studies have reported the discovery of novel receptors that could serve as targets for the development of new anti-cancer therapeutics.

4.1 Surgery

Breast-conserving surgery (BCS) and mastectomy are primary candidates in TNBC treatment. TNBC status, traditional clinicopathological variables, and patient preference determine whether mastectomy or lumpectomy is the optimal treatment choice. A 2016 population-based study published in *Lancet Oncology* reported a higher survival in patients subjected to BCS and radiotherapy as opposed to patients that underwent mastectomy (39). Another study concluded that post BCS, the local recurrence rate was lower in TNBCs than other breast cancer subtypes (40).

4.2 Chemotherapy

Cytotoxic chemotherapy remains the mainstay of TNBC treatment despite the development of novel targeted therapies. Factors such as tumor size, lymph node status, grade, and overall performance status are used to design individualized chemotherapy regimens for TNBC patients (41). Several studies have underscored the benefit of using chemotherapeutic drugs in the neoadjuvant, adjuvant, and metastatic treatment of TNBC. The administration of

neoadjuvant chemotherapy has consistently shown higher response rates (RR), thus promoting improved long-term outcomes in TNBC. Additionally, a higher pathologic complete response (pCR) related to neoadjuvant chemotherapy is observed in TNBCs when compared to luminal non-TNBC subtypes (42). Although TNBCs are initially susceptible to chemotherapy, early complete response (CR) often fails to correlate with OS. On the other hand, TNBC specific adjuvant regimens that appear to be efficacious remain incompletely defined for both early advanced stages of the disease. Currently, the chemotherapeutic strategies employed in the management of TNBC are a) platinum compounds and taxanes targeting DNA repair complexes and p53, b) anthracycline-based regimens targeting cell proliferation, and c) third-generation chemotherapeutics using either dose-dense or metronomic polychemotherapy.

4.2.1 Platinum Salts

Due to the improvements in managing the non-specific toxicity of platinum agents, a renewed interest in using DNA cross-linking agents (cisplatin and carboplatin) in TNBC treatment has emerged. Further, the histological similarities between breast cancer type 1 susceptibility (BRCA1)-mutated breast cancers and TNBCs, render platinum agents, a desirable therapeutic strategy. The cytotoxicity of platinum agents is primarily exerted through the formation of mono adducts, thus distorting the DNA double helix, to generate single and double-strand DNA breaks (43). Preoperative TNBC therapy with platinum agents has yielded promising results. For instance, a phase II study evaluating single-agent cisplatin in women with stage II or III TNBC reported a pCR rate of 22%, with 36% of the patients demonstrating a Miller-Payne score of 4 or 5 which included both complete and near-complete responses (44). The success of platinum agents in preoperative settings further bolstered the rationale behind their use in advanced TNBCs. In the TBCRC009 trial, mTNBC patients received either cisplatin or carboplatin for three weeks.

A median progression-free survival (PFS) of 89 days was observed, with 33% of patients reporting a PFS less than six weeks, while another 33% had a PFS longer than six months (45).

4.2.2. Taxanes

Taxanes are a class of diterpenes that function through the disruption of microtubule function (46). While taxanes remain an essential treatment modality in TNBCs, it does not demonstrate any specific benefit over non-TNBCs (42). In an MD Anderson Cancer Center (MDACC) study evaluating 1,118 patients treated with neoadjuvant anthracycline and taxane combination therapy, the pCR rates were observed to be significantly higher in TNBC patients, but both PFS and 3-year OS were substantially worse (22). The benefit of using taxanes in adjuvant TNBC therapy has gained traction only recently. In the CALGB 9344/INT1048 trial, randomized patients with node-positive operable breast cancer received three doxorubicin doses followed by four paclitaxel cycles every three weeks. The addition of paclitaxel was associated with significant improvements in the HER-2 negative, TNBC patient cohort (47). Abraxane, a novel nanoparticle albumin-bound (nab) formulation of paclitaxel, demonstrated a significantly improved PFS in mTNBC patients both alone and in combination with other chemotherapy (48). However, the NSABP B28 trial comparing cyclophosphamide and doxorubicin with or without paclitaxel found no significant difference in the relative risk of disease recurrence or OS based on hormone receptor status (49). In the metastatic setting, several trials reported no specific benefit of using taxanes in TNBC treatment. The CALGB9342 trial, which evaluated three different paclitaxel doses for metastatic hormone receptor-positive tumors and mTNBCs, reported no statistically significant difference in RR, but a significantly worse OS for TNBCs (50).

4.2.3 Anthracyclines and Cyclophosphamides

Anthracyclines act through multiple mechanisms, including DNA intercalation, topoisomerase-II mediated toxicity, reactive oxygen species (ROS) generation, and DNA adduct formation, making them one of the most efficacious anti-cancer treatments ever developed (51). On the other hand, cyclophosphamide promotes the formation of phosphoramidate mustards, that irreversibly crosslink with DNA to facilitate tumor cell apoptosis. In the study by Dees and colleagues, the pathological and clinical RRs for neoadjuvant anthracycline and cyclophosphamide (AC) combination chemotherapy were reported to be significantly higher in TNBC patients than in other subtypes (52). Another study by Rouzier and collaborators reported a pCR rate as high as 45%, following preoperative paclitaxel treatment combined with fluorouracil, doxorubicin, and cyclophosphamide (53). The WSG 01 trial corroborated the benefit of using adjuvant anthracycline therapy in young patients with TNBC. Most of the patients showed a 5-year event-free survival rate (54). The anthracyclines doxorubicin, epirubicin, and etoposide are commonly used in the treatment of mTNBC (55).

4.2.4 Anti-Metabolites

Anti-metabolites hinder cancer cell proliferation through the incorporation of chemically altered nucleotides or the depletion of deoxynucleotides required for DNA replication. In the clinical trial conducted by Kroman and collaborators, the addition of gemcitabine to paclitaxel promoted an increase in RR (40.8% vs. 22.1%) and more prolonged survival (median survival 18.5 vs. 15.8 months) in patients with advanced mTNBC (56). Further subgroup analysis of two large randomized adjuvant capecitabine trials indicated that the addition of capecitabine to anthracyclines and taxanes regimens was particularly effective in TNBC populations (57, 58).

4.3 Novel Potential Therapies

As mentioned previously, TNBC patients demonstrate a relatively poorer disease prognosis than other breast cancer subtypes. Extensive molecular and genetic profiling studies have identified several different targetable mutations. In addition to the mutations in *PIK3CA* and *p53*, other potential targets such as *PTEN*, *INPP4B*, *KRAS*, *BRAF*, *EGFR*, *FGFR*, *IGFRI*, *KIT*, and *MET* have been explored (59). The recent characterization of TNBC's diverse subtypes and molecular drivers has provided extensive insight into its heterogeneity. Further, it has led to the evolution of *in vitro* and *in vivo* models that accurately recapitulate TNBC tumorigenesis, thus providing the pre-clinical platforms required to develop novel therapeutic strategies.

4.3.1 Poly ADP-Ribose Polymerase Inhibitors

Some TNBCs resembling basal-like breast carcinomas frequently harbor defects in DNA double-strand break repair due to BRCA-1 dysfunction. Such BRCA1-deficient tumors exhibit high sensitivity to poly ADP-ribose polymerase (PARP) inhibition. PARP enzymes play a pivotal role in the processing and repair of DNA breaks (60). *In vitro*, pre-clinical studies have revealed that breast cancer cells lacking BRCA1/2 function exhibit a higher sensitivity to PARP inhibitors (61). Olaparib and Iniparib are the PARP inhibitors showing the most potential. A clinical trial using DNA-damaging agents and PARP inhibitors (olaparib) in conjunction has shown promising results in BRCA1/2-deficient TNBC patients with advanced disease progression (62, 63). Further, a randomized phase II study revealed that the clinical benefit rate, overall RR, and PFS in mTNBC patients was significantly higher when Iniparib was added to carboplatin and gemcitabine (64). A similar improvement in mTNBC patients was observed when Iniparib was administered with gemcitabine and carboplatin (65).

4.3.2 PI3K-AKT-mTOR Pathway Inhibitors

Owing to its multi-faceted role in promoting protein translation, tumor angiogenesis, cancer cell proliferation, and migration, the mammalian target of rapamycin (mTOR) is a lucrative anti-cancer therapeutic target (66). Currently, rapamycin and its analogs everolimus, temsirolimus, and deforolimus are undergoing clinical evaluation in TNBC treatment (67). The mesenchymal TNBC subtype, enriched in EMT and stem-cell like features, has demonstrated some benefit from mTOR inhibition. Further, the MDA-MB-435 TNBC cell line harboring phosphatase and tensin homolog (PTEN) deficiency has shown increased sensitivity to mTOR inhibition (68), thus prompting the use of mTOR inhibitors in TNBC patients with PTEN loss (13). Several reports have attributed cisplatin resistance to mTOR activation, a phenomenon reversed by everolimus administration. Beuvink and colleagues revealed that the addition of everolimus to cisplatin increased the loss of viability by 5- fold *in vitro* (69). Additionally, clinical trials are also exploring the potential of targeting the AKT pathway in TNBC patients. For instance, a phase II study reported a longer PFS and OS in 140 mTNBC patients upon the addition of the AKT inhibitor capivasertib to paclitaxel (70).

4.3.3 Immune Checkpoint Inhibitors

The inception of immune checkpoint inhibitors (ICI) targeting programmed death-1 (PD-1), programmed death-ligand 1 (PD-L1), and cytotoxic T lymphocyte antigen-4 (CTLA-4) has drastically altered the treatment landscape for cancers like TNBC with a high mutational burden (71). Several studies have suggested that the TNBC subtype is an attractive candidate for cancer immunotherapy due to the presence of PD-1 positive TILs (tumor-infiltrating lymphocytes) and higher rates of PD-L1 expression by the tumor and the immune cells (72, 73). Pembrolizumab, a PD-1 inhibitor, was recently evaluated in a phase II, single-arm study in patients with advanced TNBC (74). Results from the phase I trial evaluating the PD-L1 inhibitor

atezolizumab in TNBC revealed an OR of 10% in a cohort of 112 patients, and a notable 11 responders were alive at two years (74). As monotherapy for advanced TNBCs, ICIs have resulted in RRs ranging between 5% to 19%, with higher RRs based on PD-L1 status (75-77). However, median PFS was observed to be only about 1.4 to 2.1 months. To date, atezolizumab is the only FDA approved ICI used as first-line therapy in patients with advanced TNBC (78).

4.3.4 EGFR Inhibitors

Overexpression of EGFR is a common phenomenon observed in TNBC. This tyrosine kinase receptor plays a crucial role in regulating PI3K–AKT–mTOR pathway and ras/raf/mitogen-activated protein kinase/ERK kinase (RAS-MEK) pathway mediated tumor cell proliferation, survival, and differentiation (79). Anti-cancer monoclonal antibodies (mAbs) targeting dysregulated EGFR activity act through the following mechanisms: a) tumor cell death through inhibition of receptor dimerization, inhibition of cell survival signaling and ligand-receptor blockade (80, 81), b) activating antigen-specific T cell immunity (82), c) complement-mediated cytotoxicity (83). Cetuximab is a chimeric IgG1 mAb that binds and blocks ligand-induced EGFR in tumor cells (84). In pre-clinical studies, cetuximab effectively inhibited TNBC tumor growth alone and in combination with chemotherapy (85). Further, in phase 2 trials, TNBC patients receiving cetuximab combined with cisplatin had a significantly longer median PFS than patients treated with cisplatin alone (86). When Lapatinib (an EGFR tyrosine kinase domain inhibitor) was combined with rapamycin, they produced a gradual dose-dependent growth inhibition in MDA-MB-231 and MDA-MB-468 TNBC cell lines *in vitro* (87).

4.3.5 Angiogenesis Inhibitors

Tumor-specific vascular endothelial growth factor (VEGF) expression is observed to be significantly higher in TNBCs when compared to non-TNBC presentations. The anti-VEGF

agent, Bevacizumab (Avastin®), has received controversial attention despite showing potential in several clinical trials. However, multiple Phase III trials are investigating the efficacy of bevacizumab in the mTNBC setting (88). In the E2100 trial, the addition of bevacizumab to paclitaxel, doubled the median PFS (5.3 versus 10.6 months), while reducing the risk of progression by 51% in first-line mTNBC patients (89). The AVADO trial demonstrated a 47% reduction in mTNBC disease progression when bevacizumab was added to docetaxel (90). In the neoadjuvant setting, the GeparQuinto trial studying the effect of combining bevacizumab with anthracycline–taxane chemotherapy, demonstrated a statistically significant improvement in pCR rates (N = 663; 39.3% versus 27.9%, P = 0.003) for patients receiving bevacizumab compared with chemotherapy (91).

5. Mechanisms of Triple-Negative Breast Cancer Chemoresistance

Despite numerous advances in cancer therapeutics, chemotherapy remains the mainstay in systemic TNBC treatment. Neither anti-HER-2 agents nor hormonal therapies are efficacious owing to the absence of their targets in the TNBC setting (92). Cytotoxic chemotherapy induces cancer cell death primarily through apoptosis. As depicted in Figure 1, although chemotherapy administration initially promotes tumor regression, chemoresistance is eventual as tumor cells evade drug exposure by turning to alternative cellular fates, thus promoting metastatic recurrence (41). The findings below highlight some of the mechanisms of TNBC chemoresistance.

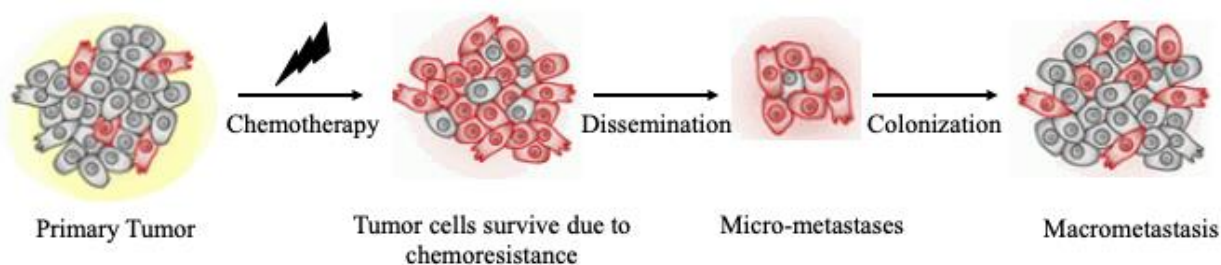


Figure 1: Chemoresistance promotes metastatic recurrence. Primary tumor cells that survive chemotherapy administration acquire an invasive phenotype and undergo metastatic dissemination to distant organs.

5.1 ATP-Binding Cassette Transporters

Transporter-mediated drug efflux is one of the most extensively validated mechanisms of chemoresistance (93). ATP-binding cassette (ABC) transporters utilize ATP binding to translocate various substrates, including anti-cancer drugs across the cell membrane. The three ABC transporters most frequently upregulated in TNBCs are a) multidrug-resistant protein-1 (MRP-1), which confers resistance against vinca alkaloids, high-dose methotrexate, and anthracyclines. b) P-glycoprotein (MDR-1), which effluxes a broad spectrum of taxanes such as paclitaxel out of cancer cells, and c) breast cancer resistance protein (ABCG-2), which pumps out drugs such as doxorubicin (94).

5.2 Mutations in DNA Replication and Mismatch Repair Enzymes

DNA damage is the primary mechanism of action of most conventional chemotherapeutics. Several studies have suggested chemoresistance to be a result of aberrant DNA damage repair due to altered DNA mismatch repair enzyme function. For instance, chemoresistance against anthracyclines and epipodophyllotoxins was attributed to mutations in

the critical DNA replication and repair enzyme topoisomerase II (95, 96). The study by Fedier and colleagues further confirmed that the resistance to topoisomerase II inhibitors was due to inhibited expression of DNA-mismatch repair proteins (97).

5.3 Tumor Dormancy

Following chemotherapy administration, chemoresistant tumor cells sometimes exist in a dormant state for several years before resuming proliferation. These dormant cancer cells adapt by entering quiescence and undergo alterations in their signaling pathways, protein expression, and modulation to survive chemotherapy-induced cytotoxic stress. Post-treatment, these cells re-initiate tumor growth, which promotes disease recurrence after an initial response. Tumor dormancy may be established through chemotherapy-induced cellular senescence (CIS), which results in permanent cell cycle arrest without cell death. Although this stress response reduces tumor growth, cancer cells often exit CIS and regain proliferative capacity. The effect of chemotherapy on the senescence-linked signaling via p53, p16Ink4a, p21Waf1/Cip1, and p27Kip1, resulting in tumor dormancy, continues to be a hotly debated topic.

5.4 Epithelial to Mesenchymal Transition

Several recent studies suggest the involvement of EMT in antagonizing chemosensitivity in several cancers, including TNBC. As discussed previously, EMT entails the dynamic transition promoting the acquisition of invasiveness, resistance to apoptotic stimuli, motility, and a mesenchymal phenotype by epithelial cancer cells (98). Aberrant expression of the Snail family of transcription factors not only initiates EMT but also confers resistance to apoptosis induced by genotoxic stress in MDA-MB-468 and MDA-MB-231 TNBC cell lines *in vitro* (99). Compelling evidence also demonstrated that the EMT inducer Twist up-regulated ABC transporter expression, which leads to multidrug resistance in human breast cancer cell lines (100,

101). Twist is implicated in the activation of the β -catenin signaling pathway and AKT pathways, known to reinforce the loss of chemosensitivity (102).

5.5 Cancer Stem Cells

Growing evidence indicates that cancer recurrence is caused by multipotent self-renewing cancer-initiating cells, commonly referred to as cancer stem cells (CSCs). The CSC paradigm has emerged based on the notion that some, but not all, cancer cells have the potential to recapitulate the phenotypic diversity of the original tumor upon transplantation. The biological features of CSCs largely overlap with those of drug-resistant cancer cells. Recent studies suggest that upon exposure to conventional chemotherapy, TNBC biopsies demonstrate an increase in RNA transcripts of genes associated with the CSC phenotype. For instance, treatment with taxanes like paclitaxel significantly increased TGF- β signaling and other CSC properties in several TNBC cell lines and mouse xenografts (103). The TGF- β cytokine family and its receptors are often overexpressed in CSCs. Through TGF- β induced EMT, CSCs promote TNBC relapse (104). Another study reported elevated expression and transcriptional activity of hypoxia-inducible factors (HIFs) post gemcitabine administration in TNBC cell lines. This eventually promoted CSC enrichment through upregulated IL-6 and IL-8 signaling (105).

5.6 Hypoxia

A prominent feature of the tumor milieu is hypoxia, where an inadequate supply of oxygen occurs due to tumor cells outgrowing their vasculature (106). Clinically, TNBC tumors are found to be more hypoxic than their non-TNBC counterparts (41). By varying the oxygen levels within the TME, hypoxia propagates a chemoresistance phenotype that is accompanied by tumor aggressiveness and metastatic dissemination. Hypoxia promotes the development of an acidic TME, thus compromising chemotherapy drug uptake (107). Further, hypoxia protects

tumor cells against immune surveillance by acting as a barrier to immune effector cells (108). Additionally, hypoxia stimulates cellular adaptations including; a) upregulated ABC transporter expression, b) decreased proliferation, c) autophagy induction, d) upregulation of pro-angiogenic factors, e) enhanced genetic instability and subsequent clonal selection of aggressive phenotypes and f) E-cadherin repression which furthers cancer progression (109).

5.7 Cell-Signaling Pathways

5.7.1 NF- κ B Pathway

A crucial regulator of carcinogenesis, the NF- κ B signaling pathway, inhibits apoptosis, controls the inflammatory response, and angiogenesis. Hyperactivation of the NF- κ B pathway is often implicated in TNBC progression and poor prognosis. In 2018, Huang and colleagues demonstrated that doxorubicin administration stimulated the overexpression of pleiotrophin (PTN) and its cognate receptor protein tyrosine phosphatase zeta (PTPRZ1) in several TNBC cell lines. The upregulated PTN/ PTPRZ1 signaling axis subsequently promoted chemoresistance evolution through the activation of the NF- κ B signaling pathway *in vitro* (110). Alternatively, that NF- κ B signaling can also be up-regulated by hypoxia (111).

5.7.2 PTEN and PI3K-AKT-mTOR Pathway

PI3K-AKT-mTOR (PAM) pathway is a critical mechanism governing cancer cell survival, growth, proliferation, and motility. Frequent up-regulation of the PAM pathway accounts for the adverse prognosis, aggressive nature, and poor outcome observed in most TNBCs (112). Further, the skewed expression of the PAM pathway components is also associated with TNBC chemoresistance (113). Additionally, the PAM pathway's AKT induces HIF-1, which plays a notable role in chemoresistance onset (114).

5.7.3 JAK/STAT pathway

Aberrant JAK/STAT signaling plays a pivotal role in mediating the metastatic cascade (115). Genetic profiling of chemotherapy-refractory TNBCs revealed a pro-inflammatory gene signature due to JAK/STAT pathway extracellular ligand (Interleukin (IL)-6/IL-8) overexpression (116). STAT-3, which is a downstream component of the JAK/STAT signaling axis, is frequently overexpressed in TNBC. STAT-3 interacts with NF- κ B to promote chemoresistance in TNBC (117). Moreover, through the up-regulation of both HIF-1 and ABC transporter expression, STAT-3 also induces hypoxia-mediated chemoresistance in TNBC (118).

5.7.4 TGF- β Pathway

While the TGF- β signaling pathway is synonymous with EMT, proliferation, angiogenesis, and subsequent metastatic progression, it is mostly recognized for regulating breast CSCs (119). Post chemotherapy administration in a TNBC setting, elevations in the TGF- β signaling was observed (103). Further, the exposure of several TNBC cell lines to TGF- β promoted EMT and the acquisition of CSC properties, including chemoresistance (120).

5.7.5 Wnt/ β -Catenin Pathway

Wnt signaling is predominantly associated with tumor initiation, stemness, and metastatic dissemination (121). Several studies have highlighted the pivotal role played by Wnt/ β -catenin signaling in promoting the tumorigenic behavior associated with the TNBC subtype. For instance, TNBC patients with aberrant Wnt/ β -catenin signaling were reported to be more susceptible to metastatic progression, especially to the brain and lung (122). In another seminal study, the Wnt signaling was identified to be vital for development, enhanced proliferation, increased migration, and chemotherapy resistance in TNBCs (123). Further, β -catenin was demonstrated to have a synergistic effect with Nek2B on chemotherapy resistance in TNBC (124).

Other constituents of the Wnt/ β -catenin pathway, such as FZD-8 (a member of the Frizzled receptor family) was overexpressed in TNBC and linked to TNBC chemoresistance following neoadjuvant chemotherapy (125).

5.8 Receptor Tyrosine Kinases

The PAM and JAK/STAT signaling pathways are employed by numerous growth factors to mediate tumorigenesis. The upstream regulators of these pathways, namely the insulin-like growth factor-1 receptor (IGF-1R) and EGFR, are often implicated in TNBC chemoresistance. EGFR expression is markedly higher in TNBCs, making it a prominent TNBC hallmark. Several studies have confirmed the correlation between EGFR amplification and expression with worse outcome in TNBC (126, 127). Via the regulation of ABCG-2 expression and function, the EGFR pathway is observed to promote chemoresistance in TNBC cell line and xenograft models (128). IGF-1R is a transmembrane receptor overexpressed in TNBCs and is frequently associated with poor survival (129). Insulin-like growth factors (IGFs) bind to their receptors, activate the downstream signaling cascade to promote chemoresistance evolution via ABC transporter expression, and apoptosis inhibition (130). Through its interaction with the Wnt/ β -catenin pathway, IGF-1 enhances CSC growth and self-renewal potential (131).

6. Tumor-Targeting Peptides

The efficacy of most anti-cancer agents is often hindered by its inability to target, penetrate cellular membranes, and eventually localize within the tumor. Unlike standard chemotherapeutic agents that induce non-specific cytotoxicity, targeted therapies are often cytostatic. Their deliberate interaction with ‘molecular targets’ expressed on the cancer cell surface inhibits cancer growth and progression (132). Targeted therapies like nanoparticles or antibodies possess a high molecular weight (MW), high affinity, and low diffusion coefficient

that impede tumor penetrability (133). On the other hand, smaller MW entities like peptides offer fundamental advantages, including easy synthesis, higher cell membrane penetration, and lesser immunogenicity (134).

Tumor-targeting peptides (TTPs) are two-dimensional linear chain amino acid sequences (135), modified to either directly target cancer cell surface receptors or act as chaperones delivering cytotoxic drugs to the TME, tumor vasculature, and cancer cells. Targeting and concentrating these peptides to specific cancer tissue components is achieved via tumor-specific biomarkers. TTPs can be coupled with either cargo or an apoptotic domain. The homing domain can be identified through antibody-based screens, bio-panning of phage-displayed peptide libraries, identified in silico using random generation algorithms, or through imitation of protein fragments known to bind to the receptor of interest (135).

6.1 Phage Display Screening for the Isolation of Tumor-Targeting Peptides

In 1985, Nobel laureate George Smith demonstrated that filamentous phages could be genetically modified to display peptides as fusions on the virus capsid protein (136). This opened the possibility of isolating phage-displayed peptides by selecting for those with the highest binding affinity to the desired target. As shown in Figure 2. below, The multivalent display of foreign polypeptides is achieved by cloning the peptide encoding combinatorial DNA sequences into the M13 phage's pIII or pVIII gene. Each phage-displayed peptide is designed as a linear chain of variable random amino acid residues ($X_n, 6 \leq n \leq 12$), resulting in the generation of phage-displayed peptide libraries with complexities up to a 10^{13} magnitude. To reduce conformers and improve affinity, the random sequences are enclosed within two cysteine residues to generate cysteine-to-cysteine disulfide cyclized phage-peptide libraries (137).

The isolation of phage-displayed peptides homing to the target of interest is carried out via an affinity selection process, alternatively known as bio-panning. Homogenous in situ phage

library bio-panning using immobilized antigens can be used to isolate peptides with high affinity and specificity (138). However, to facilitate the identification of peptides that mimic naturally occurring receptor ligands or target heterogeneous environmental conditions, screens were performed *in vitro* (139), *in vivo* (140), *ex vivo* (141), and inpatient (142) settings.

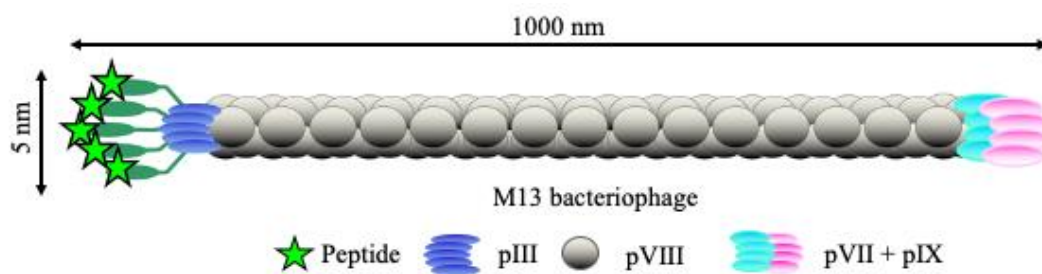


Figure 2. A diagrammatic representation of M13 bacteriophage. Each bacteriophage is 1,000 nm in length and 5 nm wide. The peptides are displayed as fusions on the pIII minor coat protein.

6.2 Tumor-Targeting Peptides Specific to the TME

Owing to its indispensable role in carcinogenesis, the TME serves as an alternative target for future therapies. Due to their low production cost, high specificity, and tumor penetrability, there has been a renewed interest in using phage display technology to identify peptides that efficiently target the TME. The findings below highlight some TTPs targeting various stromal constituents of the TME.

6.2.1 Peptides Targeting Tumor Vasculature

The tumor vasculature, with its consistently high angiogenic marker (i.e., VEGF receptor (VEGFR) and integrins) expression, pronounced hypoxic regions, ‘leaky’ nature, and pivotal role in tumorigenesis, serves as an attractive therapeutic target. A prominent example of

a tumor vasculature specific therapy is the “RGD” peptide. Isolated using *in vivo* phage display technology in prostate tumor-bearing mice, the cyclic RGD peptide (sequence: CDCRGDCFC) was identified to bind with $\alpha\beta v$ -3 and $\alpha\beta v$ -5 integrins over-expressed on tumor blood vessels (143, 144). Subsequently, another pioneering study by Arap and colleagues led to the discovery of the “NGR” motif bearing cyclic peptides (sequence: CNRGC) that targeted tumor vasculature in melanoma, breast carcinoma and Kaposi’s sarcoma (145). This peptide homed to the aminopeptidase N (APN/CD13) receptors detected in tumor vasculature (146).

6.2.2 Peptides targeting Extra-Cellular Matrix

The extracellular matrix (ECM) is composed of immensely diverse components, including fibronectins, tenascin C (TNC), collagen, and connective tissue growth factor, to name a few. Tumor-associated fibronectin (TAF) plays a vital role in promoting cancer cell survival, proliferation, invasiveness, and metastatic dissemination (147). During tumor driven ECM remodeling, TAF undergoes alternative splicing, which results in extra domains A and B (EDA and EDB). Through *in situ* phage library bio-panning, an EDB binding scaffold-like peptide named APTEDB was identified (138). This peptide was further modified to a targeting ligand that could be conjugated with anti-cancer drugs to reduce systemic toxicity, deliver cargo, including siRNA, oligonucleotides, and imaging probes (148, 149).

The TNC glycoprotein mediates the assembly of other ECM molecules and plays a part in mediating cell adhesion, permeation, migration, and differentiation. TNC is specifically associated with several solid tumor malignancies, including breast, colon, and oral cavity (150). This led to the isolation of a TNC targeting peptide (sequence: FHKHKSPALSPV) that selectively bound to TNC in both xenograft mouse tissues and patient tumors and acted through the reduction of TNC-induced cell rounding and migration (138). More recently, Yeow and

collaborators ingeniously tackled tumor ECM targeting by conducting the first three rounds of bio-panning in Matrigel™ *in vitro* and the last round *in vivo*. Following the four rounds, a disulfide cyclized peptide (sequence: CSGRRSSKC) that exclusively homed to laminin-nidogen receptor complexes of the ECM was isolated (151).

6.2.3 Peptides targeting Matrix Metalloproteases

Abrogated ECM remodeling triggers the release of biophysical and biochemical cues that set the events of neoplastic evolution in motion. MMPs are one of the most studied ECM remodeling enzymes due to their up-regulation in the TME and roles in angiogenesis regulation, tumor cell migration, and invasion. Despite being secreted proteins, MMP-2 and MMP-9 mediate phage homing by binding to integrins expressed by tumor vasculature. Based on this principle, peptides targeting the gelatinase members of the MMP family (sequences: CRRHWGFEFC and CTTHWVGLMS) and subsequently inhibiting MMP-2 and MMP-9 activity were discovered (152). In 2019, Bicycle therapeutics pioneered *in vitro* phage display technology to develop BT1718, a peptide-drug conjugate targeting the ECM enzyme MMP-14. This drug is currently undergoing Phase I clinical trials in patients with advanced solid tumors (133).

6.2.4 Peptides targeting Cancer-Associated Fibroblasts

Within the TME, cancer-associated fibroblasts (CAFs) are often found to reside within the proximity of tumor cells. Unlike tumor cells that express diverse cell surface markers, CAFs predominantly overexpress specific proteins, including fibroblast-activated protein-alpha (FAP- α) and alpha-smooth muscle actin (α -SMA) (153). Thus, CAF targeting may be an alternative strategy to improve anti-tumor efficacy. In a seminal study combining *in vivo* phage display and the PHASTpep software, two peptides (sequences: APPIMSV and HTTPKV) targeting CAFs were identified (154). The peptides selectively bound to only α -SMA positive pancreatic CAFs

in mice. Several studies have reported that the CAFs within the TME of colon, breast, and prostate were carcinomas dependent on the urokinase plasminogen activator (uPA) receptor signaling axis to mediate the events implicated in early tumor development. This prompted the isolation of a peptide (sequence: LWXXAr (Ar = Y, W, F, H) XFXXYLW) that acted as a potent antagonist against the uPA receptor (155).

6.2.5 Peptides targeting Tumor-Associated Macrophages

Derived from circulating monocytes within the TME, tumor-associated macrophages (TAMs) are specified as a separate myeloid population of the TME. Tumor-secreted cytokines (IL-4 or M-CSF) mediate macrophage polarization into anti-inflammatory M2-skewed TAMs that promote tumor angiogenesis, immunosuppression, and neoplastic transformation (156). M2-skewed TAMs traverse the TME's complex milieu with either the aid of collagen-interacting proteins, including collagenases, MMP-9, and mannose receptors (CD206/MRC-1) or through tumor vasculature via VEGF secretion (157). The *in vitro* phage-displayed peptide library bio-panning performed by Cieslewicz and collaborators yielded M2Pep (sequence: YEQDPWGVKWWY), which selectively targeted M2-skewed mouse TAMs in mouse colon carcinoma tumors (158). To improve its affinity, the authors synthesized a tetravalent version of the peptide, which coupled was to a C-terminal cysteine on a maleimide scaffold. This peptide was then conjugated with a pro-apoptotic domain, which augmented its toxicity towards M2 TAMs (158). In 2017, *in vivo* phage display in metastatic breast cancer-bearing mice led to the identification of a CD206-binding peptide termed mUNO (159). The internalization of mUNO by M2 TAMs was mediated through the minimal binding CSPGAK sequence motif present in all CD206-binding collagens. Interestingly, the mUNO peptide also binds to human recombinant CD206, indicating future therapeutic potential in cancer patients (159).

6.3 Tumor-Targeting Peptides Specific to Overexpressed Tumor Receptors

Post administration, anti-cancer therapies often modulate the expression of cell-surface receptors implicated in carcinogenesis. Agents such as antibodies, peptides, or small molecule inhibitors, can serve to inhibit the receptor's downstream activity by directly binding to them, thus halting cancer progression. In the following section, a few prominently over-expressed receptors used in cancer cell-specific targeting have been discussed.

6.3.1 Peptides Targeting EGFR

Through its complex signaling cascade, EGFR modulates several events implicated in carcinogenesis, including cancer cell survival, proliferation, differentiation, adhesion, and migration. In 2014, Wang, Zho, and Joshi were awarded an international patent (Patent No. WO2016029125A1) for 17 EGFR-specific peptides identified through in situ phage library screening of Ph.D.-7 heptapeptide and Ph.D.-12 decapeptide random libraries from New England Biolabs (160). Li and colleagues are credited with isolating the prominent GE11 peptide, internalized preferentially by both EGFR overexpressing cancer cells in vitro and tumor xenografts *in vivo* (161). Another group identified two short peptides (sequences: SYPIPDT and HTSDQTN) via an *in vitro* cell-based subtractive bio-panning approach in EGFR overexpressing A-431 cells. These peptides effectively inhibited EGF-induced phosphorylation of EGFR in a concentration-dependent manner (162).

6.3.2 Peptides Targeting VEGFR

VEGFR belongs to the VEGFR receptor family (VEGFR 1, 2, 3, and neuropilin 1). The overexpression of VEGFR and its cognate VEGF ligand is observed in several malignancies (163-165). To identify novel ligands specific to VEGFR-3, Qin and coworkers used phage-displayed peptide library screening to isolate the peptide P1 (sequence: CSDXXHXWC, where X is any

amino acid) which bound to all VEGFR-3 positive tumor cells with a high degree specificity (166). In another study, using the novel BRASIL method, Giordano and colleagues sorted for cell-surface binding peptides based on differential centrifugation. They isolated 21 phage-displayed peptide clones that bound to VEGF-stimulated HUVEC cells (167).

6.3.3 Peptides Targeting Interleukin 11 Alpha Receptor

Upon up-regulated expression, IL-11 confers several tumor intrinsic “hallmarks” to neoplastic cells. An integral member of the IL-6 family of cytokines, it dictates the progression of the metastatic cascade via downstream JAK/ STAT-3 signaling pathway activation (168). Pasqualini and colleagues first explored the potential of using IL-11 α R as an anti-tumor target via *in vivo* bio-panning of a 7-mer library in chemotherapy-refractory B cell malignancy bearing patient (142). In a companion study, the authors isolated a phage clone (sequence: CGRRAGGSC) that bound to IL-11 α R overexpressed in the prostate, which was further validated in prostate tumor-bearing mice and human prostate cancer tissue samples (169). When conjugated with a pro-apoptotic moiety, this peptide also demonstrated acute cytotoxicity on cultured prostate cancer cells (165).

6.3.4 Peptides Targeting Folate Receptor Alpha

Folate receptor-alpha (FR α) overexpression often co-relates with high tumor grade, stage, malignancy, and aggressiveness (170), thus serving as a potential target for tumor therapy and diagnosis. Xing and coworkers isolated the FR α specific C7 peptide (sequence: MHTAPGWGYRLS) by screening a Ph.D.-12 phage library displaying random dodecapeptides in an ovarian cancer mouse model. The C7 peptide was further validated outside the phage context, through *in vivo* phage homing experiments and fluorescence imaging (171).

6.3.5 Peptides Targeting PDGFR beta

A transmembrane glycoprotein in the receptor tyrosine kinase family, PDGFR-beta (PDGFR β), is implicated in cancer cell proliferation, differentiation, and development (172). Owing to its upregulation in a variety of solid tumors, this receptor represents an attractive target in the treatment and molecular imaging of oncological diseases. PDGFR-P1 (sequence: IPLPPPSRPFFKY-NH₂) is a synthetic peptide designed to bind to PDGFR β overexpressing cells *in vitro*. *In vivo* biodistribution studies in the BxPC3 tumor mouse model revealed a high accumulation of PDGFR-P1 peptide in BxPC3 tumors than in normal organs (173).

6.4 Design of Tumor-Specific Hunter-Killer Peptides

A unique feature of anti-microbial peptides (AMPs) is the amphipathic α -helix, which grants its membrane permeabilization and resultant cytotoxic potential. The synthetic (KLAKLAK)₂ moiety, which mimics AMP features and demonstrates significant anti-microbial activity, was generated based on this principle. The (KLAKLAK)₂ moiety is highly selective to the anionic membranes of prokaryotes and is poorly permeabilized by eukaryotic plasma membranes. To promote tumor cell internalization, the (KLAKLAK)₂ moiety is fused with TTPs to generate hunter-killer peptides that act through mitochondrial disruption (174). For instance, the hunter-killer R7- (KLAKLAK)₂ peptide consisting of the homing domain (R7 or RRRRRRRR) shows increased cellular uptake and efficient apoptosis in several tumor cell lines and human xenografts (175). Along the same principles, the NH₂-terminus of TCTP (human translationally controlled tumor protein) was fused to the (KLAKLAK)₂ moiety resulting in the hunter-killer TCTP-(KLAKLAK)₂ peptide. This peptide promoted the regression of lung carcinomas implanted in mice (176). Our own group has generated a proteolysis-resistant targeted hunter-killer peptide D-WAT. This peptide is composed of a cyclic domain CSWKYWFGEC homing to adipose

stromal cells and pro-apoptotic domain (KFAKFAK)₂ (177). The addition of the (KFAKFAK)₂ moiety was observed to improve the cytoablative properties of D-WAT. The above examples underscore the potential use of TTPs fused to a cytotoxic peptide, to produce a highly efficacious, tumor cell ablating complex.

Chapter 2: Statement of Objective

1. Knowledge Gap

An insurmountable challenge encountered in the clinical management of TNBCs is metastatic progression. Metastatic dissemination continues to be a major perpetrator of TNBC patient mortality. Owing to the unresponsiveness of TNBCs to hormone therapy, chemotherapy remains a mainstay in mTNBC treatment. Despite chemotherapy eliciting a brief response in the tumors, drug resistance gradually develops. Several studies suggest that chemotherapy appears to select for cells with CSC properties that drive cancer toward more aggressive stages (178). There are no bio-markers specific to chemoresistant metastatic tumor cells. Moreover, there is a dearth of drugs available to selectively target them. Therefore, it is imperative to develop novel targeted therapies to ablate these stubborn tumor cell populations. The isolation and development of peptides selectively targeting these chemoresistant metastatic tumor cells would be pivotal for cancer medicine, as they would enable targeting the mortality-responsible cell population with minimal side effects. This rationale encouraged us to formulate the following hypothesis.

2. Hypothesis

Metastatic chemoresistant TNBC cells display novel cell surface biomarkers, which can be used in the identification of new compounds homing to these unique cell populations and specifically ablating them.

3. Aims and Experimental Approach

Aim 1: Identify phage-displayed peptides homing to chemoresistant metastatic tumor cells.

Experimental Approach

- Perform an *in vivo* phage-displayed peptide library screen in a spontaneous TNBC lung metastasis model to isolate phage-displayed peptide candidates homing to metastatic tumor cells.

- Compare the homing of the phage-displayed peptide candidates between vehicle control and cisplatin-treated *in vitro* and *in vivo* models.
- Identify the most enriched breast lung metastasis peptide (BLMP) candidate.

Aim 2: Conversion of phage-displayed peptides into hunter-killer peptides that ablate metastatic tumor cells *in vitro* and *in vivo*

Experimental Approach

- Validation of the chemically synthesized hunter-killer peptide candidates *in vitro*.
- *In vivo* studies to validate the ability of hunter-killer peptides to ablate TNBC pulmonary metastases.

4. Graphical Abstract

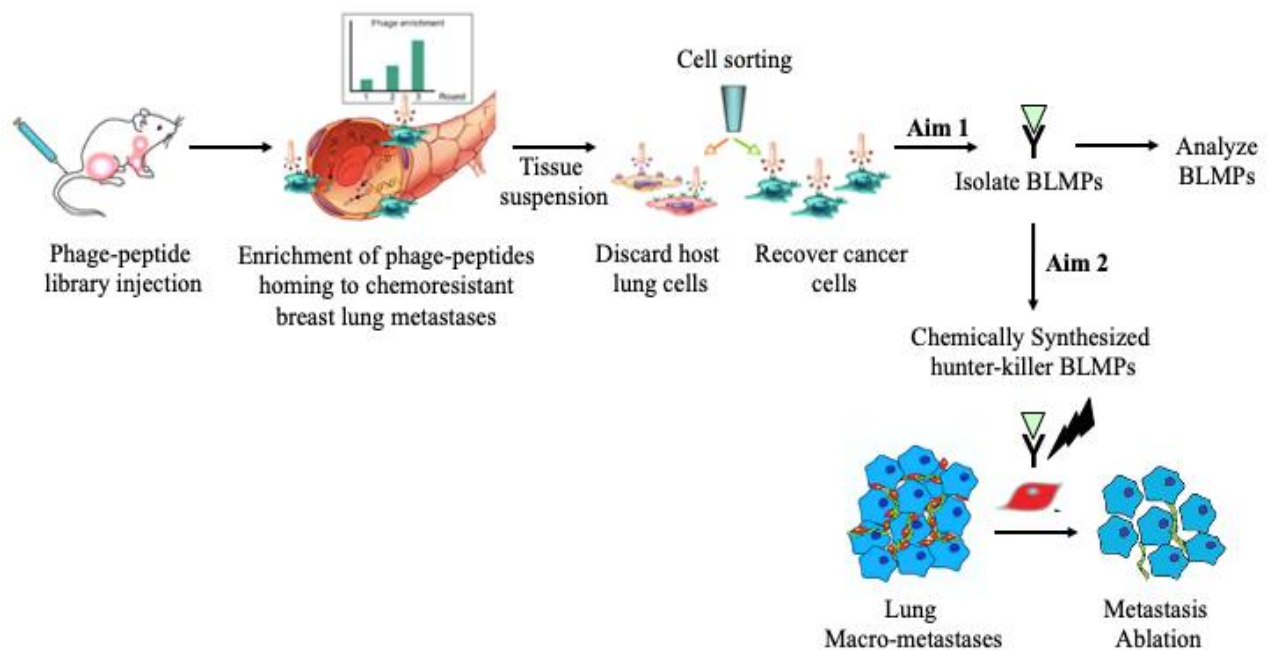


Figure 3: Schematic depiction of the study

Chapter 3: Materials & Methods

1. Cell Lines and Cell Culture

Murine fibroblast 3T3L1 (ATCC® CRL-1658™), murine melanoma B16-F10 (ATCC® CRL-6475™), murine mammary breast adenocarcinoma E0771 (ATCC® CRL-2755™) cell lines were obtained from the ATCC (Manassas, VA). The human mammary adenocarcinoma MDA-MB-231 cell line was kindly provided by Dr. Wenliang Li's lab (IMM-UTHealth, Houston, TX). The mammary adenocarcinoma murine 4T1 cell line with dual luciferase and mCherry expression (4T1 - Luc⁺ mCherry⁺) was kindly provided by Dr. Sendurai A. Mani's lab (MDACC, Houston, TX). The murine mCherry labeled 4T1.2 (4T1.2 - mCherry⁺) breast tumor cells (derived from spontaneous adenocarcinoma in a Balb/cfC3H mouse) was kindly provided by Dr. Naoto Ueno's lab (MDACC, Houston, TX). Its cisplatin-resistant cell lineage, 4T1.2/CTX, was generated with a biweekly treatment of cisplatin (Tocris Biosciences, Minneapolis, MN; 180ng/mL) to maintain consistent drug resistance. The cell lines were cultured in DMEM media (Hyclone Laboratories Inc., Logan, UT) supplemented with 1% penicillin-streptomycin (Gibco) and 10% FBS (Atlas Biologicals, Fort Collins, CO). All cell lines were cultured on plastic plates maintained at 37°C and 5% CO₂. Sub-culturing was performed at 70% cell confluency. Adherent cells were washed with 1X PBS (Phosphate-Buffered Saline) solution (Fisher Scientific, Waltham, MA) and detached with 0.25% trypsin-EDTA (Gibco) and then sub-cultured.

2. Murine Model of Experimental Lung Metastasis

All mouse experiments were performed in accordance with the bioethical principles adopted by the Institutional Animal Care and Use Committees of UTHealth and MDACC. Female C57BL/6 mice (Jackson, Bar Harbor, ME) were aged eight weeks prior to experimental manipulation. The mice were anesthetized using tribromoethanol (150mg/kg) administered through intraperitoneal injections. Murine melanoma B16-F10 cells (100,000 cells suspended in 100µl DMEM) were injected into the mice intravenously. Following this procedure, the mice were

kept warm under a heat lamp and monitored until recovery. Upon resuming mobility, the mice were housed back in their cages. Ten days post tumor implantation; the mice were randomized into vehicle and chemotherapy-treated cohorts. The mice were administered either vehicle (1X PBS solution) or cisplatin (Tocris Biosciences; 2.5mg/kg) retro-orbitally once a week for three weeks. Upon exhibiting distress, the mice were euthanized, and their organs (brain, spleen, liver, kidney, and lung) surgically resected. After excision, the tissues were fixed in 10% neutral-buffered formalin (Thermo Fisher Scientific, Waltham, MA) for histopathological analysis.

3. Orthotopic Murine Model of Spontaneous Lung Metastasis

Female Balb/c mice (stock 000651, Jackson) were six weeks old at the start of the experiment. Prior to cell injection, the animals were anesthetized through 2-4% isoflurane (Fisher Scientific) inhalation. The site of tumor implantation was prepped with 70% ethanol solution and shaved with hair clippers. 4T1-Luc⁺ mCherry⁺ (20,000 cells suspended in 20μl DMEM) were subcutaneously injected into the mammary gland of the syngeneic Balb/c mice. The correct injection of cancer cells was validated through the visual confirmation of fat pad swelling. Once palpable, the growing primary tumors were measured biweekly with calipers with tumor volume calculated using the $(\text{length} \times \text{width}^2)/2$ formula. After the tumor volumes reached ~ 200mm³, the mice were randomized into two cohorts, vehicle and chemotherapy-treated, respectively. The mice were administered either vehicle (1X PBS) or cisplatin (Tocris Biosciences; 2.5mg/kg) retro-orbitally once a week for three weeks. Multiple row t-tests were performed to account for the differences observed in tumor volume between the two groups. Upon exhibiting adverse effects such as labored breathing or ulcerated tumors, the mice were humanely euthanized. This was followed by surgical resection of organs (brain, spleen, liver, kidney, and lung) and tumors. After excision, the tissues were then fixed in 10% neutral-buffered formalin.

4. Non-Invasive Bioluminescence Imaging to Monitor Metastatic Progression *In Vivo*

4T1 Pulmonary metastases bearing mice were injected intraperitoneally with D-luciferin (Promega, Madison, WI; 150 mg/kg) and anesthetized 9 minutes before the peak luciferin uptake time (according to manufacturer's procedures) with 5% isoflurane. At the optimal imaging time, the mice were transferred to the imaging chamber (IVIS SPECTRUM, PerkinElmer Inc., Boston, MA) with their mouths and noses firmly set within the anesthetic tubing maintained at 2% isoflurane until BLI was completed. In the fat pad spontaneous metastasis model, weekly *in vivo* bioluminescence imaging BLI was initiated at the time of tumor implantation. Due to differences in tumor burden, an autoexposure (1 second–1.5 minutes) was used for each mouse to account for any variabilities in the bioluminescence signal. BLI imaging of the primary tumors was performed in the following setting: emission filter: open, f/stop: 1, binning: medium, 1 scan/minute, exposure time: 1–15 second. While imaging metastatic lesions in the thoracic cavity, bleed-over from the implantation site was avoided by masking the primary tumor/injection site with an X-ray sheet encased in aluminum foil. Metastatic burden was then evaluated by drawing a standard circular ROI (same size over all the time points) over the lung region. Luminescence was expressed as photons/sec/ROI minus background luminescence for a region of similar size. Bioluminescent signals were quantified to radiance intensity using Living Image 3.0 (Caliper Life Sciences, Alameda, CA).

5. *In-situ* Lung Perfusion and Fixation

The animals bearing pulmonary metastases were anesthetized using tribromoethanol (150mg/kg) administered through intraperitoneal injections. When the mice's reflexes were no longer observed, the mice were splayed on a Styrofoam board with their limbs secured in position with push pins. The fur was wet with 70% ethanol to slick the hairs down. The chest cavity was opened with surgical scissors, and a "V" shaped incision was made from the sternum apex through

the ribs to the upper left and right shoulder. This was followed by cutting the vena cava caudalis underneath the liver. Using a 20 mL syringe equipped with a 21G needle, 15mL 1X PBS was slowly injected into the right ventricle of the beating heart until the lungs were inflated, and the heart stopped beating (asystole). Using forceps, the heart and lungs were pulled out as one unit by firmly grasping the lung hilus directly above the heart. The heart was separated from the lungs carefully by pulling the heart with forceps, and by transecting connective tissue ligaments and blood vessels. The lungs were then fixed in 10% neutral-buffered formalin.

6. Enumerating Pulmonary Metastasis in Mice

The lungs bearing pulmonary metastases were fixed in 10% neutral-buffered formalin until the metastatic nodules were bleached to amelanotic gray/white nodules. Using forceps, the fixed lungs were pried apart into individual lobes. At 10X magnification, the tumor nodules on each lobe were enumerated blindly beneath a dissecting microscope. For consistency between the mice, the foci number on the lobe surface was first counted, and then the lobe was inverted. Doing each of the four lobes individually allowed for more accuracy in counting. The average number of nodules for all mice within both treatment groups was determined.

7. *In Vivo* Phage-Peptide Library Bio-panning for Lung Metastases Targeting Peptides

7.1 Round 1 of *In Vivo* Phage-Displayed Peptide Library Bio-panning

Phage-displayed peptides were selected from fUSE5 phage-peptide libraries, which were kindly provided by Dr. Erkki Koivunen (University of Helsinki, Finland). Library amplification was conducted as described previously (179). Phage transducing units (TU) were determined through titration with K91 *Escherichia coli*. A mouse bearing 4T1 pulmonary metastases from the chemotherapy-treated cohort was anesthetized through 2-4 % isoflurane

inhalation. A 10^{10} TU mixture of cyclic CX₇C and CX₈C (C: disulfide-bonded cysteines; X: any amino acid) phage-displayed peptide libraries suspended in 1X PBS was injected intravenously and allowed to circulate for 3 hours. The mouse was perfused with 15mL of 1X PBS solution as described previously in Section 5, to facilitate phage elimination from normal vasculature and other non-lung metastasis specific antigens. The mouse was euthanized, and its organs (lungs, liver, kidney, primary tumors, brain, and spleen) resected.

7.2 Lung Tissue Digestion for Cell Isolation

Lungs bearing 4T1 pulmonary metastases were minced manually and digested with collagenase (Worthington, Franklin County, OH; 250 U/ml in PBS) and dispase (Roche, Indianapolis, IN; 2.4U/ml in PBS) for 30 minutes at 37°C with intermittent shaking. Enzymatic digestion was neutralized with growth media (DMEM with 2% FBS). The samples were centrifuged at 300 x g for 8 minutes. The supernatant lysate was discarded, and the cell pellet resuspended in growth media (DMEM with 5% FBS). The samples were passed through a 70µm cell strainer (Fisher Scientific), washed once in growth media (DMEM with 2% FBS), and incubated in Red Blood Cell Lysis buffer (BD Pharmingen, San Jose, CA) for 15 minutes at room temperature in the dark. After centrifugation at 200 x g for 5 minutes, the supernatant was carefully aspirated, and the pellet was resuspended in growth media (DMEM with 2mM EDTA and protease inhibitors; Thermo Fisher Scientific). The samples were transferred into 35µm strainer-capped flow cytometry tubes for flow cytometric analysis.

7.3 FACS Recovery of Pulmonary Metastatic 4T1-Luc+mCherry+ Tumor Cells

For fluorescence-activated cell sorting (FACS) analysis of the prepared single-cell suspensions of mouse lung tissue samples, the cells were prepared at a concentration of 1 million

cells/ mL and pre-gated to exclude non-viable cells, tissue debris and cell clumps. Lung cells recovered from a healthy tumor-free mouse were used as gating control. 4T1-Luc⁺ mCherry⁺ tumor cells from pulmonary metastases were recovered based on gating with mCherry fluorescence. 50,000 mCherry⁺ singlets were analyzed per sample with a FACS Aria II /FlowJo software (BD Biosciences, San Jose, CA).

7.4 Recovery of Phage-Displayed Peptides from Metastatic Tumor Cells

The FACS sorted 4T1-Luc⁺ mCherry⁺ tumor cells recovered from pulmonary metastases were resuspended in growth media (DMEM with 10% FBS). The cell suspension was homogenized in 1mL glass douncers (Sigma Aldrich, St. Louis, MO) to rupture the cells and extravasate the internalized phage-displayed peptides. Following centrifugation at 14,000 rpm, the bound phage was eluted, and used to infect K91 *E. coli* host cells. Bacteriophage was isolated from K91 *E. coli* by polyethylene glycol (PEG) precipitation, amplified, purified, and resuspended in PBS as described previously (179). Through K91 *E. coli* infection, bacteriophage enumeration was performed using the double-layer agar technique in LB agar plates (20g/L LB Agar, 0.01g/L Tetracycline and 0.05g/L Kanamycin; Thermo Fisher Scientific).

7.5 Enrichment of Peptides in Rounds 2 and 3 of *In Vivo* Bio-panning

10¹⁰ TU of phage recovered from Round 1 of selection was used as input phage for the next round of *in vivo* selection and were recovered after 3 hours of circulation as described from Sections 7.1 to 7.4. Between each round, the foreign DNA inserts and encoded peptide sequences were determined for the top 10 most enriched phage clones to gauge the selection process and the absence of contamination, as described in Section 7.6. These phage-displayed peptide clones were bulk-amplified and subsequently pooled as described for the next round of *in vivo* selection (179). A total of three rounds of selection was performed.

7.6 PCR, DNA Sequencing and Insert Analysis

Following the final round of *in vivo* selection, the eluted phages were used to infect K91 *E. coli* host cells. The bacteriophage-infected K91 host cells were serially diluted in LB Broth (25g/L LB Broth, 0.01g/L Tetracycline, and 0.05g/L Kanamycin; Thermo Fisher Scientific). 1000-fold dilutions were plated using the double-layer agar technique in LB agar plates and incubated for 12 hours at 37 °C to form plaques. Individual clones were isolated using sterile toothpicks and stored in 50% glycerol (Fisher Scientific) stocks in a 96 well format for future amplification. The insert size of each phage clone was analyzed by PCR. Insertless Fd-Tet and D-WAT phages were used as negative and positive controls. The PCR reactions were carried out in a 10µL reaction volume containing a single colony of phage infected K91 *E. coli*, 5µL Azura 2X Taq Mix (Azura Genomics Inc., Raynham, MA), 2µL of the forward primer 5'-TTAACTCCCTGCAAGCCTCA-3' and 2µL of the reverse primer 5'-CCCTCATAGTTAGCGTAAGC-3' and 1µL PCR grade water (Thermo Fisher Scientific). The PCR reactions were performed using a Mastercycler Pro Thermal Cycler (Eppendorf, Hauppauge, MA) at the following conditions: 25 cycles of denaturation at 94°C for 10 seconds; annealing at 60°C for 30 seconds; and extension at 72°C for 60 seconds. The product size was assessed by 1.8% agarose gel electrophoresis in 1X TAE buffer (Tris-Acetate EDTA Buffer) at 80 volts for 40 minutes. PCR product clean up and DNA sequencing to ascertain the displayed foreign peptide of each phage was carried out by Epoch Life Sciences (Houston, TX). Sanger sequencing was done using the M13-pIII sequencing primer 5'-TTAACTCCCTGCAAGCCTCA-3'. The automated Sanger sequences were represented as chromatograms, analyzed using the Chromas software (Technelysium Pty Ltd, Queensland, Australia). The amino acid sequences of the fused peptide inserts were deduced from the DNA sequence using the ExPASy Bioinformatics Resource Portal (SIB, University of Lausanne,

Switzerland). Multiple sequence alignment of the selected phage-displayed BLMP clones from each round was performed using ClustalΩ (Omega) software (EMBL-EBI, Cambridgeshire, UK). The sequences were then analyzed by the BLAST algorithm (NLM, Bethesda, MD) for homology with known or putative cancer correlations, identify the presence of consensus motifs, and to define clones for further analyses.

8. *In Vitro* Phage-Displayed Peptide Homing Validation

8.1 Phage-Displayed Peptide Internalization Assay

The relative specificity of phage-displayed BLMP clones was assessed individually *in vitro*. Cells were grown to 60% confluency in a 24-well tissue culture plate (Costar, Fisher Scientific) overnight at 37°C in growth medium (DMEM with 10% FBS). The growth media was removed and a new medium (DMEM with 2% FBS) with either 10⁹ TU of BLMP clones or insertless phage separately and incubated at 37°C for 5 hours. Insertless Fd-Tet phage was used as a negative control. The adherent cells were washed thrice with 1X PBS solution, detached with 0.25% trypsin-EDTA, and resuspended in 2mL growth media (DMEM with 10% FBS). Cell count for each sample was determined individually using a hemocytometer. The internalized BLMP clones were recovered by rupturing the cell membranes using glass douncers. The individual phage-displayed BLMP clone samples were centrifuged at 14,000rpm for 5 minutes. The cell lysate of each sample containing the extravasated BLMP clones was used to infect K91 *E. coli*. The bacteriophage infected K91 host cells were serially diluted in LB Broth. 1000-fold dilutions were plated using the double-layer agar technique in LB agar plates and incubated for 12 hours at 37°C to form plaques. The homing specificity of each BLMP clone was quantified as a ratio of TU recovered to the total number of cells.

8.2 Phage-Displayed Peptide Internalization Validation by Immunofluorescence

Cells were grown to 60% confluency in a 24-well tissue culture plate (Costar, Fisher Scientific) overnight at 37°C in growth medium (DMEM with 10% FBS). The growth media was removed and 0.2L new medium (DMEM with 2% FBS) with either 10⁹ TU of BLMP clones or insertless phage separately and incubated at 37°C for 5 hours. Insertless Fd-Tet phage was used as a negative control. The adherent cells were washed thrice with 1X PBS solution to remove non-specific unbound phage. The cells and bound phage were fixed by the addition of 4% formaldehyde in PBS solution and blocked with a Serum-free protein block (Pierce, Thermo Fisher Scientific) for 1 hour at room temperature. The internalization of phage by the cells was probed by the addition of a rabbit polyclonal anti-Fd bacteriophage primary antibody (Sigma Aldrich; 1:500) incubated at 4 °C for 12 hours. The wells were extensively washed with TBS (PBS/0.05% Tween-20, Thermo Fisher Scientific) three times before being incubated with donkey anti-rabbit Cy3-conjugated (Jackson ImmunoResearch Laboratories, INC, West Grove, PA; 1:300) Secondary IgG for one hour in the dark at room temperature. Nuclei were stained with Hoechst 33258 (Invitrogen, Grand Island, NY). Fluorescence images were acquired with a Nikon Eclipse TE2000E Widefield Fluorescence Microscope (Nikon Instruments Inc, Melville, NY).

9. *In Vivo* Phage-Displayed Peptide Homing Validation

Individual phage-displayed BLMP clones were injected into vehicle and cisplatin-treated (2.5mg/kg) treated spontaneous and experimental metastasis murine models. The BLMP clones were allowed to circulate for three hours, after which the mice were anesthetized using tribromoethanol (150mg/kg) administered through intraperitoneal injections. Lung perfusion, organ resection, and subsequent fixation were performed as described in Sections 2, 3, and 5. The tissues harvested from the mice were embedded in paraffin. Slides with sections of formalin-fixed tissues and tumors embedded in paraffin were deparaffinized and rehydrated as described (180).

Antigen retrieval was performed by heating the slides in 10mM sodium citrate buffer (Pierce, Thermo Fisher Scientific) at 95°C for 20 minutes and slowly cooled to room temperature for another 20 minutes. The tissue sections were blocked with a Serum-free protein block solution and incubated at room temperature for 2 hours. Primary antibodies (4°C, 12–16 hours) and secondary antibodies (RT, 1 hour) were applied in TBS. The following primary antibodies were used: rabbit anti-Fd (Sigma-Aldrich; 1:500), goat anti-mouse CD31 (Santa Cruz Biotechnology, Santa Cruz, CA, 1:150), mouse anti-E Cadherin (BD Biosciences, San Jose, CA; 1:100), mouse anti-N Cadherin (BD Biosciences, San Jose, CA; 1:100) and mouse anti-Cytokeratin (MyBioSource, San Diego CA; 1:200). Secondary IgG used were as follows: donkey anti-mouse Alexa 488-conjugated (Invitrogen, 1:300) and donkey anti-rabbit Cy3-conjugated (Jackson ImmunoResearch Laboratories, INC; 1:300). Nuclei were stained with Hoechst 33258. Fluorescence images were acquired with a Nikon Eclipse TE2000E Widefield Fluorescence Microscope (Nikon Instruments Inc). Hematoxylin and eosin (H&E) staining was performed by histology CORE (IMM-UTH, Houston, TX). Images of H&E stained tissue sections were obtained with Zeiss Axio Scope Brightfield Microscope (Carl Zeiss Meditec, Inc., Dublin, CA).

10. Design and Synthesis of Hunter-Killer Peptides

All hunter-killer peptides were made as proteolysis-resistant “all D-amino acid” peptides. The apoptotic domain, a cationic amphipathic sequence (KLAKLAK)₂, was linked to the targeting domain via an amino hexanoic acid linker (NH-(CH₂)₅-CO). Peptides were synthesized by conventional peptide chemistry, cyclized via cysteines, purified to >90% by HPLC, and quality controlled (mass spectroscopy). Peptide instability and proteolytic cleavage *in vivo* were addressed via L-amino acid to D-amino acid sequence conversion accompanied by terminal N or C- terminus blockade. Lyophilized peptide acetate salt powder was reconstituted in PBS solution to a concentration of 10 mmol/L, and aliquots were stored at -20°C until dilution in

PBS, filtration, and use. The following hunter-killer peptides were designed and purchased from Celtek Bioscience (Franklin, TN):

1. HK-BLMP7: Composed of breast lung metastasis (BLM) homing peptide BLMP7 (sequence: CLRHSSKIC) conjugated to apoptotic (KLAKLAK)₂ domain.
2. HK-BLMP8: Composed of BLM-homing peptide BLMP8 (sequence: CRAGVGRGC) conjugated to apoptotic (KLAKLAK)₂ domain.

The following peptides were designed and purchased from Ambipharm (North Augusta, SC):

1. D-CAN: Composed of Adipose stromal cell (ASC) homing peptide WAT7 (sequence: CSWKYWFGEC) conjugated to apoptotic (KLAKLAK)₂ domain.
2. (KLAKLAK)₂: Composed of uncoupled lytic amphipathic sequence (KLAKLAKKLAKLAK).

11. Biotin-labeled HK-BLMP Internalization Assay *In Vitro*

HK-BLMP7 and HK-BLMP8 peptides were labeled with biotin using the Sulfo-NHS-LC-Biotin Kit (APExBIO, Houston, TX) according to the manufacturer's guidelines. Cells were cultured as specified above and incubated with biotin-labeled HK-BLMP7 (30 μmoles/L) or HK-BLMP8 (20 μmoles/L) peptides for 5 hours at 37°C. The adherent cells were fixed and blocked, as described in Section 8.2. The internalization of the biotin-labeled peptide by the cells was probed by the addition of Streptavidin-Cy3 (Zymed, Thermo Fisher Scientific; 1:50) for one hour in the dark at room temperature. Nuclei were stained, and fluorescence images were acquired as described in Section 8.2.

12. *In Vitro* Assay for Cell Viability

Cells were grown to 60% confluency in 48-well tissue culture plates (Costar, Fisher Scientific) overnight at 37°C in growth medium (DMEM with 10% FBS). HK-BLMP7, HK-BLMP8, D-CAN, or uncoupled (KLAKLAK)₂ was added to each well. Peptide concentrations ranging from 1 to 300 µmoles/L were added to 0.2 mL serum-free media in each of the wells and incubated for at 37°C for 8 -24 hours. Trypan blue exclusion assay and the cleaved-caspase3 assay was used to determine cell viability in peptide-treated cell lines.

12.1 Validation of Cell Viability by Trypan-Blue Staining

Following hunter-killer peptide treatment, live and dead cells were distinguished by staining with 0.4% Trypan Blue solution (MP Biomedicals, Santa Ana, CA) for 10 minutes. The solution was slowly decanted and replaced with 4% formaldehyde in PBS solution to fix the cells. The cells were imaged and analyzed with a Nikon Eclipse TE2000E Widefield Fluorescence Microscope (Nikon Instruments Inc.).

12.2 Validation of Apoptosis induction by Cleaved-Caspase 3 Staining

Following hunter-killer peptide treatment, cells were fixed and blocked, as described in Section 8.2. Cell viability was probed by the addition of primary antibody: anti-Asp175-cleaved Caspase3 (Cell Signaling Technology, Beverly, MA; 1:100) incubated at 4 °C for 12 hours. Secondary donkey anti-rabbit Cy3-conjugated (Jackson ImmunoResearch Laboratories. INC; 1:300) (Invitrogen; 1:150) for one hour in the dark at room temperature. Nuclei were stained, and fluorescence images were acquired as described in Section 8.2.

13. *In Vivo* Metastasis Ablation Study with HK-BLMP8

Female Balb/c mice (stock 000651, Jackson) were ten weeks old at the start of the experiment. The mice were implanted with 4T1 breast tumors, as described in Section 3.3. Once the tumors were palpable, the mice were split into two cohorts (n=5). Mice in each cohort were administered twelve doses of either vehicle (1X PBS) or HK-BLMP8 peptide (10mg/kg) subcutaneously into the lower back over a period of 4 weeks. During this period, the mice were periodically monitored and subjected to weekly BLI to monitor and image metastatic progression. Upon reaching morbidity, the animals were then euthanized.

14. Statistical Analysis

Statistical analysis was carried out using GraphPad Prism 8 software (GraphPad, La Jolla, California). Multiple row t-tests were used to compare changes in tumor volume between vehicle control, cisplatin-treated, and hunter-killer peptide treated mice. Two-way Anova was used to compare the binding efficiency of the six BLMP clones across different cell lines. The Log-rank (Mantel-Cox) test was used to compare the survival probability between vehicle control and hunter-killer peptide treated mice. Data were represented as Mean \pm SEM.

Chapter 4: Results

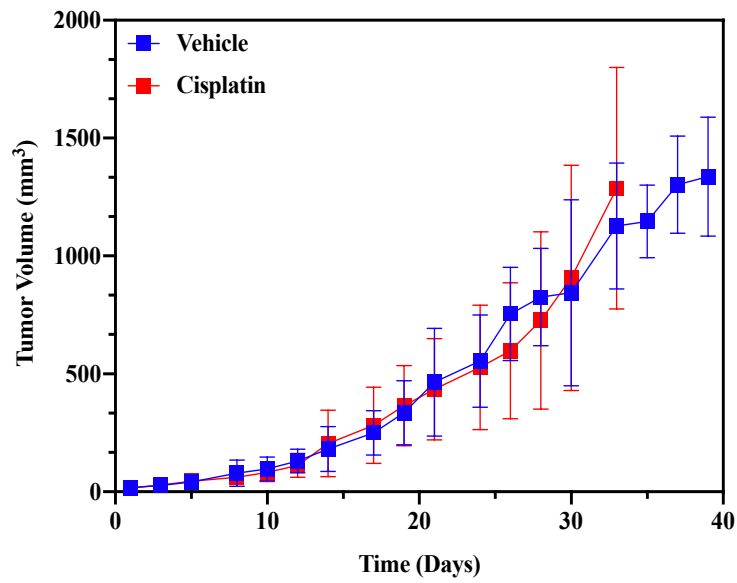
1. Cisplatin treatment elicits no tumor response but exacerbates metastatic burden

In order to conduct the *in vivo* phage-displayed peptide library screen for chemoresistant TNBC pulmonary metastases, the 4T1 orthotopic syngeneic murine model was selected. This *in vivo* model of spontaneous metastasis has been well characterized and has been used in several studies for the elucidation of the mechanisms implicated in chemoresistance evolution and subsequent metastatic progression (181-184). Dual-luciferase and mCherry labeled 4T1 adenocarcinoma cells obtained from Dr. Sendurai Mani's lab, were orthotopically implanted into the mammary fat pad of Balb/c mice. Once the tumors reached a volume of 200mm³, the mice were randomized into two groups (n=20/cohort) and treated with vehicle control or 2.5mg/kg cisplatin retro-orbitally for three weeks. The tumor volumes were measured thrice a week until the mice attained morbidity. Further, metastatic progression was measured weekly using non-invasive bioluminescence imaging until the mice succumbed to metastasis-induced mortality.

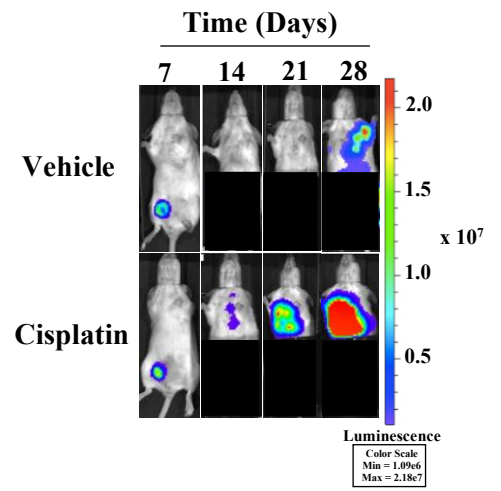
Based on Welch's t-test analysis, no significant difference ($p=0.5735$) in tumor volumes was observed between the two groups during the treatment period (Figure. 1A). These observations were sustained even upon treatment completion (Figure. 1A). These results suggest that cisplatin administration had no effect on primary tumor growth. However, upon analysis of non-invasive bioluminescence images of the mice, a significant difference in metastatic burden was indicated between the groups (Figure. 1B). In the cisplatin-treated mouse cohort, cancer progression and subsequent pulmonary metastatic burden were significantly higher when compared to the vehicle-treated mouse cohort (Figure. 1B). These observations were further corroborated through pulmonary metastases nodule quantification. At the experimental endpoint, mice were euthanized, and their lungs subjected to PBS perfusion. The lungs were then fixed in formalin until the metastatic nodules were bleached to amelanotic gray/white nodules (Figure. 1C). This was followed by a blind enumeration of metastatic lung nodules of both mice cohorts. The cisplatin-treated mice demonstrated a significantly higher ($p \leq 0.01$) pulmonary

metastatic nodule burden when compared to the vehicle control group (Figure. 1D). Together, these data suggest that cisplatin administration elicits no primary tumor response but does exacerbate cancer progression and metastatic burden (Figure. 1).

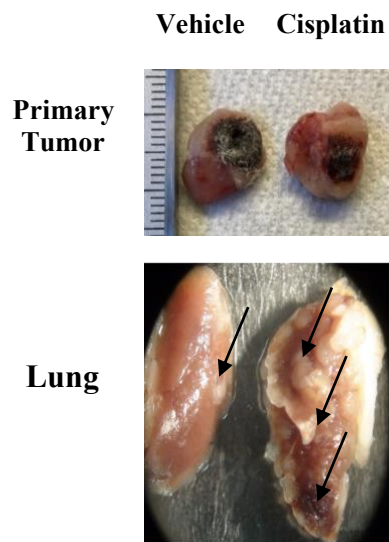
A



B



C



D

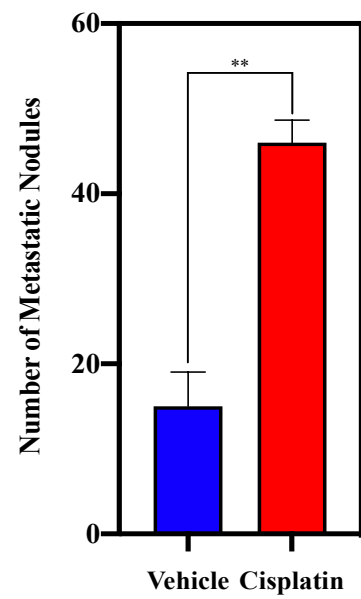


Figure. 4: Cisplatin treatment elicits no tumor response but exacerbates metastatic burden

- A. Primary Tumor growth curves for vehicle versus cisplatin treated cohorts (n = 20/cohort).
Vehicle and cisplatin (2.5mg/kg) were administered retro-orbitally weekly, for three weeks.
Tumor volumes were calculated using the formula : length x (width)² x 0.52. Tumor volumes are shown as mean ± SEM.
- B. Non-invasive bioluminescence imaging to monitor metastatic progression. The luciferase signal and luminescence were assessed in vehicle and cisplatin-treated cohorts respectively.
- C. Quantification of metastatic nodules of vehicle and cisplatin treated mice cohorts (n = 5 /cohort) at experimental endpoint (**, p ≤0.01). Metastatic nodule number shown as mean ± SEM.
- D. Representative images of primary tumors and lung metastases in vehicle and cisplatin-treated cohorts.

2. A screen for phage-displayed breast lung metastasis homing peptides

In order to isolate peptides specifically homing to chemoresistant breast lung metastases (BLM), the *in vivo* phage display methodology was adopted to investigate the interactions between phage-peptides mimicking the ligands of novel receptors expressed preferentially on the tissues or organs of interest (140, 142, 185). *In vivo* phage display screening was performed in the 4T1 chemoresistant spontaneous TNBC metastasis model described above (Figure. 4). This model was chosen because it supports the basis of our hypothesis that upon chemoresistance evolution, mammary tumor cells acquire an aggressive phenotype that promotes metastatic progression and malignancy-associated morbidity (181, 182).

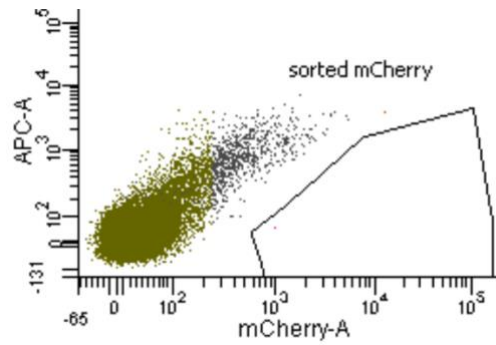
In vivo phage display bio-panning was combined with the isolation of metastatic tumor cells by fluorescence-activated cell sorting (FACS) from BLM cell suspensions. We focused on the isolation of phage-peptides that specifically bound to the mCherry positive cell sub-population of BLM from the lung (Figure. 5A). Prior to *in vivo* phage-peptide bio-panning, insertless Fd-Tet phage was intravenously injected into the mouse model for non-specific phage-peptide binding normalization. Three rounds of *in vivo* bio-panning were performed. At the start of the first round, a mixture of cyclic CX₇C and CX₈C (C: disulfide-bonded cysteines; X: any amino acid) random phage-peptide libraries were injected into the chemoresistant 4T1 spontaneous metastasis model. This approach enabled the selection of pulmonary TNBC metastasis homing phage-peptide probes from a pool of over 10¹⁰ combinatorial peptides displayed as a fusion on the pIII protein of filamentous M13 bacteriophage.

For every round, the output of the previous round was quantified, amplified, pooled, and used as the input of the subsequent rounds. Following each round of bio-panning, the phage-peptides recovered from the FACS-sorted mCherry positive and mCherry negative cell sub-populations were individually tittered using K91 *E.coli* bacterial host cells (Figure. 5B). Only

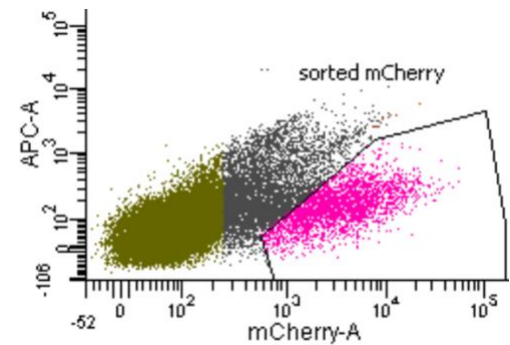
those *E.coli* cells infected with phage formed plaques on double-layered tetracycline rich LB agar plates (Figure. 5B). After titration, the phage binding efficiency was calculated by dividing the phage TU by the number of FACS sorted cells. The relative specificity of phage-displayed peptides binding to mCherry positive tumor cell populations was compared to that of the mCherry negative host cell population. In Rounds 2 and 3, a significant enrichment ($p \leq 0.001$) in the number of phage-peptides homing to mCherry positive metastatic cell populations was observed (Figure. 5C).

A

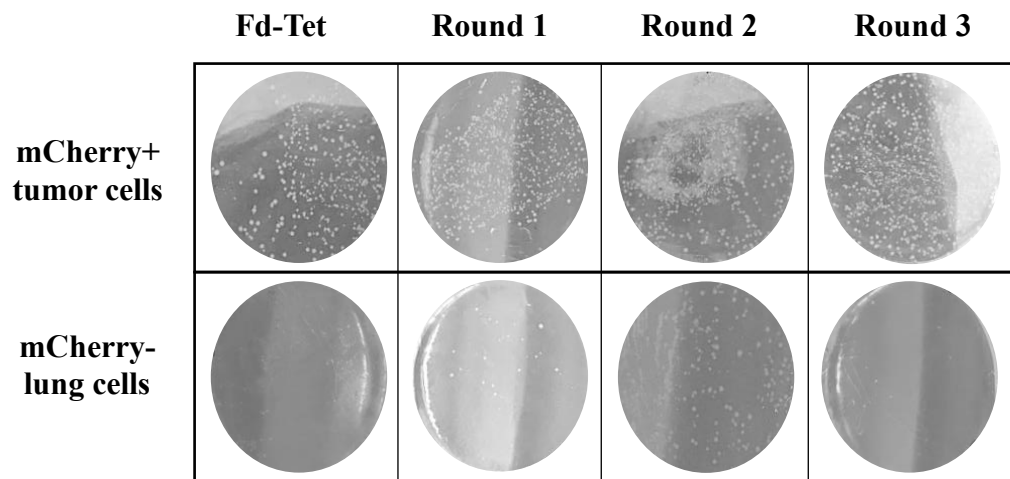
Negative Control – Healthy Lung



Lung with 4T1 Pulmonary Metastases



B



C

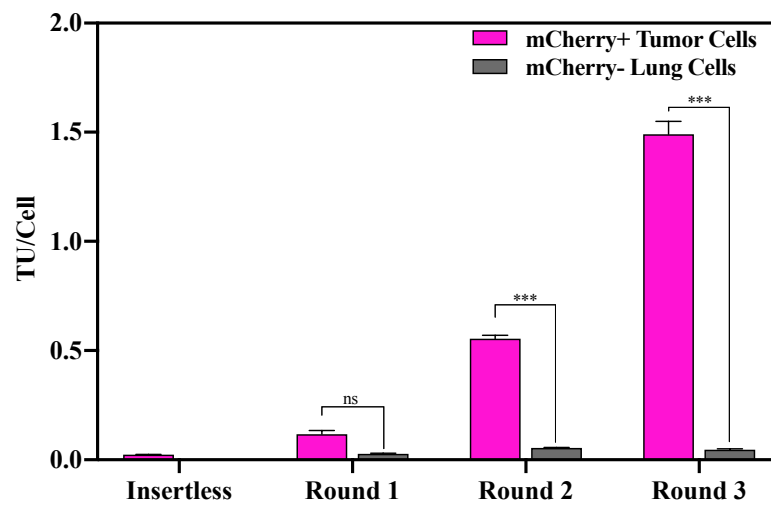


Figure. 5: An *in vivo* phage-displayed peptide library screen for peptides homing to cisplatin resistant metastatic tumor cells

- A. FACS analysis of mouse lung tissue samples. Tumor cells from pulmonary metastases were recovered based on mCherry fluorescence gating. Pulmonary cells recovered from healthy tumor-free mice used as gating control.
- B. Comparison of phage infected *E.coli* plaque density between mCherry positive tumor cells from pulmonary metastases and mCherry negative host lung cells over three rounds of *in vivo* phage-displayed peptide library bio-panning. Fd-Tet: Insertless control phage used for normalization.
- C. Phage-displayed peptides bound to metastatic mCherry positive tumor cells, in parallel with phage-displayed peptides bound to host lung cells, were quantified, amplified, pooled, and used for subsequent rounds of bio-panning. Increased recovery of phage transforming units (TU) in successive rounds reflects the enrichment of phage-displayed peptides homing to the metastatic mCherry positive tumor cells. Shown are mean \pm SEM for duplicate measurements. Two-way ANOVA indicates statistically significant differences within mCherry positive and mCherry negative groups assessed by Sidak's multiple comparisons test and is denoted as: ***, $p \leq 0.001$ and ns: non-significant ($p > 0.05$).

3. Nine novel breast lung metastasis homing phage-peptides were identified through *in vivo* screening of chemoresistant TNBC pulmonary metastases

After three rounds of synchronous *in vivo* bio-panning, nine CX7C phage-peptide clones were repeatedly recovered from chemoresistant mCherry positive metastatic tumor cells with a frequency above 1%. These phage-displayed peptides were termed breast lung metastasis peptides (BLMP), BLMP0 through BLMP8 (Figure. 6A). The homing specificity of each clone was assessed by quantifying the frequency of phage coding for each peptide. Each BLMP clone demonstrated a significant enrichment ($p \leq 0.001$) between Rounds 2 and 3 of *in vivo* phage bio-panning (Figure. 6A). BLMP7 stood out owing to its marked capacity to home to chemoresistant BLM. BLMP7 represented 59.21% of the recovered clones in Round 3. BLMP5, BLMP0, and BLMP4 were the next most enriched BLMP clones with a frequency of 8.69%, 6.67%, and 6.58%, respectively (Figure. 6A). Although BLMP1, BLMP2, and BLMP3 had relatively high homing frequency in Round 2, they were absent in Round 3 (Figure. 6A). Thus, these three BLMP clones were excluded from further analysis.

BLMP0, BLMP4, BLMP5, BLMP6, BLMP7, and BLMP8 were individually amplified in K91 E.coli. PCR was performed on the bacteriophage infected E.coli to amplify the fragment containing BLMP inserts. The products were analyzed by agarose gel electrophoresis. All BLMP clones had a 34 bp-sized insert, unlike insertless Fd-Tet phage (Figure. 6B). Individual BLMP clones were then characterized by DNA sequencing. The amino acid sequences of the BLMPs were computed from their cognate DNA sequences using the ExPASy bioinformatics portal. The amino acid sequences and the overall charge of each BLMP clone were summarized (Figure. 6C). The net charge of each clone was calculated as the total of the charge of each amino acid present in the BLMP sequence. The insert CLRHSSKIC constituted over 60% of the clones identified by the screen (Figure. 6C).

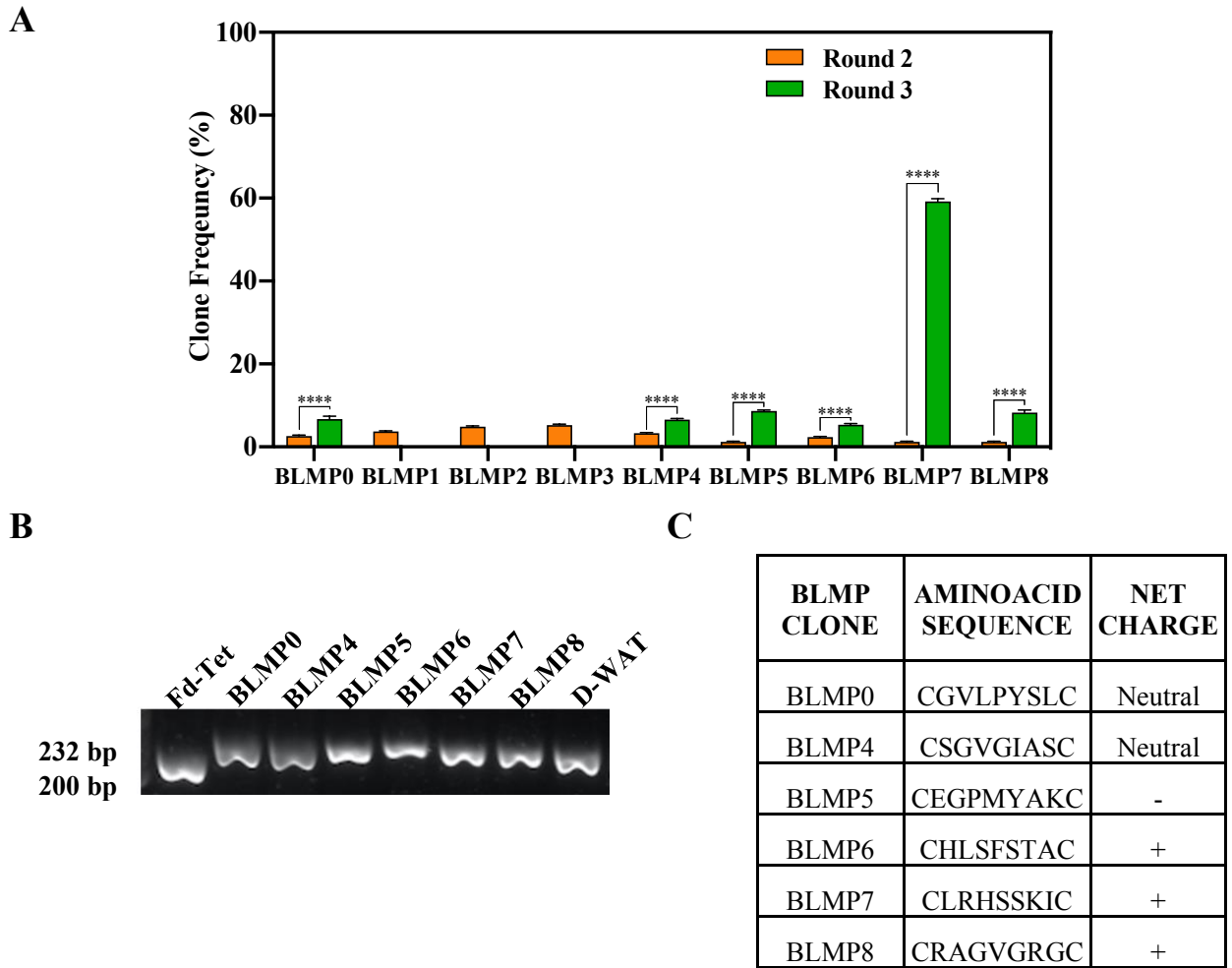


Figure. 6: Summary of top BLMP clones enriched over three rounds of *in vivo* phage-displayed peptide library bio-panning

- A. Assessment of individual BLMP clone frequencies over Round 2 and Round 3 of *in vivo* phage displayed peptide library bio-panning. Shown are mean \pm SEM for triplicate measurements. Two-way ANOVA indicates statistically significant differences within Rounds 2 and 3 by Sidak's multiple comparisons test and is denoted as: ***, $p \leq 0.001$ and ****, $p \leq 0.0001$.
- B. Analysis of PCR product size of individual BLMP clones by DNA agarose electrophoresis. Fd-Tet : Insertless control cphage. D-WAT: positive control phage.
- C. Summary of the individual BLMP clone characteristics.

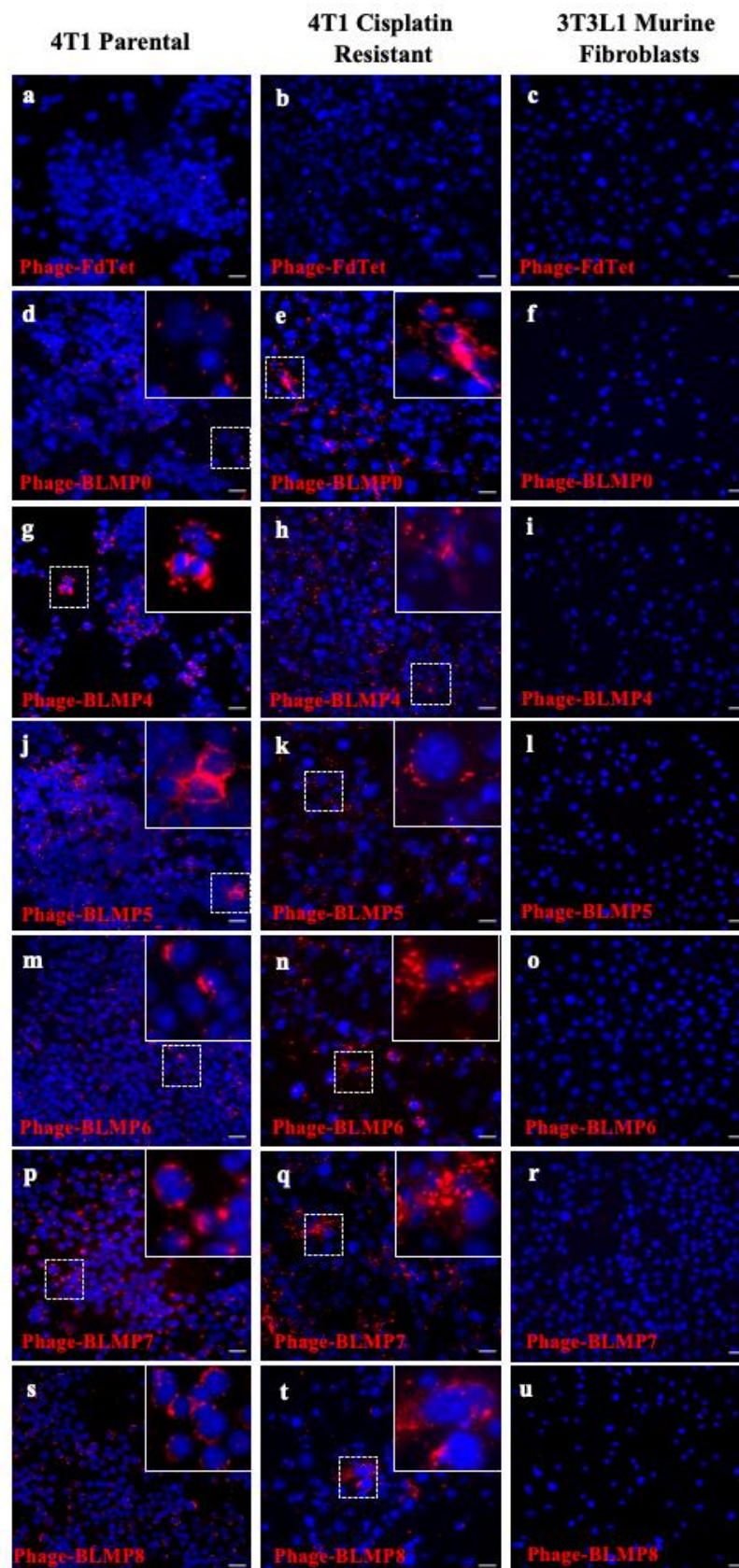
4. All BLMP clones bind specifically to murine cancer cell lines *in vitro*

The tropism of BLMP clones for TNBC cell lines was further validated through an *in vitro* immunofluorescence assay. This assay was performed using a specific antibody against M13 filamentous phage. Phage particles displaying the selected BLMP inserts were incubated with murine parental and cisplatin-resistant 4T1.2 adenocarcinoma cells and 3T3L1 murine fibroblasts overnight. Wild-type insertless Fd-Tet phage was used as negative phage control. The assay results demonstrated a pronounced red fluorescence signal for all BLMP clones in both 4T1 parental and 4T1 cisplatin-resistant TNBC cell lines. Further, no BLMP clone binding (red) was observed in murine 3T3L1 fibroblasts. These observations suggest that the BLMP clones, home specifically to only TNBC cell lines. However, no significant difference in binding capacity was observed between the 4T1 parental and cisplatin-resistant cell lines (Figure. 7A).

The relative specificity of individual BLMP clones to TNBC cancer cell lines was further probed through an internalization assay. Phage particles displaying the selected BLMP inserts were incubated overnight with the cell lines described above. Additionally, murine melanoma B16F10 cell lines were used to evaluate the possible existence of BLMP clone cross-reactivity in different murine cancer models. Upon incubation, the BLMP clones binding to each cell line were recovered, pooled, and quantified through titration against K91 *E.coli* bacteria. BLMP binding efficiency was reported as a ratio of phage TU recovered and cell count (Figure. 7B). Compared to 3T3L1 negative control, all BLMP clones except BLMP5 and BLMP6 showed significant binding efficiency ($p \leq 0.0001$) to all murine cancer cell lines. Hence, BLMP5 and BLMP6 were excluded from further analysis (Figure. 7B). BLMP4 and BLMP7 stood out owing to the significant difference ($p \leq 0.01$) in binding capacity between parental and cisplatin-resistant 4T1.2 adenocarcinoma cells. BLMP8 stood out owing to its significantly higher ($p \leq 0.0001$) binding efficiency to murine B16F10 cells (Figure. 7B).

A

Phage-displayed Breast Lung Metastasis Peptide (BLMP)



B

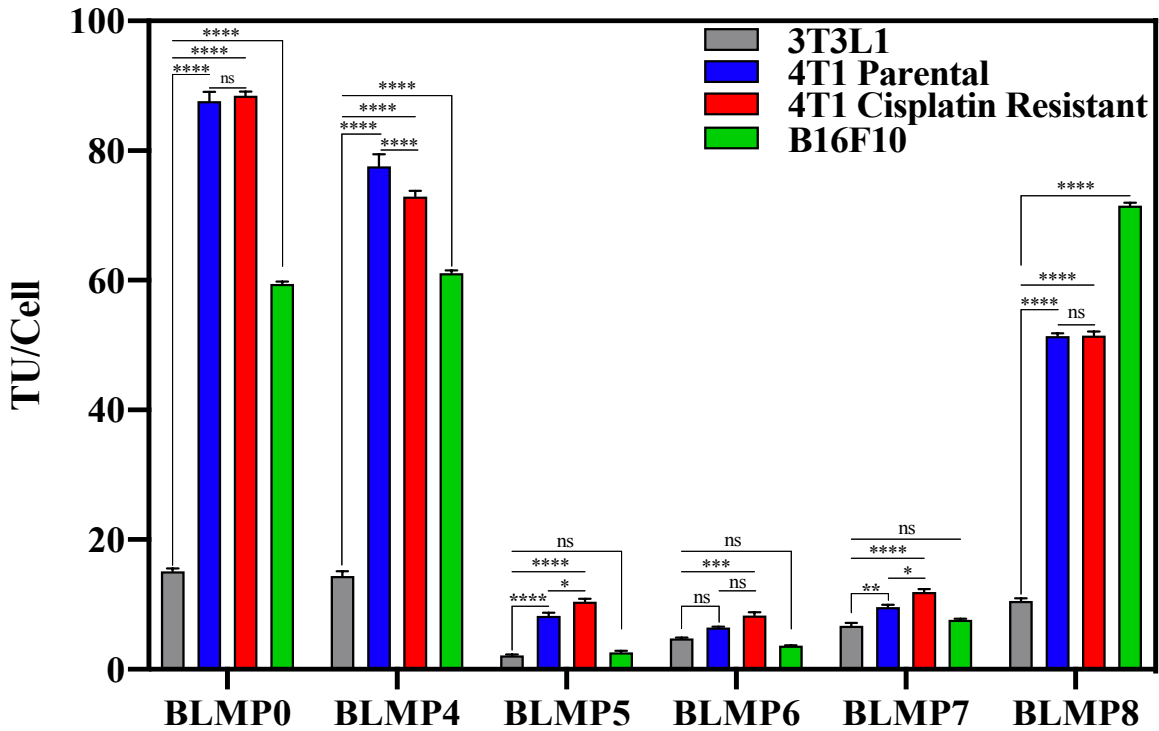


Figure. 7: Validation of phage-displayed BLMP clone specificity to cancer cells *in vitro*

- A. Anti-phage (Cy3) immunofluorescence in parental and cisplatin-resistant murine 4T1.2 adenocarcinoma and 3T3L1 fibroblast cell lines incubated with phage-displayed BLMP clones overnight. Red (anti-phage) immunofluorescence signal upon digital channel merging indicates localization of BLMP clones on 4T1 parental and cisplatin-resistant cell lines but not on 3T3L1 murine fibroblasts. Fd-Tet: Insertless control phage. Nuclear DAPI staining is blue. Scale bar: 50 μ m.
- B. Assessment of individual phage-displayed BLMP clones homing for parental and cisplatin-resistant murine 4T1.2, murine B16F10 melanoma and murine 3T3L1 fibroblast cell lines. Cells were incubated with phage-displayed BLMP clones overnight. Relative specificity of phage homing was calculated as a ratio of TU recovered and cell count. Shown are mean \pm SEM for triplicate measurements. Two-way ANOVA indicates statistically significant

differences assessed by Sidak's multiple comparisons test. *, $p \leq 0.01$; ***, $p \leq 0.001$ and ****, $p \leq 0.0001$ indicates comparison between 3T3L1 negative control and cancer cell lines for the same peptide. ***, $p \leq 0.001$ and ****, $p \leq 0.0001$ indicates comparison between parental and cisplatin-treated murine 4T1.2 adenocarcinoma cell lines for the same peptide. ns: non-significant ($p > 0.05$).

5. Both BLMP7 and BLMP8 demonstrate pulmonary metastases-specific tropism in a spontaneous TNBC metastasis model

The tropism of BLMP clones to pulmonary metastases was explored in the 4T1 adenocarcinoma spontaneous metastasis model. Phage particles bearing the BLMP inserts were intravenously injected into vehicle and cisplatin-treated mice (n = 5/cohort). Following the systemic circulation of phage for 3 hours, the mice were euthanized. Their organs (lung, primary tumor, kidney, pancreas, liver, and brain) were resected and subsequently formalin-fixed for future analysis. Immunofluorescence assay was performed in formalin-fixed paraffin-embedded organ sections of mice from both vehicle and cisplatin-treated cohorts. The assay was performed using a specific antibody against M13 filamentous phage.

In the vehicle-treated 4T1 mouse model, BLMP7 with CLRHSSKIC motif demonstrated localization (red) to the indicated areas of pulmonary metastases and liver. In contrast, the primary tumor and other control organs (pancreas, kidney, and brain) showed no BLMP7 (red) localization (Figure. 8A). Similar results were observed in the cisplatin-treated 4T1 mouse model, with additional non-specific BLMP7 (red) trapping in the kidneys and livers of cisplatin-treated mice (Figure. 8B). These results suggest that BLMP7 homes specifically to only TNBC pulmonary metastases regardless of chemotherapy administration.

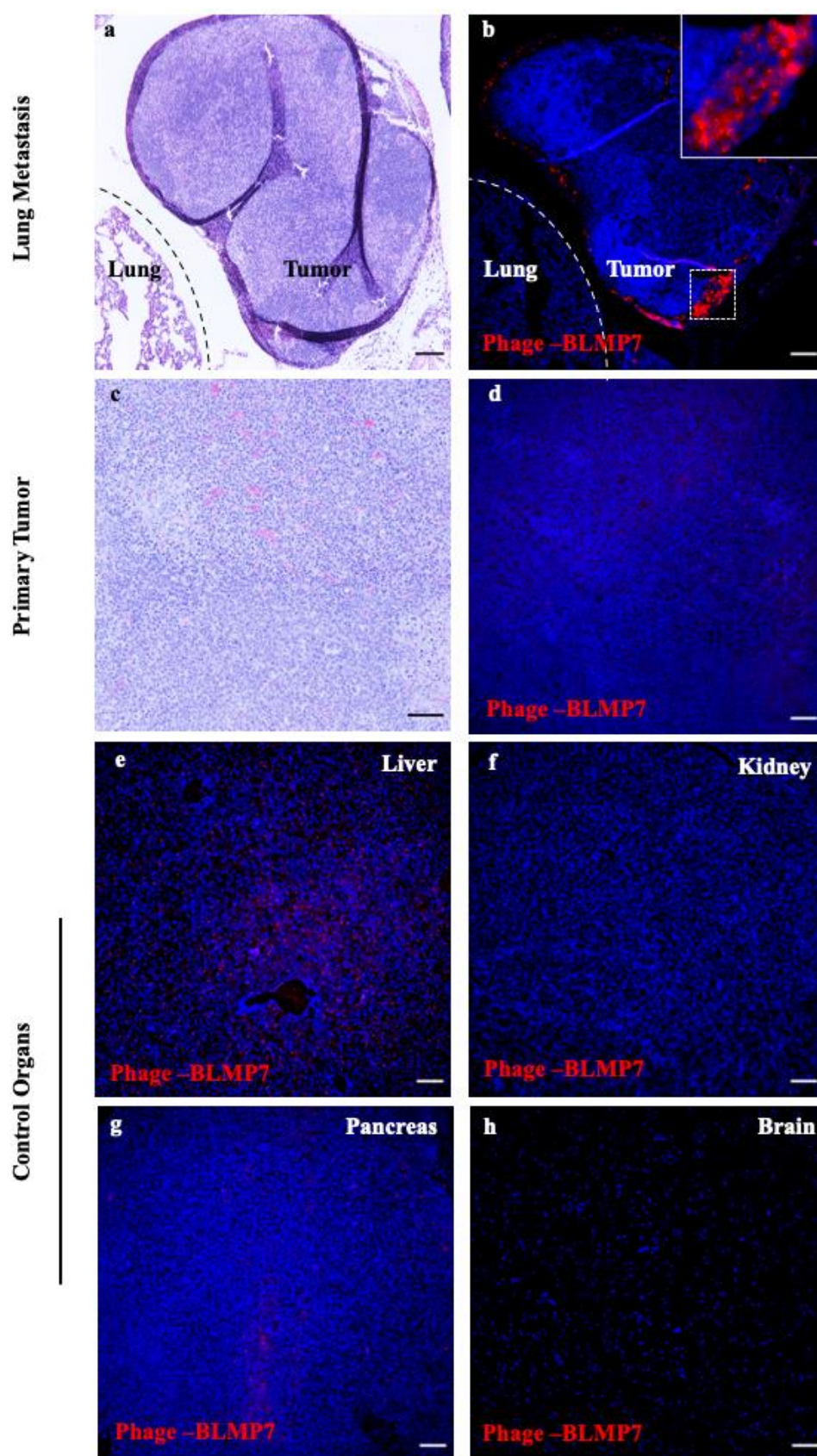
Interestingly, in addition to pulmonary metastases homing, BLMP8 with CRAGVGRGC motif, demonstrated localization (red) in the primary tumor as well. However, BLMP8 did not localize to other control organs (pancreas and brain). These observations were noticed in both vehicle (Figure. 8C) and cisplatin-treated (Figure. 8D) 4T1 mouse models. In the cisplatin-treated cohort, additional non-specific BLMP8 (red) trapping in the kidneys and liver were noted (Figure. 8D). These results suggest that BLMP8 homes not only to the spontaneous pulmonary metastases but also to the original localized TNBC primary tumors. As observed for BLMP7, BLMP8 homing was independent of chemotherapy administration.

Upon closer analysis of BLMP7 and BLMP8 homing in the indicated areas of pulmonary metastases, it was noted that the phage-displayed peptides (red) consistently localized along the invasive edges of the macro-metastases (Figures. 8 A-D). Distribution of the phage to tumor cells with metastases was further probed through immunofluorescence assay with an antibody against Cytokeratin 14 (Basal TNBC marker). In the 4T1 spontaneous metastasis model, no co-localization of phage with Cytokeratin 14 was observed (data not shown).

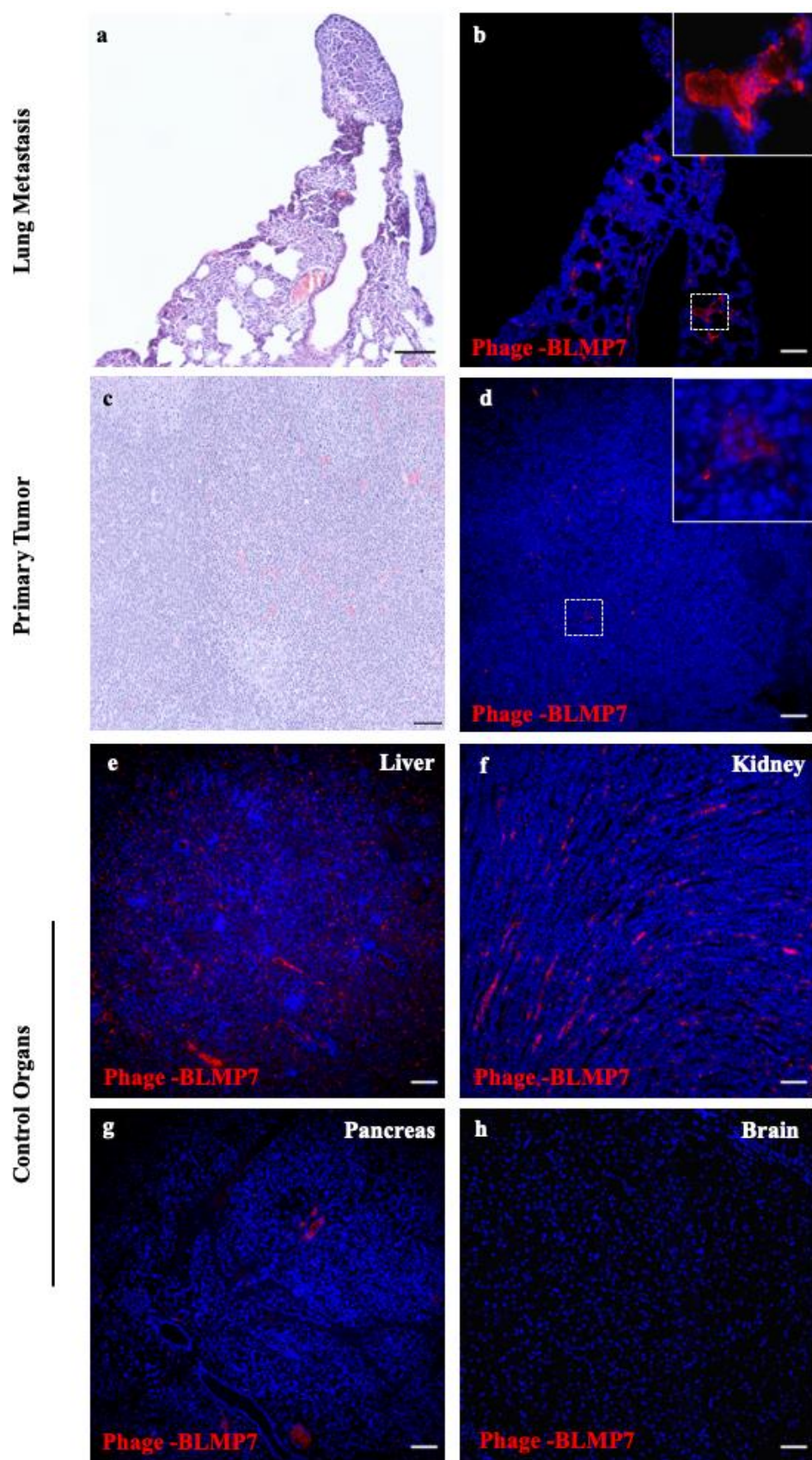
The pulmonary metastases-specific tropism demonstrated by both BLMP7 and BLMP8 clones was further corroborated in healthy metastasis-free mice. C57BL/6 mice (n=4) were intravenously injected with either BLMP 7 or BLMP8. The organs of the mice were processed as described above. Neither BLMP7 nor BLMP8 homed to lung tissue or control organs (pancreas, kidney, and brain) of healthy mice (Figures. 9A and 9B).

BLMP0 and BLMP4 clones were also administered intravenously into vehicle and cisplatin-treated mice. Contrary to *in vitro* BLMP clone homing data discussed above (Figure. 7), neither BLMP0 nor BLMP4 homed to TNBC pulmonary metastases or primary tumors (data not shown). Thus, both BLMP0 and BLMP4 were excluded from future analysis.

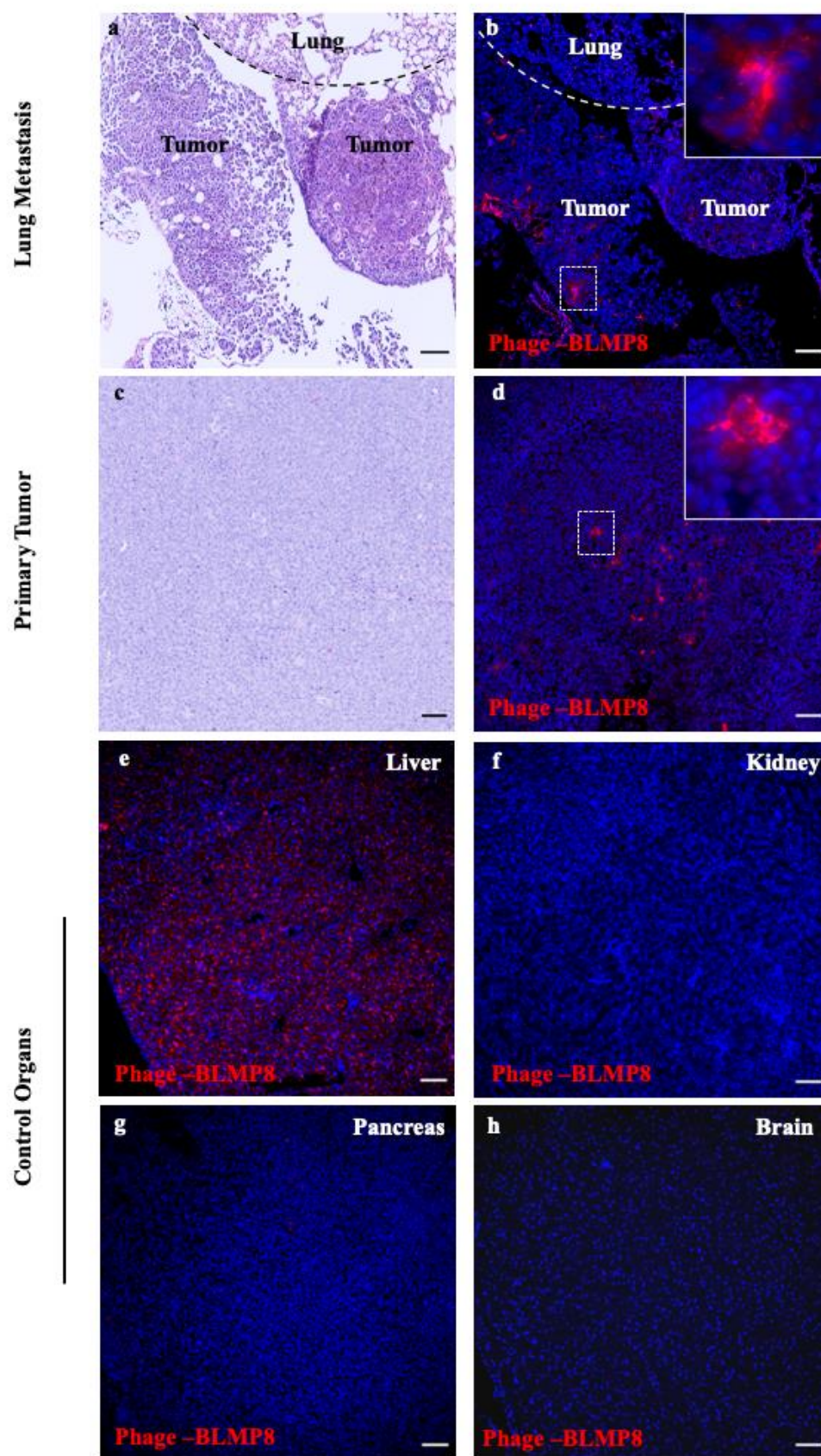
A



B



C



D

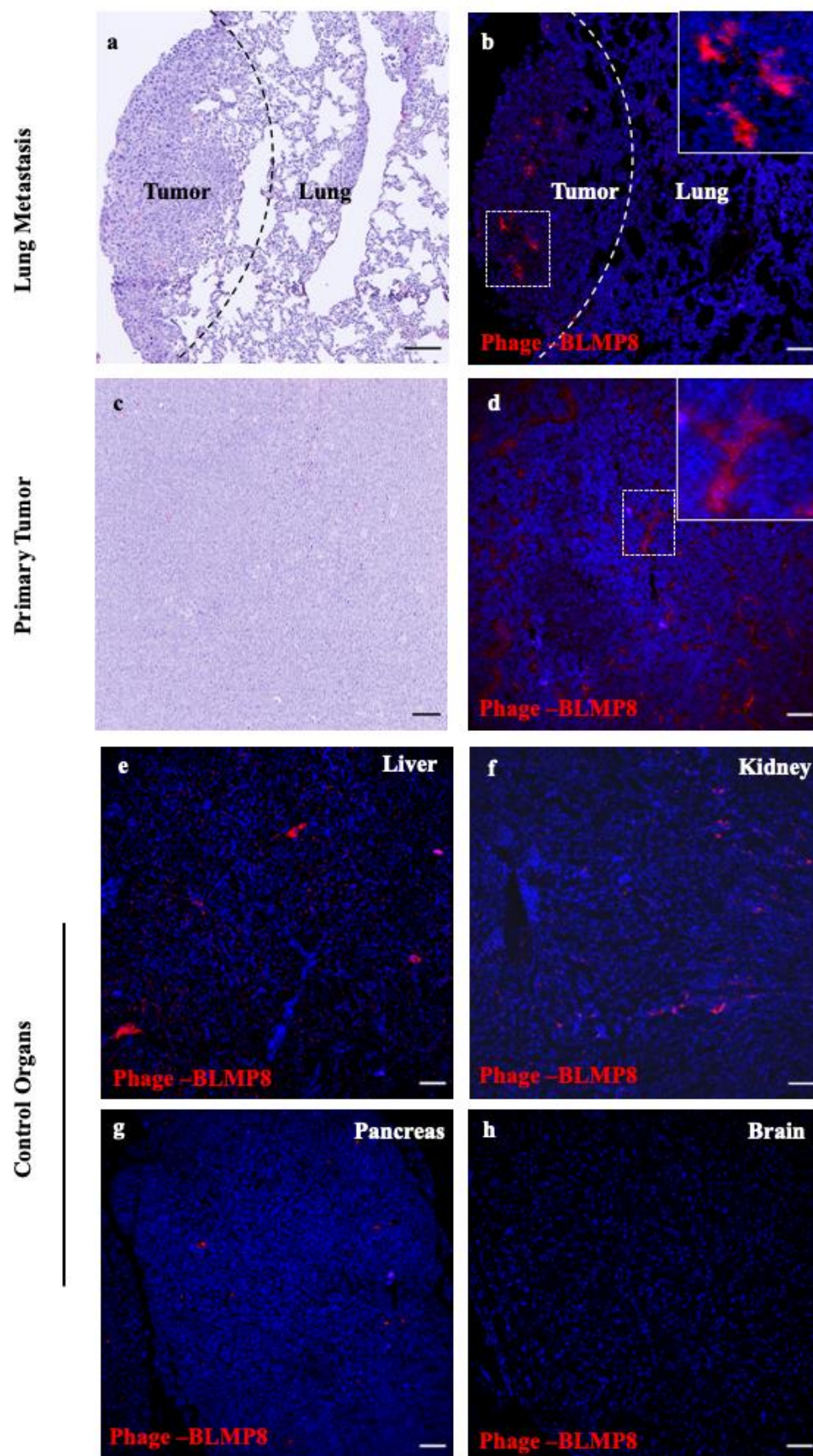
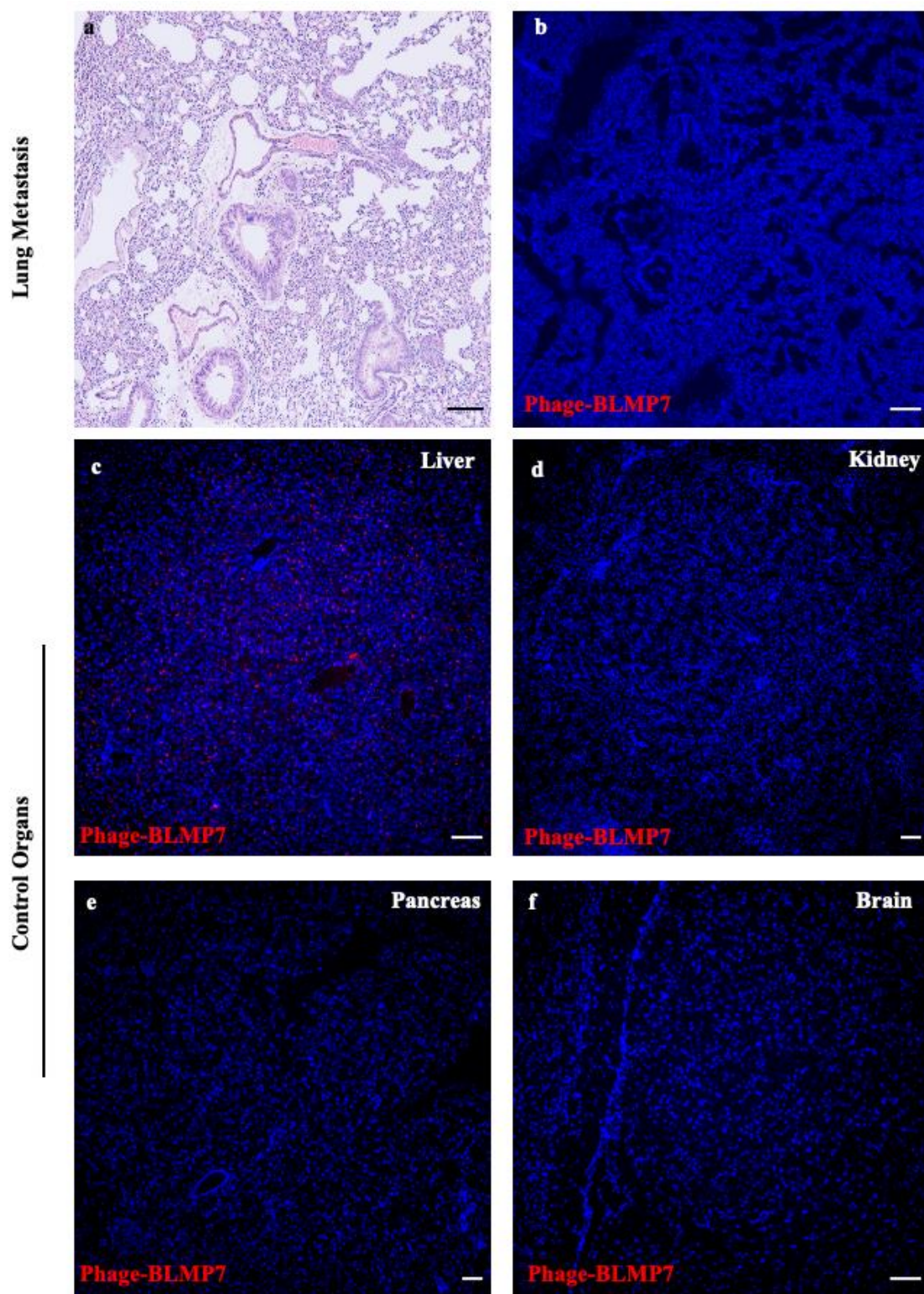


Figure. 8: BLMP7 and BLMP8 home to pulmonary metastases in the 4T1 TNBC mouse model

- A. Anti-phage (Cy3) immunofluorescence in serial paraffin sections of formalin-fixed organs of vehicle-treated mice intravenously injected with BLMP7. Red (anti-phage) signal upon digital channel merging indicates localization of BLMP7 in the indicated areas of pulmonary metastases (b), and liver (e), but not in primary tumor (d), kidney (f), pancreas (g), and brain (h). Nuclear DAPI staining is blue. Scale bar: 100 μ m.
- B. Anti-phage (Cy3) immunofluorescence in serial paraffin sections of formalin-fixed organs of cisplatin-treated mice intravenously injected with BLMP7. Red (anti-phage) signal upon digital channel merging indicates localization of BLMP7 in the indicated areas of pulmonary metastases (b), liver (e), and kidney (f), but not in primary tumor (d), pancreas (g), and brain (h). Nuclear DAPI staining is blue. Scale bar: 100 μ m.
- C. Anti-phage (Cy3) immunofluorescence in serial paraffin sections of formalin-fixed organs of vehicle-treated mice intravenously injected with BLMP8. Red (anti-phage) signal upon digital channel merging indicates localization of BLMP8 in the indicated areas of pulmonary metastases (b), primary tumor (d), and liver (e), but not in kidney (f), pancreas (g), and brain (h). Nuclear DAPI staining is blue. Scale bar: 100 μ m.
- D. Anti-phage (Cy3) immunofluorescence in serial paraffin sections of formalin-fixed organs of cisplatin-treated mice intravenously injected with BLMP8. Red (anti-phage) upon digital channel merging indicates localization of BLMP8 in the indicated areas of pulmonary metastases (b), liver (e), and kidney (f), and primary tumor (d), but not in pancreas (g), and brain (h). Nuclear DAPI staining is blue. Scale bar: 100 μ m.

A



B

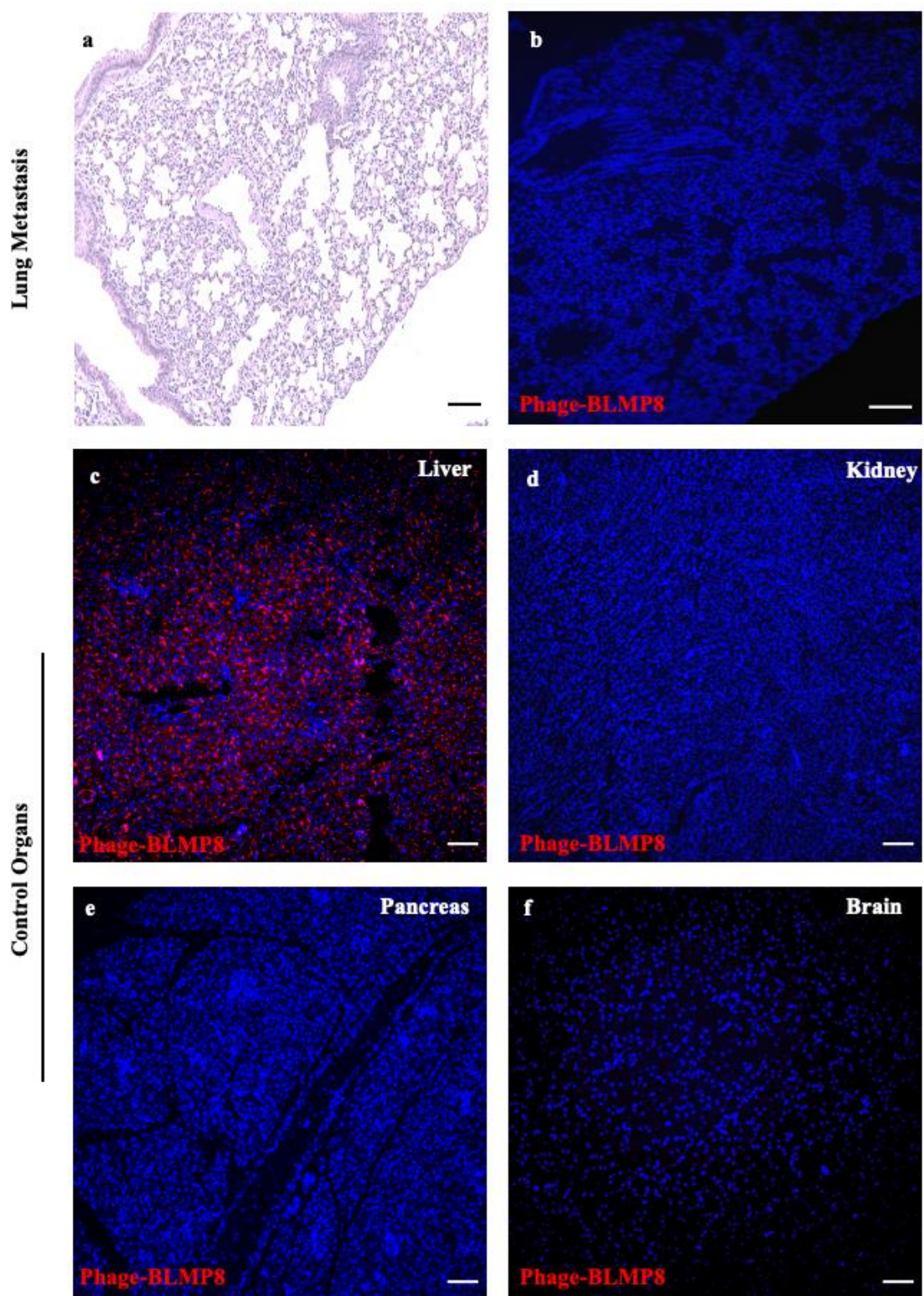


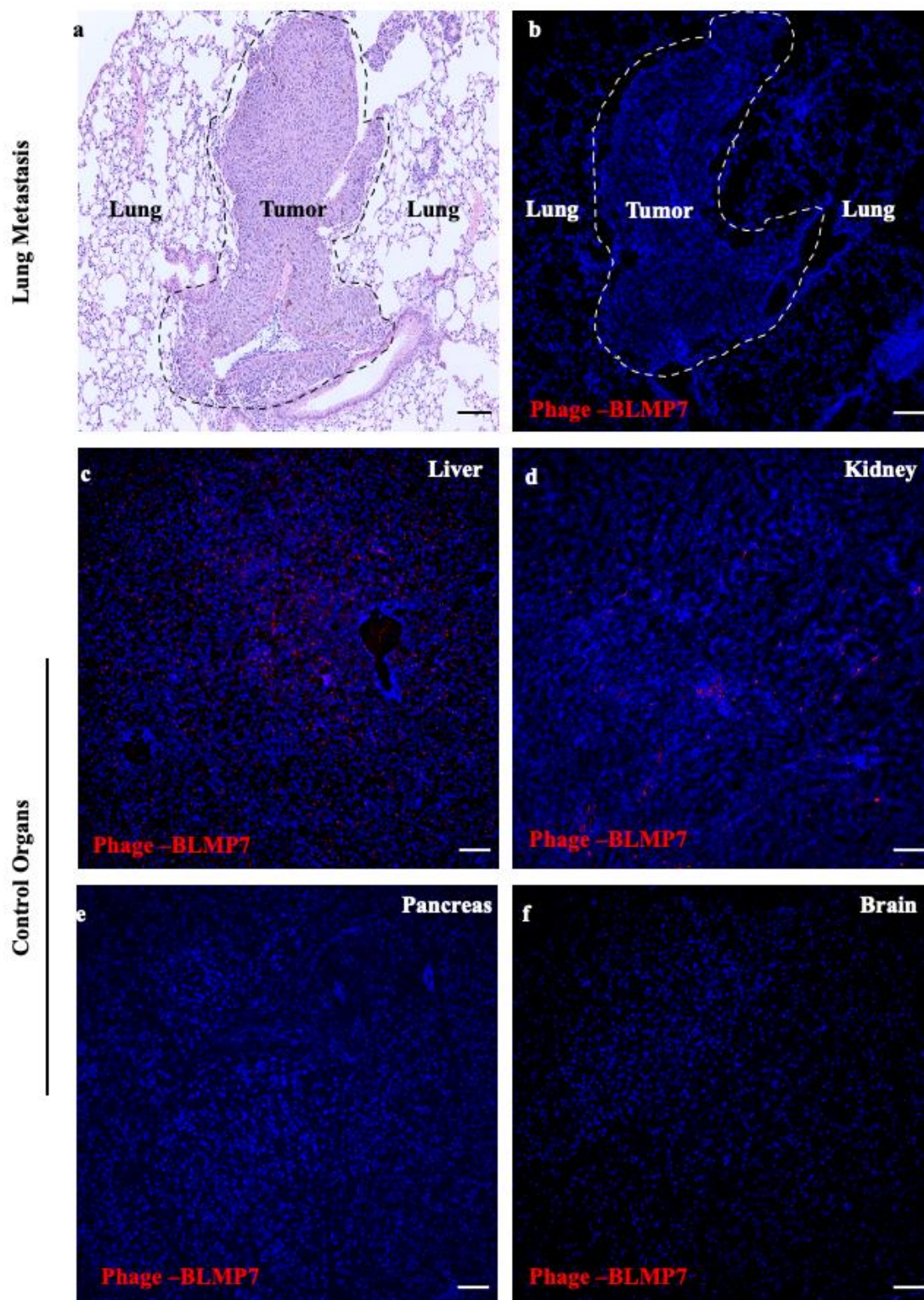
Figure. 9: Absence of BLMP7 and BLMP8 homing in metastases-free mice. Anti-phage (Cy3) immunofluorescence in serial paraffin sections of formalin-fixed organs of tumor-free mice intravenously injected with phage-displayed BLMP7 (Figure. 9A) or BLMP8 clones (Figure. 9B). Red (anti-phage) immunofluorescence signal upon digital channel merging indicates localization of phage observed for both BLMP7 (Figure. 9A) and BLMP8 (Figure. 9B) in liver (c), but not in the lungs (b), kidney (d), pancreas (e), and brain (f). Nuclear DAPI staining is blue. Scale bar: 100 μ m.

6. Only BLMP8 demonstrates pulmonary metastases-specific tropism in an experimental melanoma metastasis model

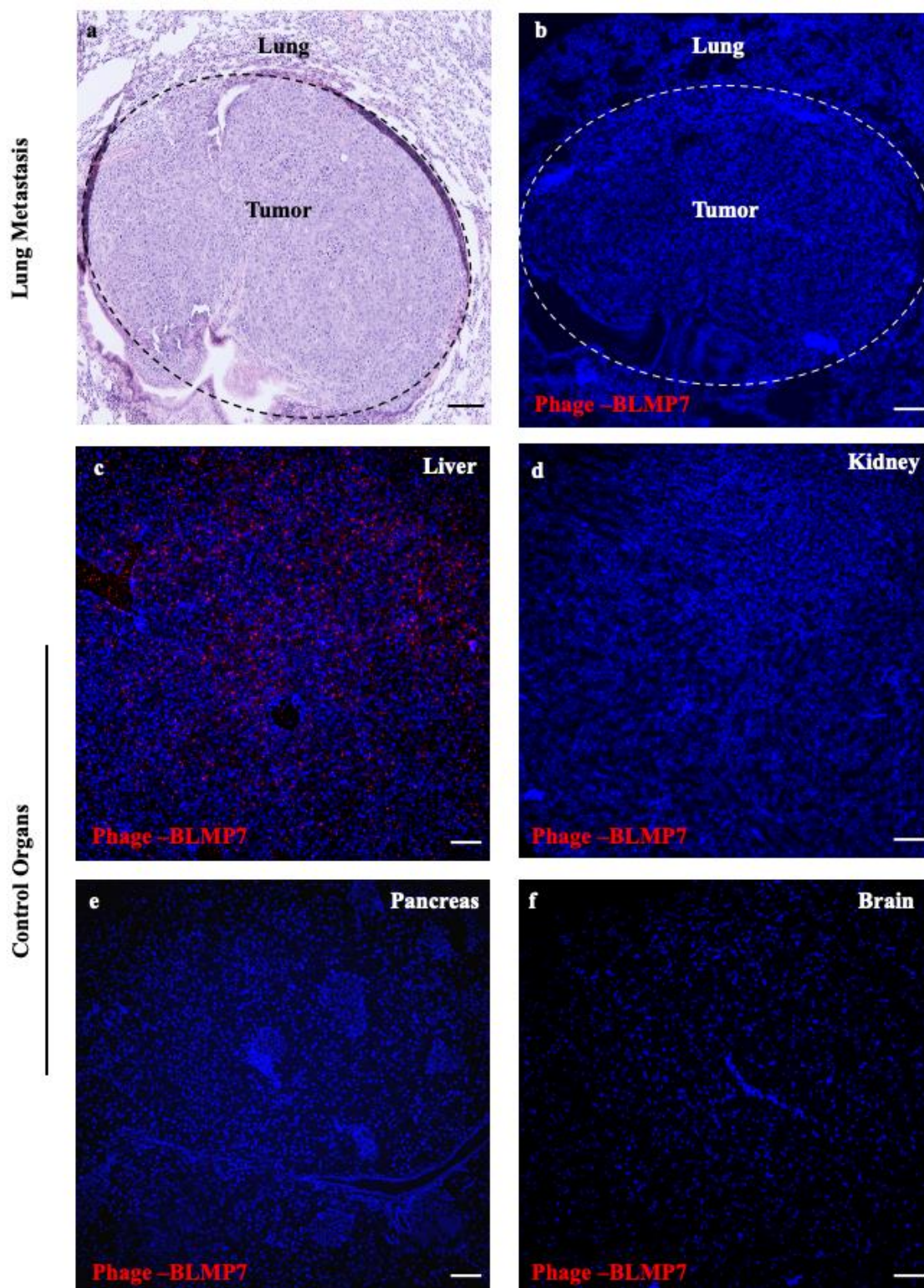
Since neither BLMP7 nor BLMP8 demonstrated chemoresistance specific pulmonary metastasis homing, we hypothesized that both BLMP7 and BLMP8 clones might home to pulmonary metastases in other cancer sub-type settings. To test this hypothesis, the B16F10 melanoma mouse model was selected for further analysis. This mouse model was chosen as BLMP8 demonstrated a significantly high binding efficiency to murine B16F10 melanoma cells *in vitro* (Figure. 7B). Further, the B16F10 melanoma model is a well-characterized model of experimental metastasis (186, 187). Phage particles bearing the BLMP inserts were intravenously injected into vehicle and cisplatin-treated B16F10 mouse models (n=3/cohort). Phage circulation, organ recovery, and immunofluorescence analysis of formalin-fixed paraffin-embedded organ sections was performed as described previously.

In both vehicle and cisplatin-treated B16F10 mouse model, BLMP7 demonstrated no localization (red) to either pulmonary metastases or control organs (Figures. 10A and 10B). These results suggest that BLMP7 homes to pulmonary metastases only in TNBC mouse models. Interestingly, BLMP8 (red) demonstrated localization in pulmonary metastases but not to the control organs of both vehicle and cisplatin-treated B16F10 mouse models (Figures. 10C and 10D). Like the 4T1 cisplatin-treated cohort, non-specific BLMP8 (red) trapping in the liver and kidneys of B16F10 cisplatin-treated mice was also noted (Figure. 10D). These results suggest that BLMP8 homes to pulmonary metastases irrespective of the cancer sub-type setting, thus corroborating the translation potential of BLMP8. Further, BLMP8 homing was independent of chemotherapy administration. Similar to the 4T1 spontaneous metastasis model, BLMP8 (red) localization within B16F10 pulmonary metastases was observed along the invasive edges of the macro-metastases (Figures. 10C and 10D).

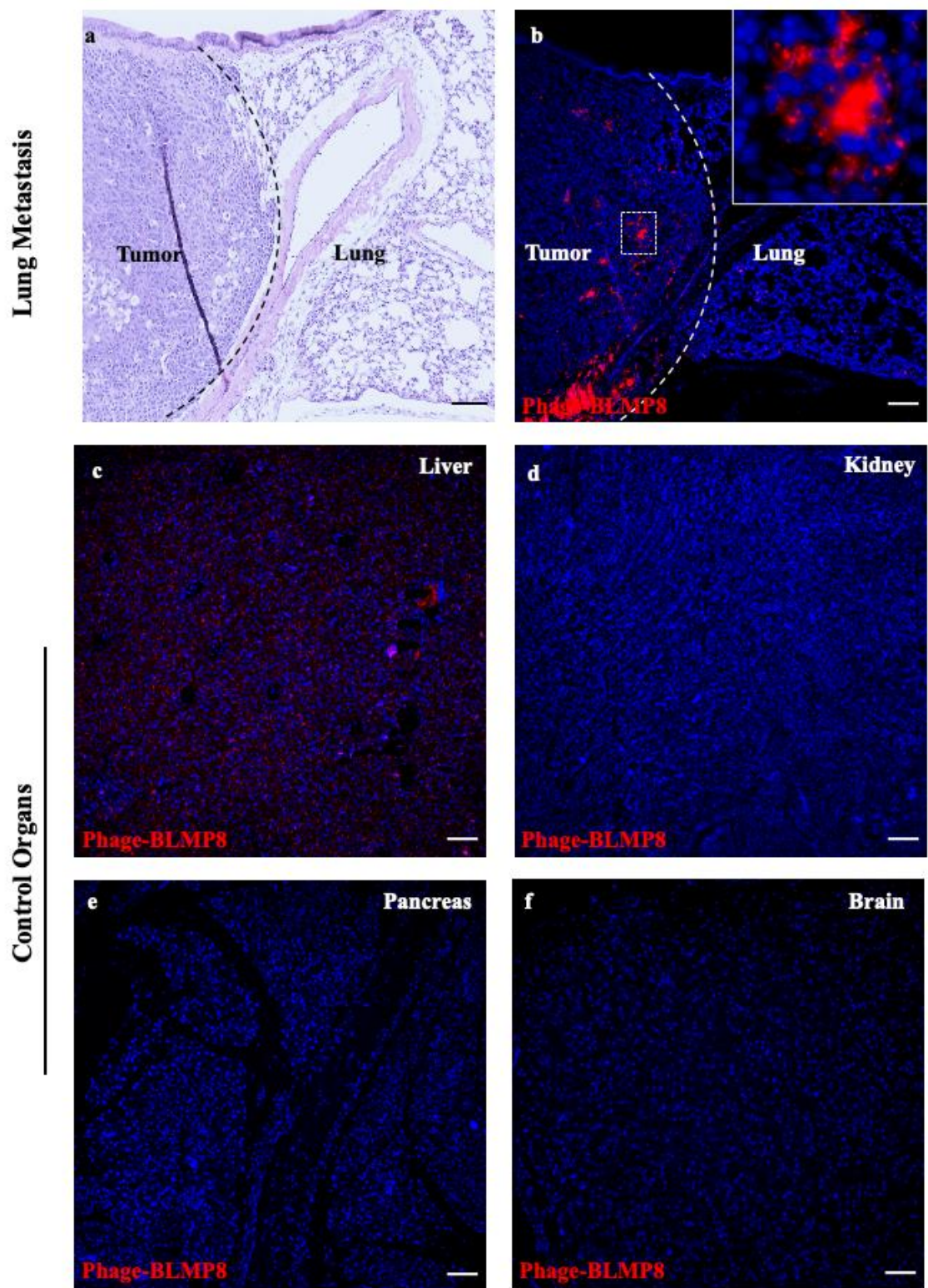
A



B



C



D

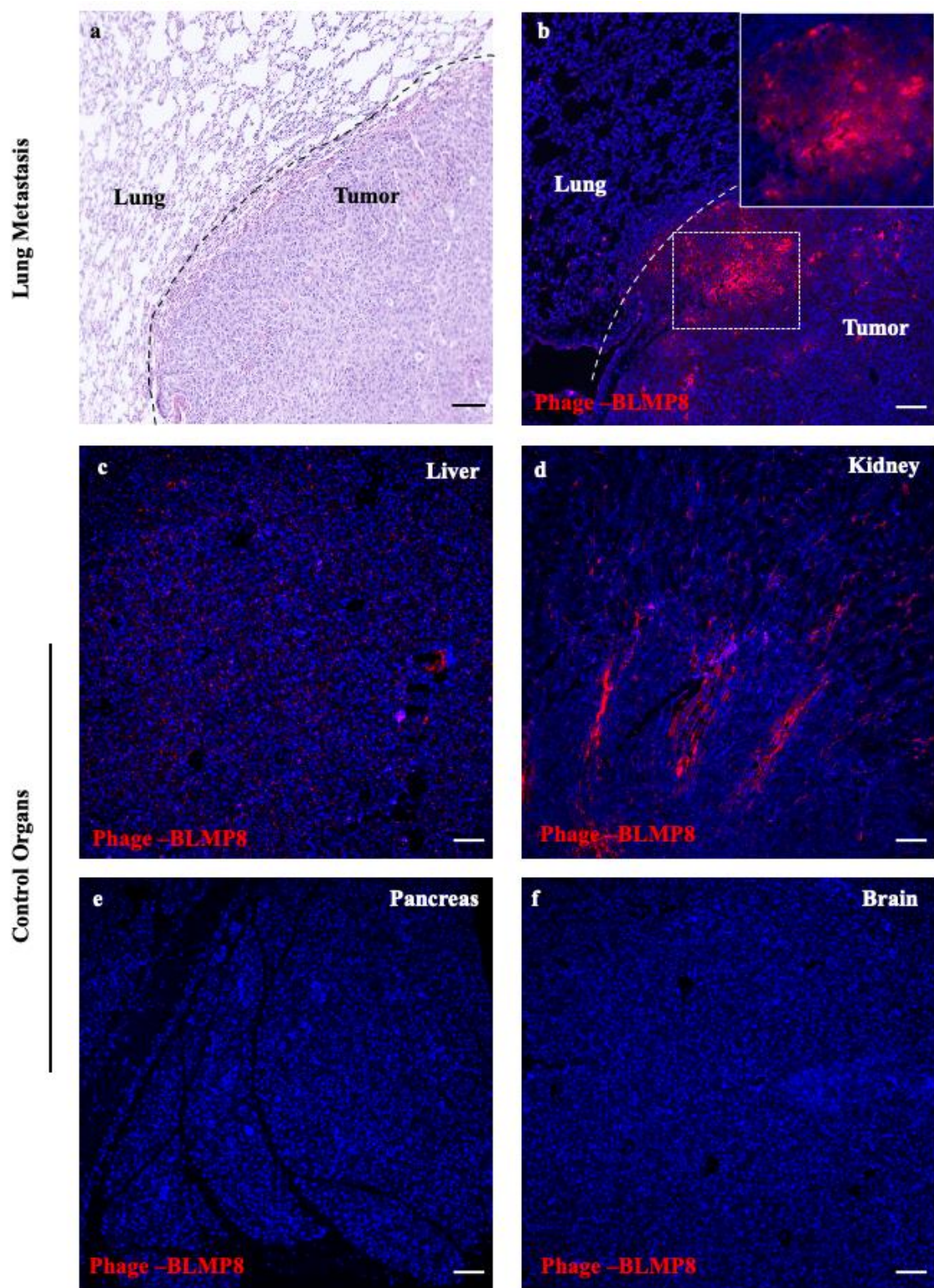


Figure 10: BLMP8 homes to pulmonary metastases in the B16F10 melanoma mouse model

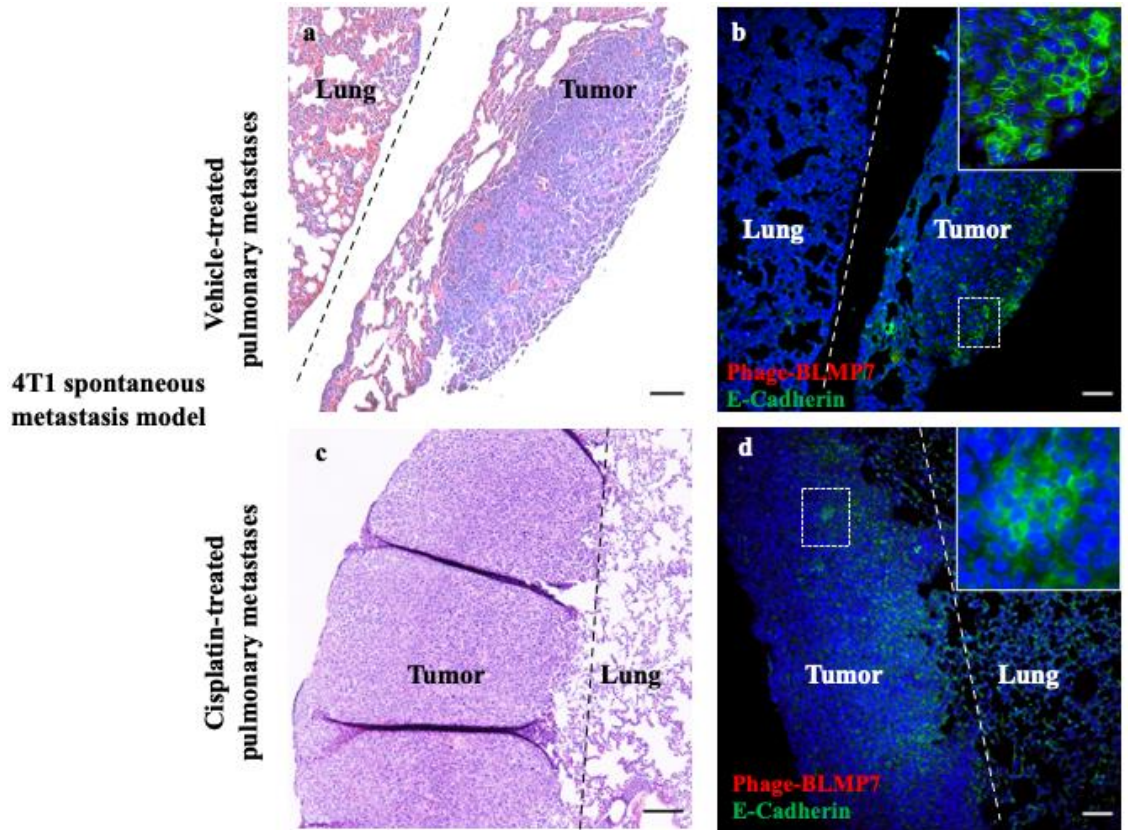
- A. Anti-phage (Cy3) immunofluorescence in serial paraffin sections of formalin-fixed organs of vehicle-treated mice intravenously injected with BLMP7. Red (anti-phage) immunofluorescence signal upon digital channel merging indicates localization of BLMP7 in liver (c), but not in the indicated areas of pulmonary metastases (b), kidney (d), pancreas (e), and brain (f). Nuclear DAPI staining is blue. Scale bar: 100 μ m.
- B. Anti-phage (Cy3) immunofluorescence in serial paraffin sections of formalin-fixed organs of cisplatin-treated mice intravenously injected with BLMP7. Red (anti-phage) immunofluorescence signal upon digital channel merging indicates localization of BLMP7 in liver (c), and kidney (d), but not in the indicated areas of pulmonary metastases (b), pancreas (e), and brain (f). Nuclear DAPI staining is blue. Scale bar: 100 μ m.
- C. Anti-phage (Cy3) immunofluorescence in serial paraffin sections of formalin-fixed organs of vehicle-treated mice intravenously injected with BLMP8. Red (anti-phage) immunofluorescence signal upon digital channel merging indicates localization of BLMP8 in liver (c), but not in the indicated areas of pulmonary metastases (b), kidney (d), pancreas (e), and brain (f). Nuclear DAPI staining is blue. Scale bar: 100 μ m.
- D. Anti-phage (Cy3) immunofluorescence in serial paraffin sections of formalin-fixed organs of cisplatin-treated mice intravenously injected with BLMP8. Red (anti-phage) immunofluorescence signal upon digital channel merging indicates localization of BLMP8 in liver (c), and kidney (d), but not in the indicated areas of pulmonary metastases (b), pancreas (e), and brain (f). Nuclear DAPI staining is blue. Scale bar: 100 μ m.

7. BLMP7 and BLMP8 home to mesenchymal tumor cells in lung metastases

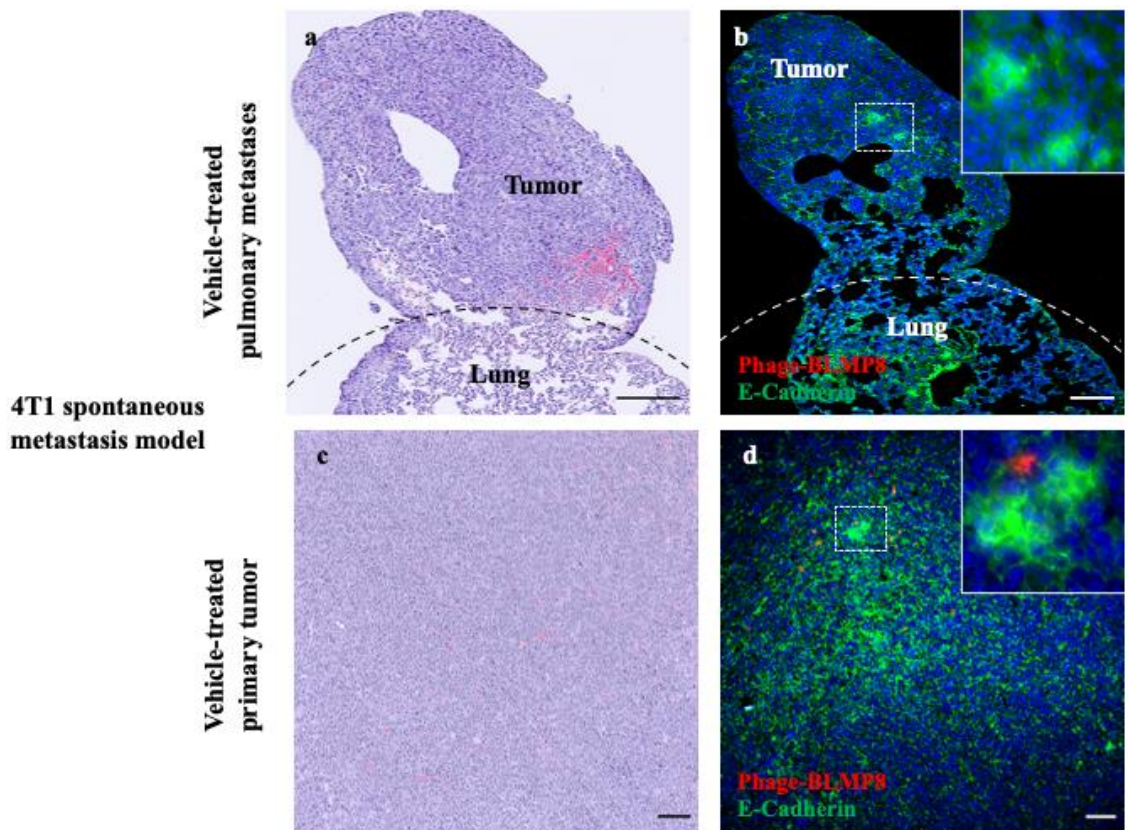
Phage-displayed BLMP localization was restricted to the invasive edges of metastases. This prompted us to explore the favorable tumor cell features that attracted phage-displayed peptide binding. Thus, the co-localization of BLMP7 and BLMP8 with markers of EMT, E-cadherin, and N-cadherin, was investigated. In the 4T1 spontaneous metastasis mouse model, BLMP7 and BLMP8 localization (red) was absent in pulmonary metastases cells positive for epithelial E-cadherin (Figure. 11 A-C). Further, a similar trend was observed in the primary tumors obtained from mice injected with phage-displayed BLMP8 (Figure. 11B and 11C). In the B16F0 experimental metastasis mouse model, BLMP8 (red) also demonstrated a localization pattern similar to 4T1 spontaneous pulmonary metastases (Figure. 11D). In this model, only BLMP8 co-localization was probed due to a lack of BLMP7 homing to B16F10 pulmonary metastases. These observations remained consistent across the vehicle and cisplatin-treated models.

However, in the 4T1 spontaneous metastasis mouse model, both BLMP7 and BLMP8 co-localized (yellow) with N-cadherin positive pulmonary metastatic tumor cells (Figure. 12 A-C). Further, a similar trend was observed in the primary tumors obtained from mice injected with phage-displayed BLMP8 (Figure. 12B and 12C). In the B16F0 experimental metastasis mouse model, BLMP8 also demonstrated a localization pattern similar to 4T1 spontaneous pulmonary metastases (Figure. 12D). In this model, only BLMP8 co-localization was probed due to a lack of BLMP7 homing to B16F10 pulmonary metastases. These observations remained consistent across vehicle and cisplatin-treated models. Taken together, these data suggest that phage-displayed BLMP7 and BLMP8 home to mesenchymal tumor cells in primary tumors and pulmonary metastases.

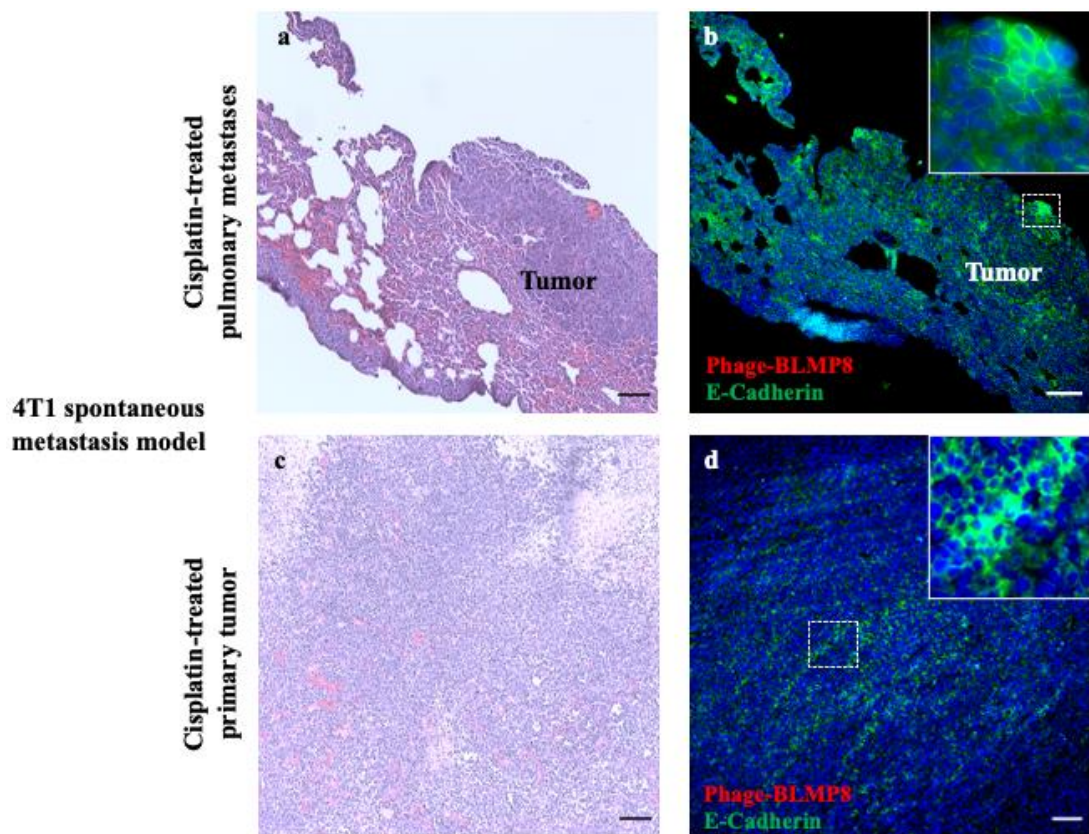
A



B



C



D

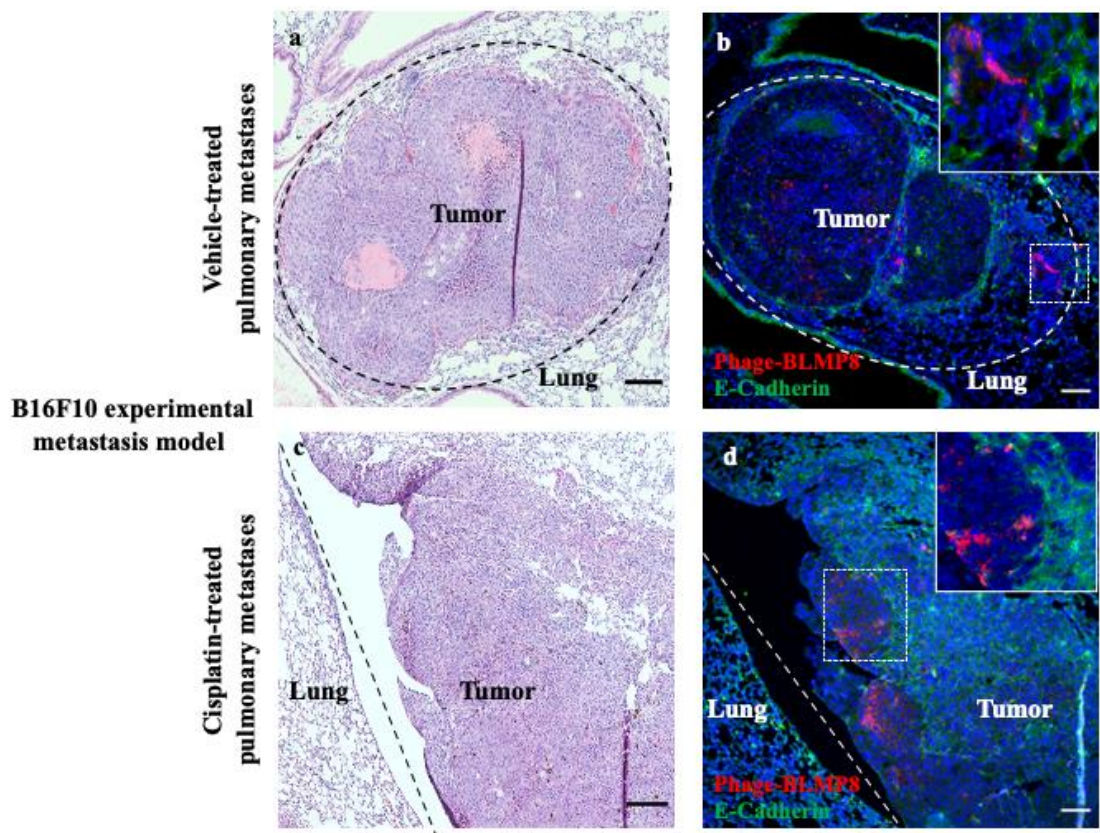
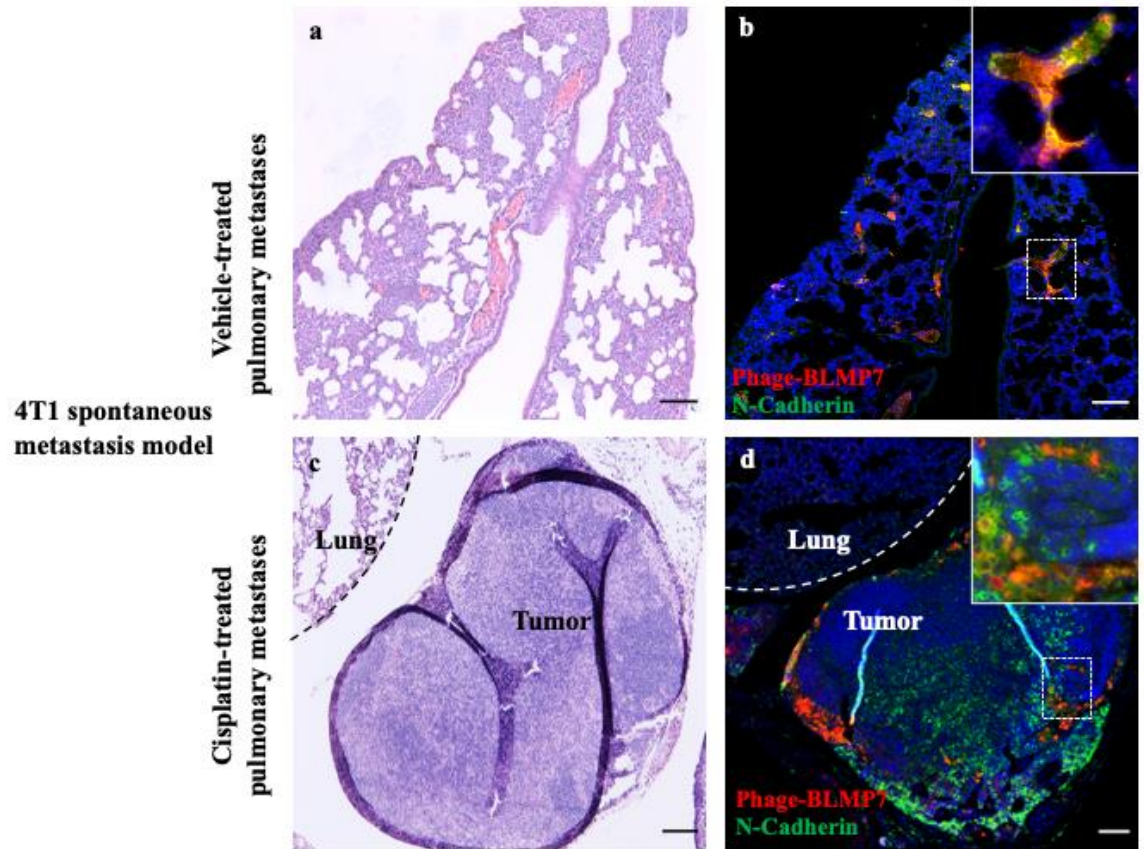


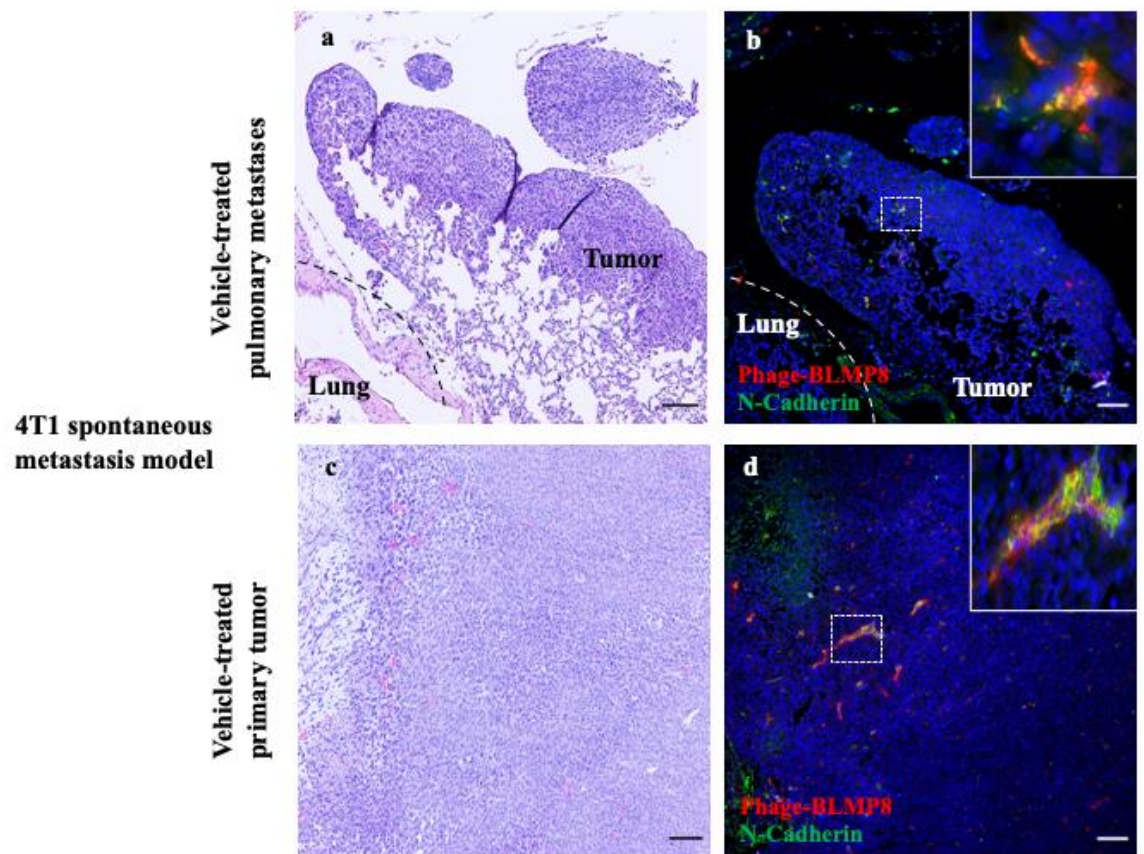
Figure 11: BLMP7 and BLMP8 do not home to E-cadherin positive tumor cells

- A. Anti-phage (Cy3) and anti E-cadherin (Alexa-488) immunofluorescence in serial paraffin sections of formalin-fixed pulmonary metastases of vehicle and cisplatin-treated 4T1 mouse models, intravenously injected with BLMP7. Upon digital channel merging, the absence of red (anti-phage) and green (E-cadherin) immunofluorescence co-localization indicates that BLMP7 doesn't home to E-cadherin positive tumor cells in both vehicle (b) and cisplatin-treated (d) pulmonary metastases. Nuclear DAPI staining is blue. Scale bar: 100 μ m.
- B. Anti-phage (Cy3) and anti E-cadherin (Alexa-488) immunofluorescence in serial paraffin sections of formalin-fixed pulmonary metastases and primary tumors of vehicle-treated 4T1 mouse model, intravenously injected with BLMP8. Upon digital channel merging, the absence of red (anti-phage) and green (E-cadherin) immunofluorescence co-localization indicates that BLMP8 doesn't home to E-cadherin positive tumor cells in vehicle-treated pulmonary metastases (b) and primary tumors (d). Nuclear DAPI staining is blue. Scale bar: 100 μ m.
- C. Anti-phage (Cy3) and anti E-cadherin (Alexa-488) immunofluorescence in serial paraffin sections of formalin-fixed pulmonary metastases and primary tumors of cisplatin-treated 4T1 mouse model, intravenously injected with BLMP8. Upon digital channel merging, the absence of red (anti-phage) and green (E-cadherin) immunofluorescence co-localization indicates that BLMP8 doesn't home to E-cadherin positive tumor cells in cisplatin-treated pulmonary metastases (b) and primary tumors (d). Nuclear DAPI staining is blue. Scale bar: 100 μ m.
- D. Anti-phage (Cy3) and anti E-cadherin (Alexa-488) immunofluorescence in serial paraffin sections of formalin-fixed pulmonary metastases of vehicle and cisplatin-treated B16F10 mouse models, intravenously injected with BLMP8. Upon digital channel merging, the absence of red (anti-phage) and green (E-cadherin) immunofluorescence co-localization indicates that BLMP7 doesn't home to E-cadherin positive tumor cells in both vehicle (b) and cisplatin-treated (d) pulmonary metastases. Nuclear DAPI staining is blue. Scale bar: 100 μ m.

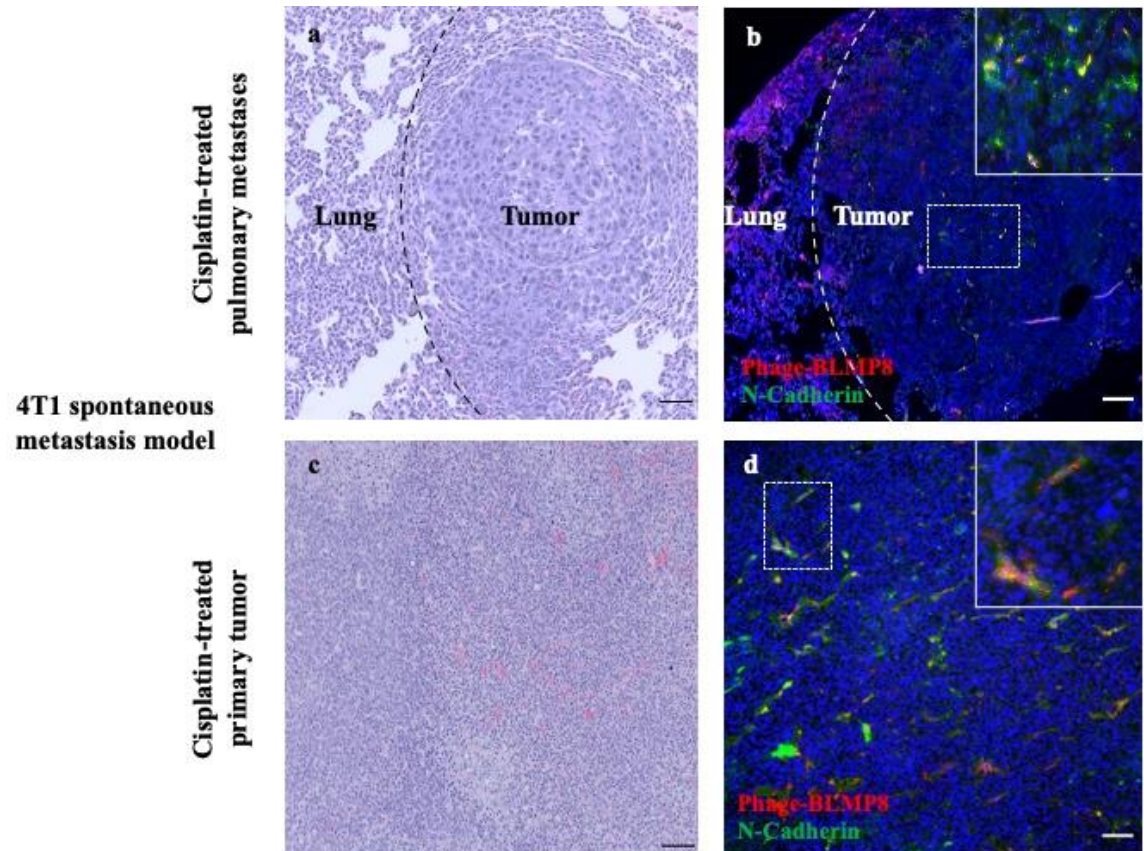
A



B



C



D

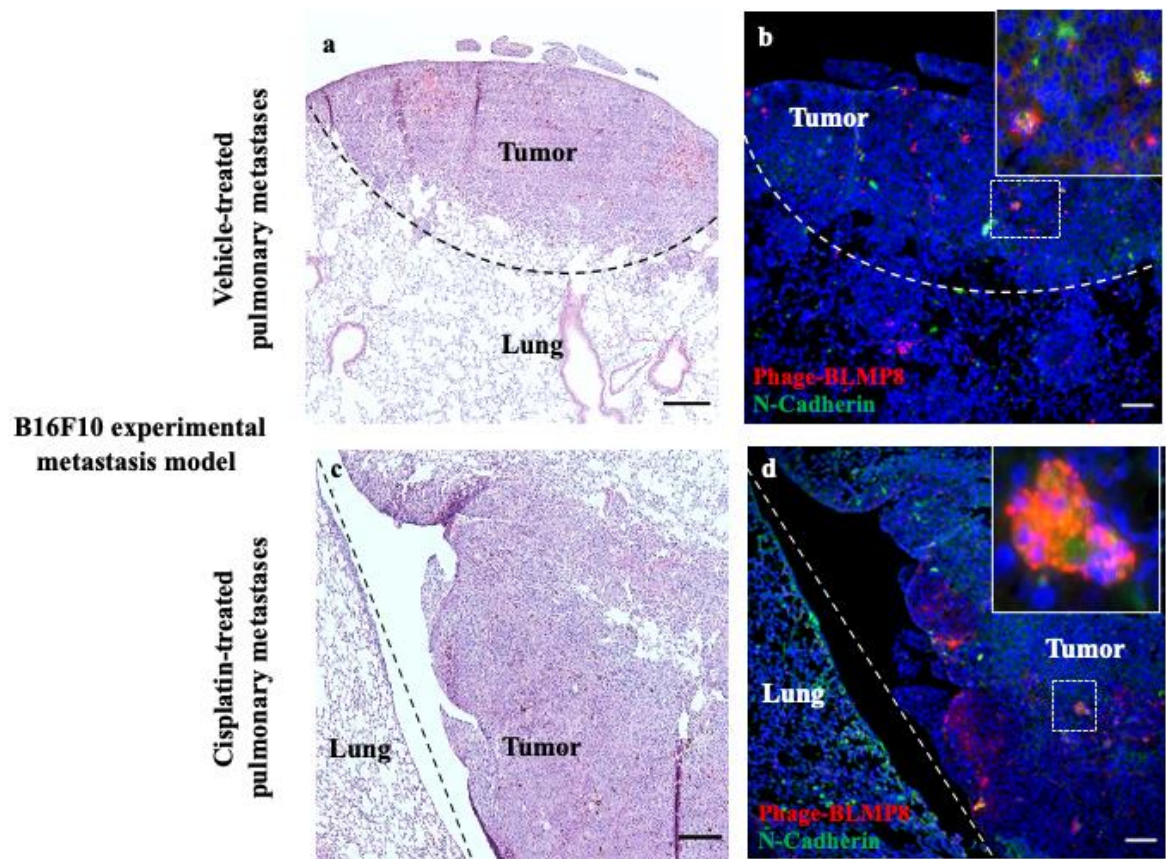


Figure 12: BLMP7 and BLMP8 home to N-cadherin positive tumor cells

- A. Anti-phage (Cy3) and anti N-cadherin (Alexa-488) immunofluorescence in serial paraffin sections of formalin-fixed pulmonary metastases of cisplatin and vehicle-treated 4T1 mouse models, intravenously injected with BLMP7. The co-localization of red (anti-phage) and green (N-Cadherin) signals upon digital channel merging indicates that BLMP7 does home to N-cadherin positive tumor cells in cisplatin (b) and vehicle-treated (d) pulmonary metastases. Nuclear DAPI staining is blue. Scale bar: 100 μ m.
- B. Anti-phage (Cy3) and anti N-cadherin (Alexas-488) immunofluorescence in serial paraffin sections of formalin-fixed pulmonary metastases and primary tumors of vehicle-treated 4T1 mouse model, intravenously injected with BLMP8. The co-localization of red (anti-phage) and green (N-Cadherin) signals upon digital channel merging indicates that BLMP8 does home to N-cadherin positive tumor cells in vehicle-treated pulmonary metastases (b) and primary tumors (d). Nuclear DAPI staining is blue. Scale bar: 100 μ m.
- C. Anti-phage (Cy3) and anti N-cadherin (Alexas-488) immunofluorescence in serial paraffin sections of formalin-fixed pulmonary metastases and primary tumors of cisplatin-treated 4T1 mouse model, intravenously injected with BLMP8. The co-localization of red (anti-phage) and green (N-Cadherin) signals upon digital channel merging indicates that BLMP8 does home to N-cadherin positive tumor cells in cisplatin-treated pulmonary metastases (b) and primary tumors (d). Nuclear DAPI staining is blue. Scale bar: 100 μ m.
- D. Anti-phage (Cy3) and anti N-cadherin (Alexa-488) immunofluorescence in serial paraffin sections of formalin-fixed pulmonary metastases of vehicle and cisplatin-treated 4T1 mouse models, intravenously injected with BLMP8. The co-localization of red (anti-phage) and green (N-Cadherin) signals upon digital channel merging indicates that BLMP8 does home to N-cadherin positive tumor cells in vehicle (b) and cisplatin-treated (d) pulmonary metastases. Nuclear DAPI staining is blue. Scale bar: 100 μ m.

8. Phage-displayed BLMP7 and BLMP8 do not home to epithelial tumor cells *in vitro*

In order to corroborate that BLMP7 and BLMP8 do home to mesenchymal tumor cells, we investigated the BLMP homing pattern *in vitro* with an immunofluorescence assay, using a specific antibody against epithelial marker E-cadherin. Phage-displayed BLMP7 and BLMP8 were incubated with murine parental and cisplatin-resistant 4T1.2 adenocarcinoma cells, murine B16F10 melanoma and human MDA-MB-231 adenocarcinoma cells overnight.

All cell lines, including B16F10 and MDA-MB-231 cells, demonstrated BLMP7 (red) and BLMP8 (red) binding (Figures. 13 A-H). Further, it was observed that 4T1 cells with pronounced E-cadherin (green) expression demonstrated less BLMP7 and BLMP8 binding (green arrow). Instead, both BLMP7 and BLMP8 (white arrow) were seen to bind better to cancer cells with very little to no E-cadherin expression (Figures. 13 A-H). Loss in the E-cadherin expression is a characteristic feature of cells undergoing EMT, to acquire a more mesenchymal phenotype. Since phage-displayed peptide homing is seen in tumor cells exhibiting predominantly mesenchymal characteristics, these data suggest that phage-displayed BLMP7 and BLMP8 home to cells that have undergone the EMT.

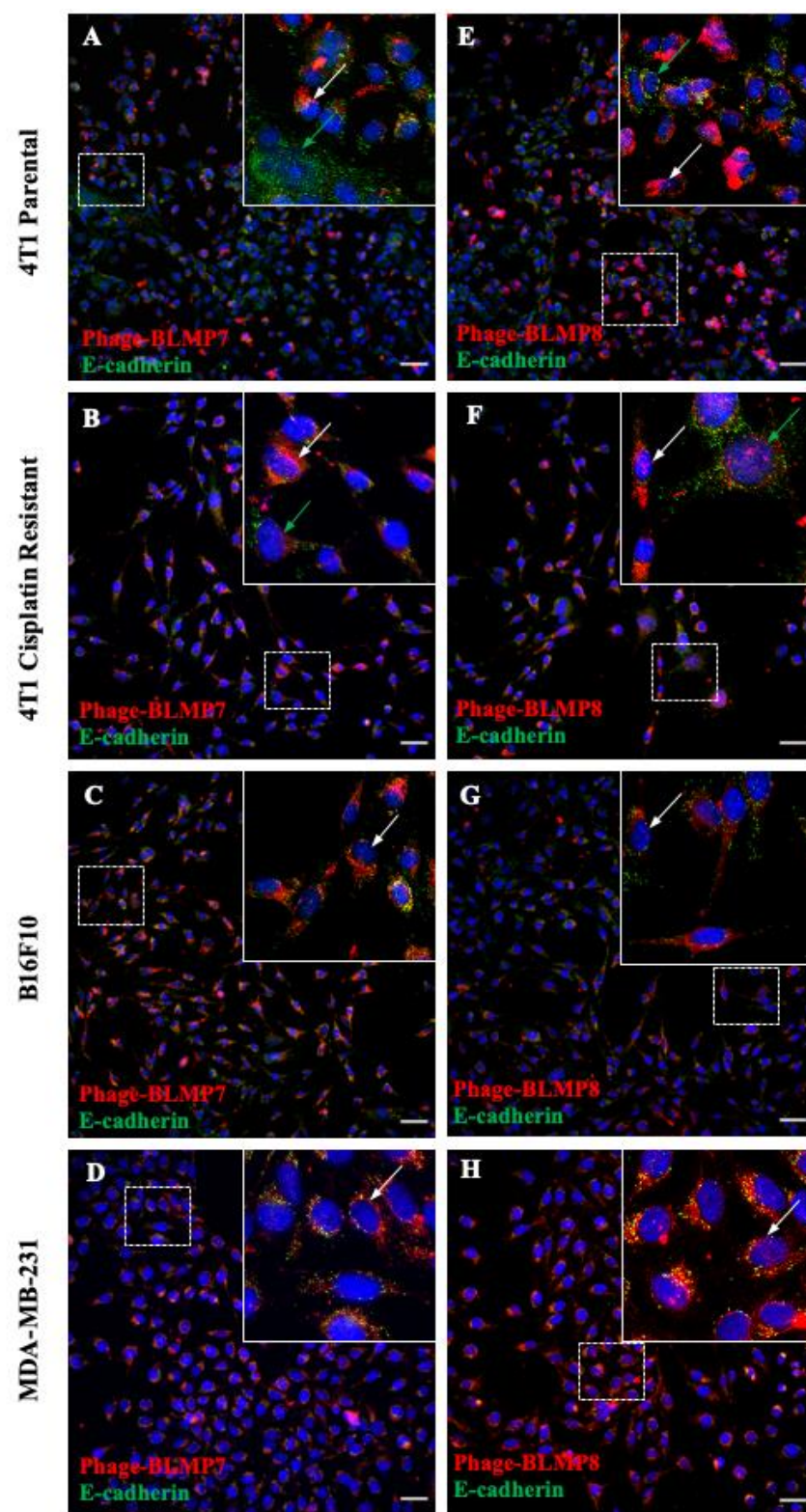


Figure 13: BLMP7 and BLMP8 home to tumor cells expressing reduced levels of E-cadherin Anti-phage (Cy3) and anti E-cadherin (Alexa-488) immunofluorescence in murine parental and cisplatin-resistant 4T1.2 adenocarcinoma, human MDA-MB-231 adenocarcinoma and murine B16F10 melanoma cell lines. Cells were incubated with phage-displayed BLMP7 and BLMP8 clones overnight. Upon digital channel merging, cancer cells exhibiting high level of green (E-cadherin) signal (green arrow), demonstrate lesser homing of BLMP7 (Cy3) and BLMP8 (Cy3) clones. However, cancer cells exhibiting little to no green signal (white arrow), demonstrate more specific homing of phage-displayed BLMP7 (Cy3) and BLMP8 (Cy3) clones. Nuclear DAPI staining is blue. Scale bar: 50 μ m.

9. Biotin-labeled HK-BLMP7 and HK-BLMP8 bind specifically to cancer cell lines *in vitro*

In order to explore the binding specificity of BLMP7 and BLMP8 outside the phage context, hunter-killer peptide versions of BLMP7 and BLMP8, termed HK-BLMP7 and HK-BLMP8, were chemically synthesized. HK-BLMP7 consists of homing motif CLRHSSKIC conjugated with the KLAKLAKKLAKLAK sequence, with an amino-hexanoic acid linker. HK-BLMP8 was designed in a similar manner, with a homing motif of CRAGVGRGC instead. The amphipathic peptide (KLAKLAK)₂ sequence, disrupts cellular mitochondrial membranes through receptor-mediated cell internalization, to promote programmed cell death (188).

The tropism of HK-BLMP7 and HK-BLMP8 for cancer cell lines was probed through biotin labeling. The pro-apoptotic potential of HK-BLMP7 and HK-BLMP8 was neutralized through the binding of biotin molecules to (KLAKLAK)₂'s lysine residues. Biotin-labeled HK-BLMP7 (B-BLMP7) and biotin-labeled HK-BLMP8 (B-BLMP8) were incubated with murine parental and cisplatin-resistant 4T1.2 adenocarcinoma cells, murine B16F10 melanoma, human MDA-MB-231 adenocarcinoma, and 3T3L1 murine fibroblasts for six hours. This was followed by an *in vitro* immunofluorescence assay using a Cy3-conjugated streptavidin binding to biotin on the labeled peptides. Human MDA-MB-231 adenocarcinoma cells were used to study the translational potential of the hunter-killer peptides. 3T3L1 fibroblasts were used as a negative control. The results of the assay demonstrated a pronounced red (Cy3) fluorescence signal for both B-BLMP7 (Figures. 14 A-D) and B-BLMP8 (Figures. 14 F-I) in all cancer cell lines. However, no signal that could result from peptide binding was observed in murine 3T3L1 fibroblasts (Figures. 14E and 14J). These observations indicate that B-BLMP7 and B-BLMP8 bind selectively to cancer cells outside the phage context.

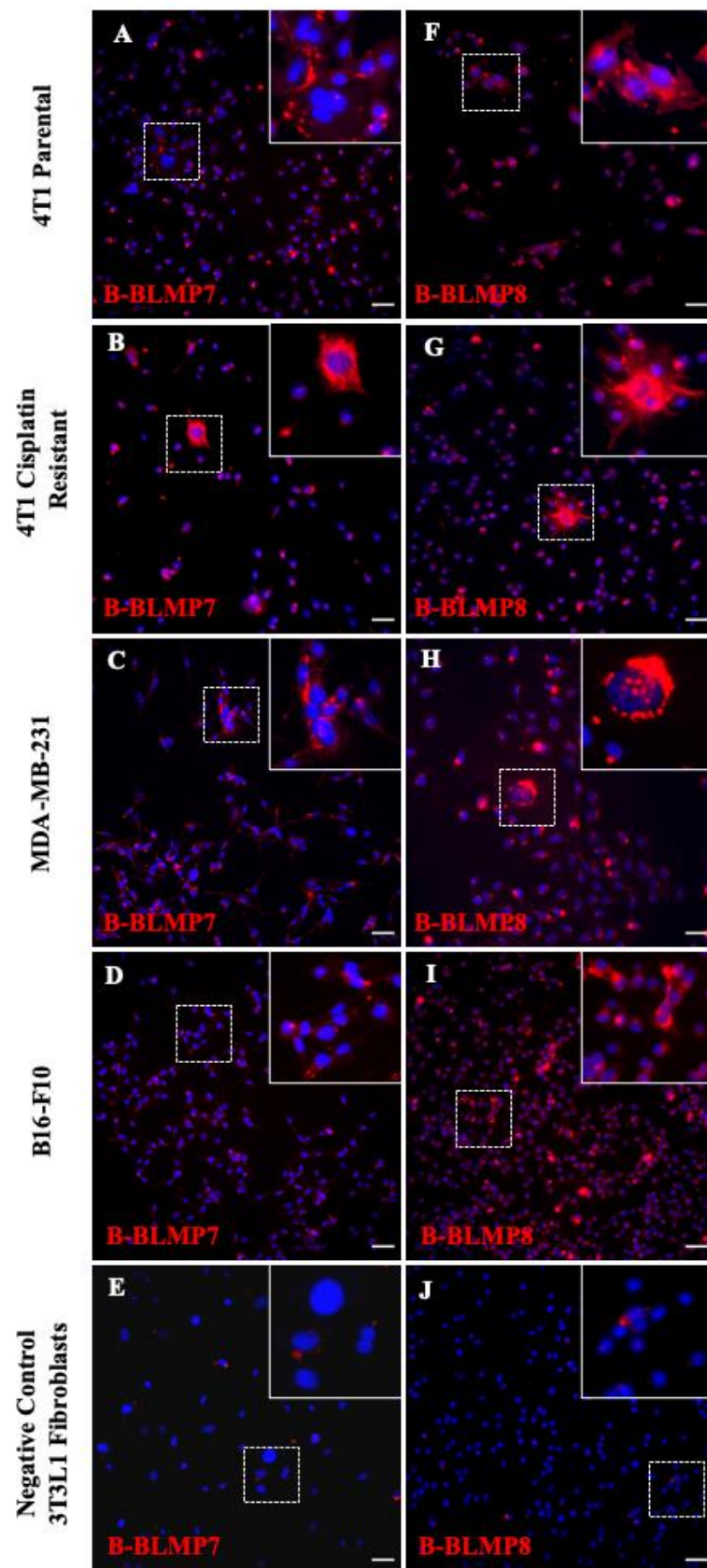


Figure 14: Validation of biotin-labeled HK-BLMP7 (B-BLMP7) and biotin-labeled HK-BLMP8 (B-BLMP8) homing specificity to cancer cells *in vitro* (A-J). Streptavidin (Cy3) immunofluorescence in murine parental and cisplatin-resistant 4T1.2 adenocarcinoma, murine B16F10 melanoma, human MDA-MB-231 adenocarcinoma, and murine 3T3L1 fibroblast cell lines. Cells were incubated with B-BLMP7 and B-BLMP8 for 6 hours. Red (Streptavidin) immunofluorescence signal upon digital channel merging indicates localization of B-BLMP7 (Cy3) and B-BLMP8 (Cy3) on 4T1 parental, 4T1 cisplatin resistant, B16F10 and MDA-MB-231 cancer cell lines but not on 3T3L1 murine fibroblasts. Nuclear DAPI staining is blue. Scale bar: 50µm.

10. Biotin-labeled HK-BLMP8 does not home to epithelial tumor cells *in vitro*

As discussed earlier, phage-displayed BLMP8 did not bind to epithelial cancer cells *in vitro* (Figures. 13 E-H). In order to corroborate that the chemically synthesized B-BLMP8 also demonstrated the same binding pattern, we investigated B-BLMP8 (red) homing *in vitro* with an immunofluorescence assay, using a specific antibody against epithelial marker E-cadherin (green). B-BLMP8 was incubated with murine parental and cisplatin-resistant 4T1.2 adenocarcinoma cells, murine B16F10 melanoma, and human MDA-MB-231 adenocarcinoma cells for six hours.

As seen with phage-displayed BLMP8, B-BLMP8 (red) was observed to bind less to cancer cells with pronounced E-cadherin (green) expression (green arrow). Instead, B-BLMP8 (white arrow) was seen to bind better to cancer cells with very little to no E-cadherin expression (Figures. 15 A-D). Loss in the E-cadherin expression is a characteristic feature of cells undergoing EMT, to acquire a more mesenchymal phenotype. Taken together, these data suggest that like phage-displayed BLMP8, its synthetically synthesized version B-BLMP8 also binds to cells with a more mesenchymal phenotype.

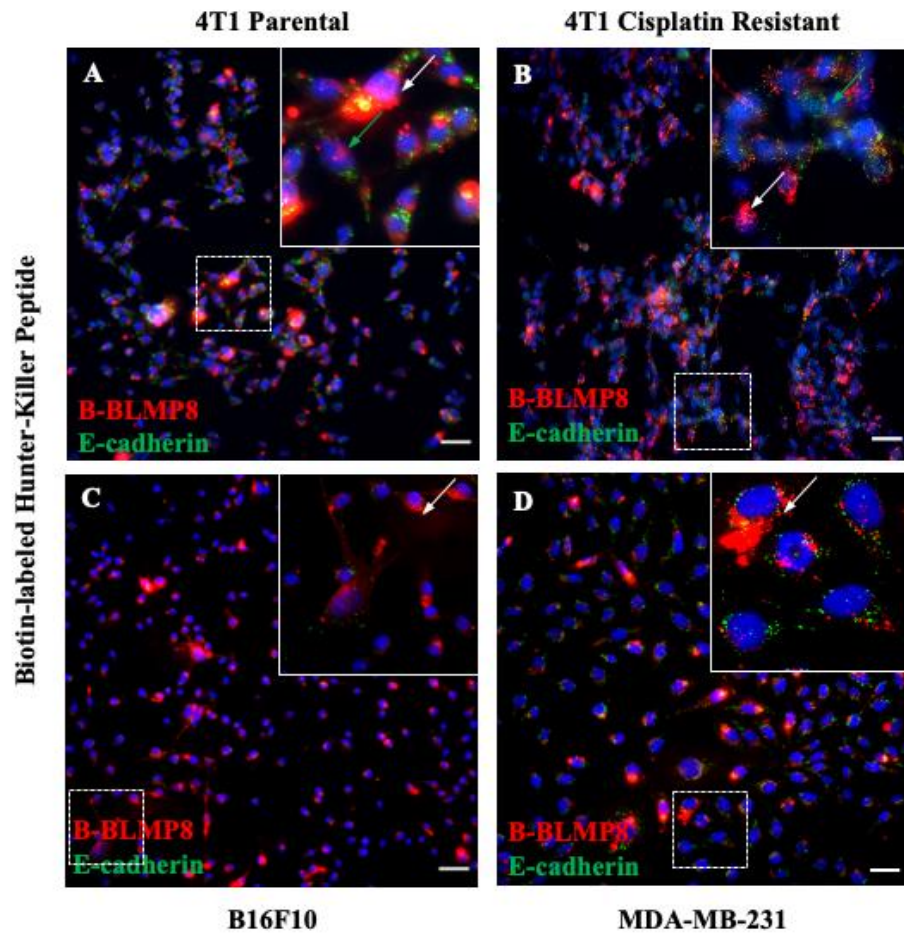


Figure 15: B-BLMP8 homes to tumor cells expressing reduced levels of E-cadherin

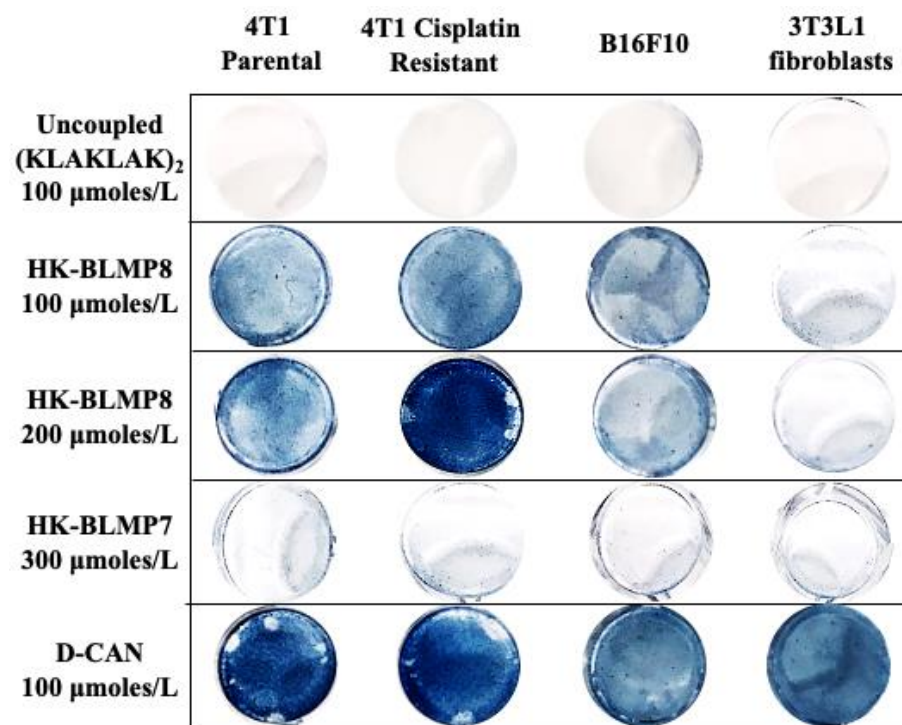
(A-D). Streptavidin (Cy3) and anti E-cadherin (Alexas-488) immunofluorescence in murine 4T1.2 parental and cisplatin-resistant adenocarcinoma, murine B16F10 melanoma and human MDA-MB-231 adenocarcinoma cancer cell lines. Cells were incubated with B-BLMP8 for six hours. Upon digital channel merging, cancer cells exhibiting high level of green (E-cadherin) immunofluorescence signal (green arrow), demonstrate lesser homing of B-BLMP8 (Cy3). However, cancer cells exhibiting little to no green immunofluorescence signal (white arrow), demonstrate more specific homing of B-BLMP8 (Cy3). Nuclear DAPI staining is blue. Scale bar: 50 μ m.

11. HK-BLMP8 induces cell death in murine cancer cell lines *in vitro*

The ability of hunter-killer peptides to induce programmed-cell death *in vivo* and *in vitro* is a well-documented phenomenon (145, 189-191). A cell viability assay using different hunter-killer peptides was performed in murine parental and cisplatin-resistant 4T1.2 adenocarcinoma cells, B16F10 melanoma, and 3T3L1 fibroblasts cell lines. The cells were treated with HK-BLMP7 (300 μ moles/L), varying concentrations of HK-BLMP8 (100-200 μ moles/L), positive-control D-CAN (100 μ moles/L), and uncoupled (KLAKLAK)₂ moiety (100 μ moles/L) for 8 hours. Cell death was then evaluated through trypan blue staining.

At the eight-hour time point, D-CAN induced non-specific apoptosis in both murine cancer cells and 3T3L1 fibroblasts (Figures. 16A and 16B). As previously described, no apoptosis induction was seen upon treatment with the uncoupled (KLAKLAK)₂ moiety owing to the absence of a homing domain (Figures. 16A and 16B). Treatment with HK-BLMP7 induced no cell death in any of the cells at the eight-hour time point. Upon treatment extension to twenty-four hours, a small degree of cell death was observed in both murine cancer cell lines and 3T3L1 cells (Figures. 16A and 16B). On the other hand, at the eight-hour time point, HK-BLMP8 induced apoptosis at both 100 μ moles/L and 200 μ moles/L concentrations, specifically in murine cancer cell lines (data not shown). To investigate if HK-BLMP8 induced apoptosis was cancer cell-specific, the treatment period was increased to twenty-four hours. At this new time point, HK-BLMP8 induced complete cell death in nearly all cancer cell lines but not in 3T3L1 fibroblasts (Figures. 16A and 16B). Although both HK-BLMP7 and HK-BLMP8 induce cancer cell apoptosis *in vitro*, HK-BLMP8 was a more suitable candidate owing to its specificity to only cancer cell lines and not 3T3L1 fibroblasts. Further, *in vitro* immunostaining corroborated that HK-BLMP8 induced cancer cell line death via cleaved caspase-3 activation (Figures. 17 A-C).

A



B

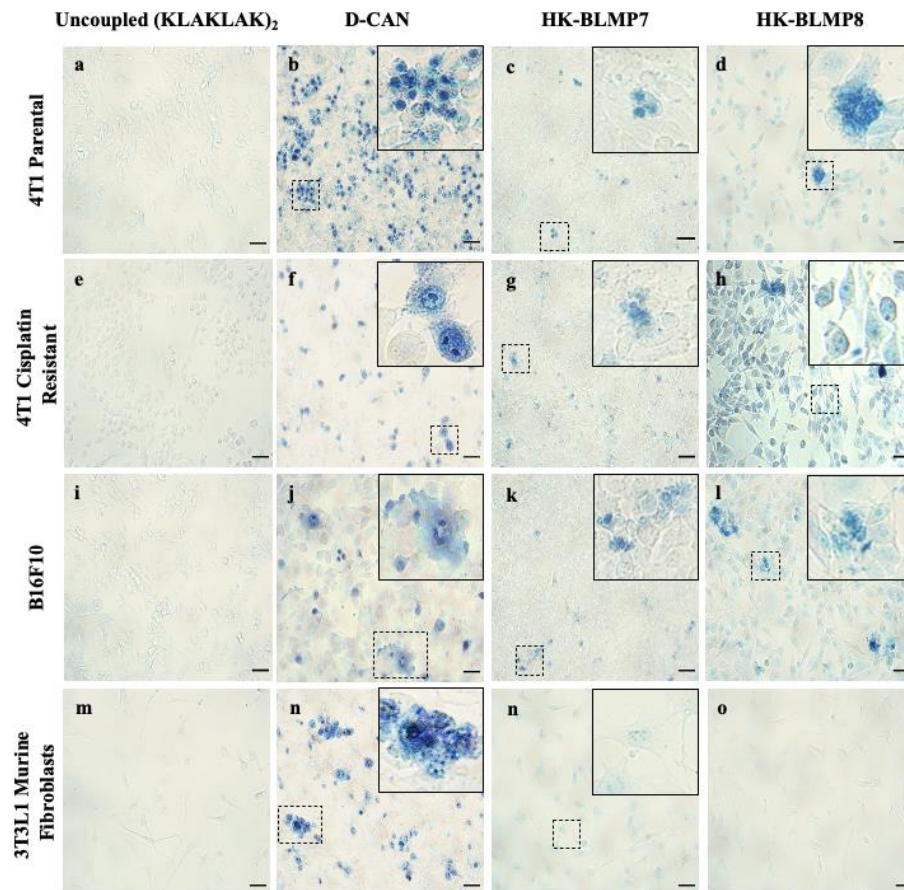


Figure 16: HK-BLMP7 and HK-BLMP8 induce apoptosis in cell culture

- A. Cell viability assay of murine 4T1 parental, 4T1 cisplatin resistant, B16F10 and 3T3L1 fibroblast cell lines following treatment with uncoupled (KLAKLAK)₂ (100 µmoles/L), D-CAN (100 µmoles/L), HK-BLMP7 (300 µmoles/L) or HK-BLMP8 (100 to 200 µmoles/L). Cell death was evaluated by Trypan blue staining. Uncoupled (KLAKLAK)₂: negative control and D-CAN: positive control.
- B. Brightfield images of dead cells (Trypan blue positive) after treatment with uncoupled (KLAKLAK)₂ (100 µmoles/L), D-CAN (100 µmoles/L), HK-BLMP7 (300 µmoles/L) or HK-BLMP8 (100 µmoles/L). Uncoupled (KLAKLAK)₂: negative control and D-CAN: positive control. Scale bar: 50µm.

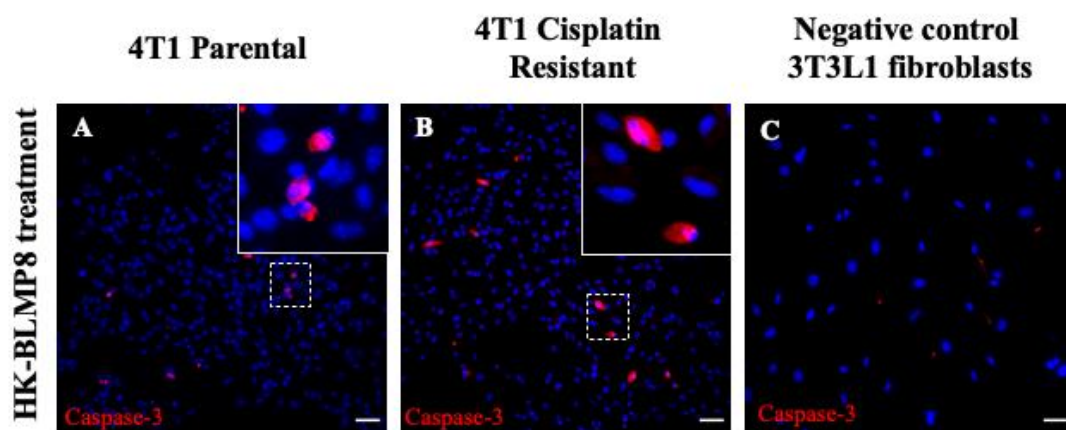


Figure 17: HK-BLMP8 induces cleaved caspase-3 mediated apoptosis in murine cancer cell lines *in vitro*. Cleaved Caspase-3 (red) immunofluorescence in murine 4T1 parental, 4T1 cisplatin resistant, and negative control 3T3L1 murine fibroblast cell lines treated with HK-BLMP8 (100 μ moles/L) for 8 hours. Red (cleaved caspase-3) signal upon digital channel merging indicates cleaved caspase-3 labeling in cancer cell lines. Nuclear DAPI staining is blue. Scale bar: 50 μ m.

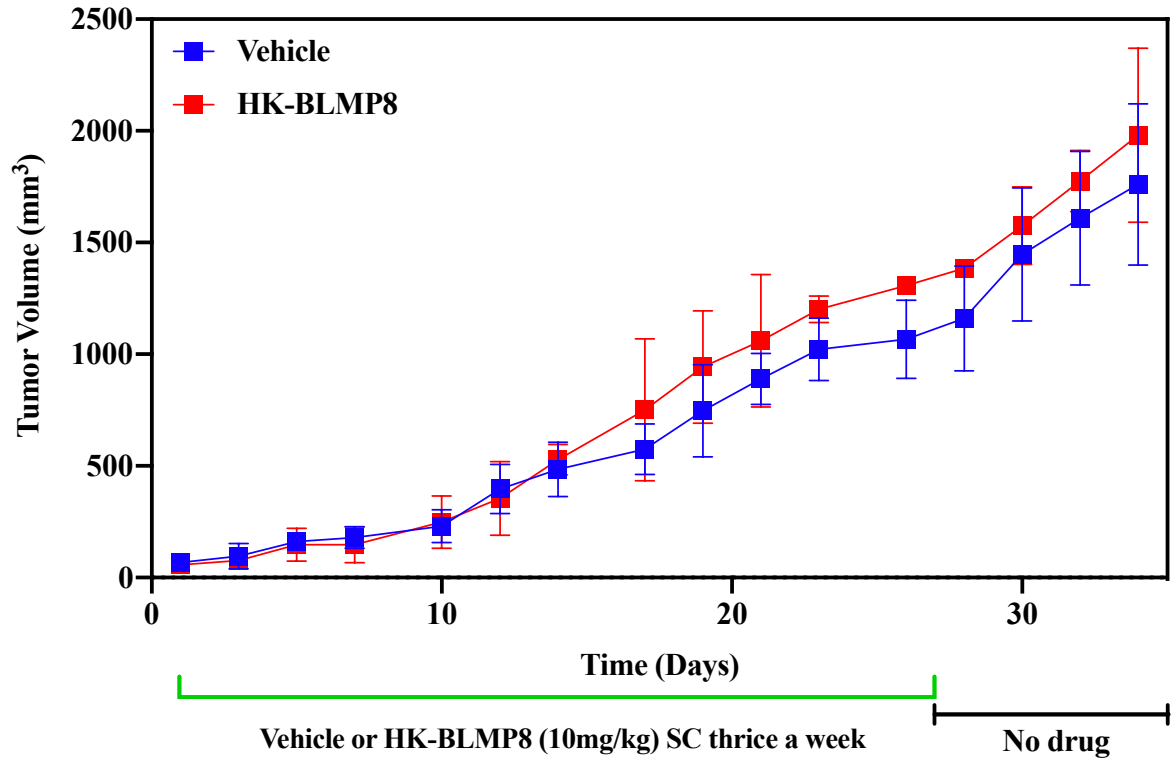
12. HK-BLMP8 administration induces a modest reduction in 4T1 pulmonary metastatic burden but does not improve overall survival

Based on the *in vitro* cell viability and cleaved caspase-3 staining results, we investigated whether HK-BLMP8 peptide could be used for the therapeutic destruction of pulmonary metastases. We injected spontaneously metastasizing dual-luciferase and mCherry labeled 4T1 adenocarcinoma cells into Balb/c mice. Once the tumors became palpable, the mice were randomized into two cohorts (n=5/cohort) and treated with vehicle control or 10 mg/kg HK-BLMP8 subcutaneously for four weeks. Tumors were measured thrice a week. Further, the effect of vehicle or HK-BLMP8 administration on metastatic progression was monitored weekly through non-invasive bioluminescence imaging. Following the administration of the last dose, the mice were monitored for survival analysis.

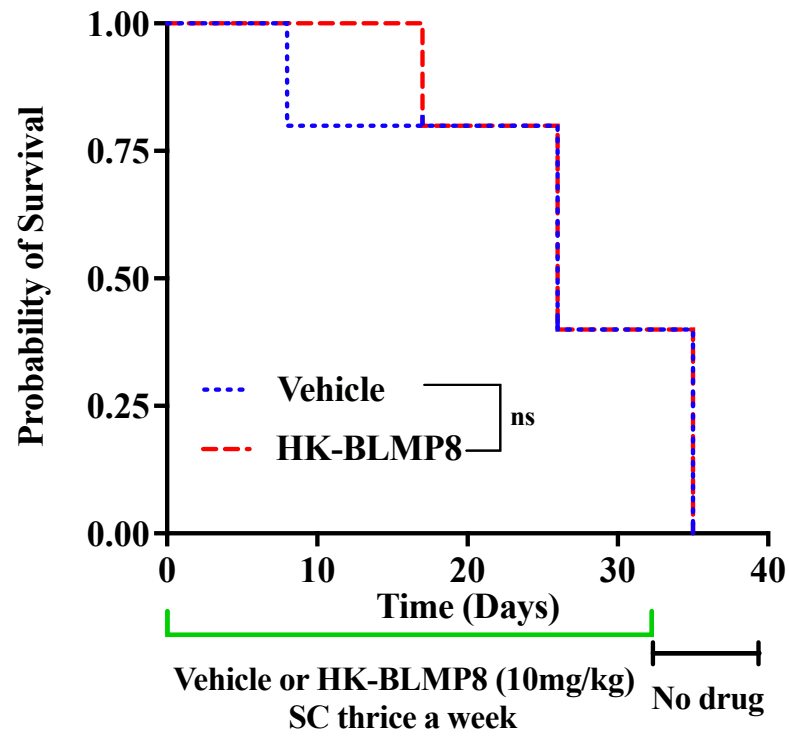
Based on Welch's t-test analysis, no significant difference ($p=0.5735$) in tumor volumes was observed between the two groups during and after treatment (Figure. 18A). These results suggest that the HK-BLMP8 administration did not affect primary tumor growth. Further, the Log-Rank (Mantel-Cox) test demonstrated no significant difference ($p = 0.9626$) in OS between the two groups (Figure. 18B). However, upon analysis of non-invasive bioluminescence images of the mice, a significant difference in metastatic burden was indicated between the groups (Figure. 18C). In the HK-BLMP8 treated mouse cohort, cancer progression and subsequent pulmonary metastatic burden were significantly lower when compared to the vehicle-treated mouse cohort (Figure. 18C). These observations were further corroborated through pulmonary metastases nodule quantification. At the experimental endpoint, the mouse lungs were subjected to PBS perfusion. The lungs were then fixed in formalin until the metastatic nodules were bleached to amelanotic gray/white nodules (Figure. 18D). This was followed by a blind enumeration of metastatic lung nodules of both mice cohorts. The HK-BLMP8 treated mice demonstrated a significantly lower ($p \leq 0.01$) pulmonary metastatic nodule burden when

compared to the vehicle control group (Figure. 18E). Together, these data suggest that HK-BLMP8 administration induces a modest reduction in metastatic burden, even though it does not improve OS (Figure. 18).

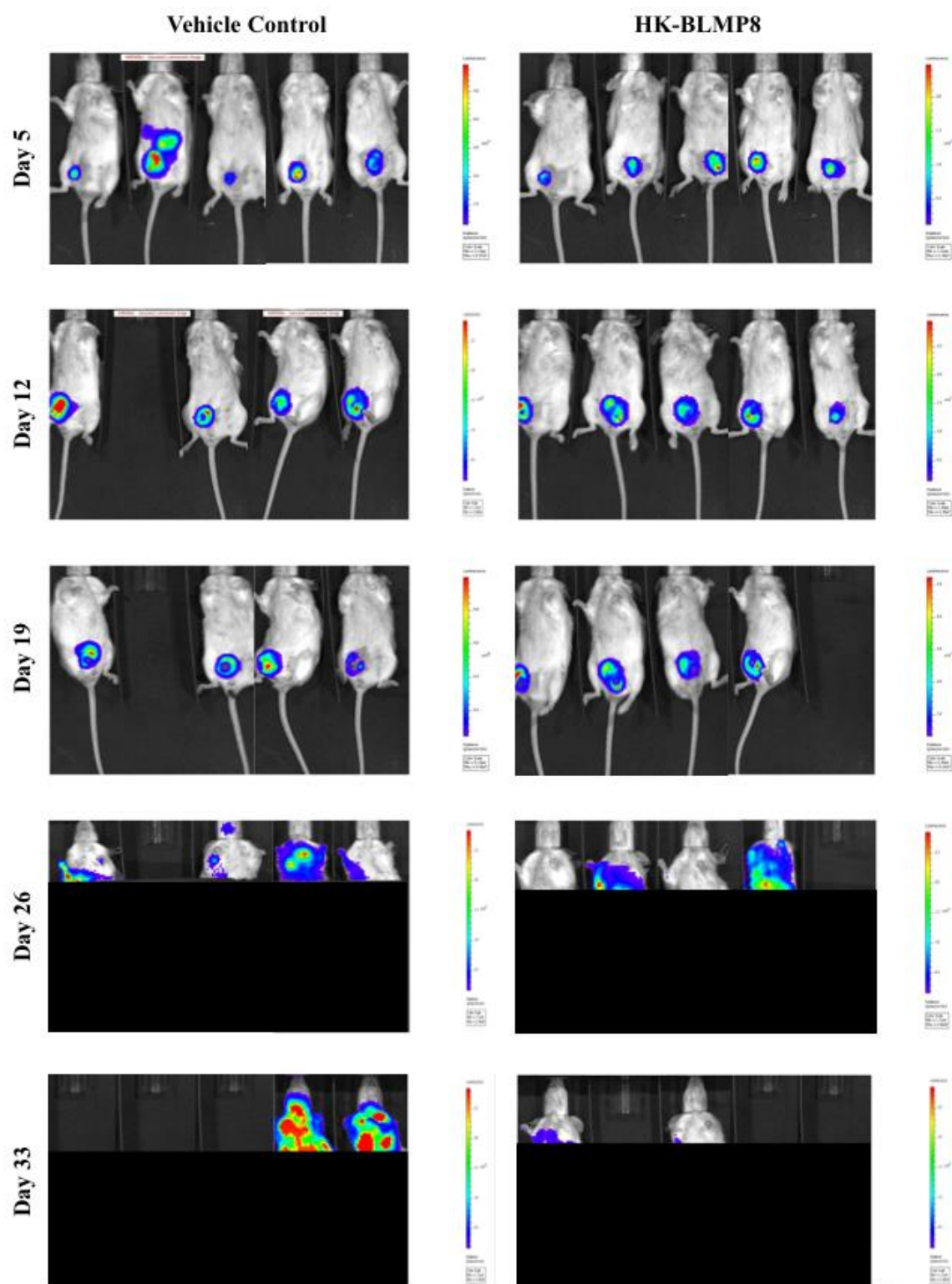
A



B



C

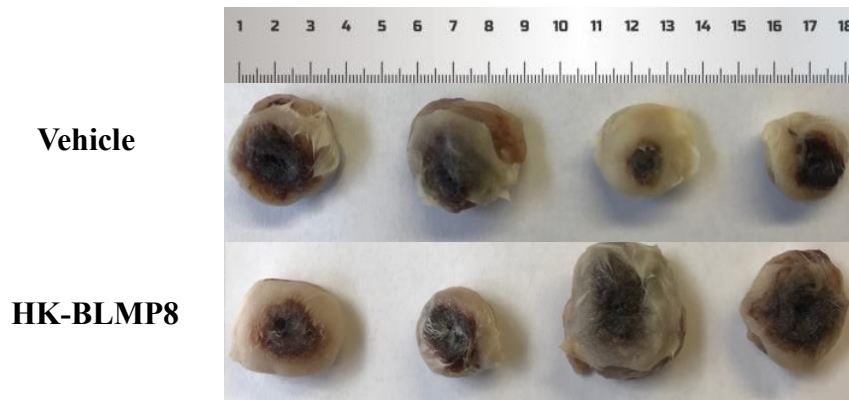


D

Lungs Bearing Metastatic Nodules



Primary Tumors



E

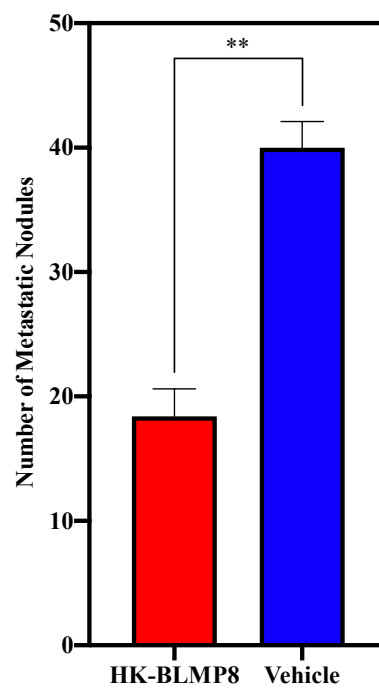


Figure 18: HK-BLMP8 administration reduces metastatic burden but does not improve overall survival *in vivo*

- A. Primary tumor growth curves for vehicle versus HK-BLMP8 treated cohorts (n = 5 mice/cohort). Vehicle and HK-BLMP8 (10mg/kg) were administered subcutaneously thrice week, for twelve weeks. Tumor volumes were calculated using the formula : length x (width)² x 0.52. Tumor volumes are shown as mean ± SEM.
- B. Survival of mice post vehicle or HK-BLMP8 (10mg/kg) administration was monitored. The probability of survival was depicted using Kaplan-Meier curves. ns, p >0.05.
- C. Non-invasive bioluminescence imaging to monitor the effect of vehicle and HK-BLMP8 (10mg/kg) on cancer progression and metastatic burden over five weeks. The luciferase signal and luminescence were assessed in vehicle and HK-BLMP8 treated cohorts respectively.
- D. Representative images of primary tumors and lung metastases in vehicle and HK-BLMP8 treated mice cohorts.
- E. Quantification of metastatic nodules of vehicle and HK-BLMP8 treated mice cohorts (n = 5 /cohort) at experimental endpoint (**, p ≤0.01). Metastatic nodule number shown as mean ± SEM.

Chapter 5: Discussions

Throughout disease progression, tumor cells undergo spatial and functional changes that manifest in a complex sub-clonal architecture, further enhanced by the application of chemotherapeutic drugs (192). The existence of spatial intra-tumoral heterogeneity accounts for the initiation of tumor clonal evolution and subsequent chemoresistance. Tumor cell diversity occurs due to progressive mutational changes that result in distinct cancer cell populations (193). Relapse and metastatic progression after a positive therapeutic effect often occur due to a resistant population that was present before therapy or originated as a result of chemotherapy. Survival, proliferation, and subsequent dominance of this population could be due to features that were absent before therapy. Thus, it is crucial to gain more insight into players implicated in the survival of these chemotherapy-tolerant metastasis-inducing tumor cell populations.

TNBCs demonstrate a lack of response to targeted therapies. Therefore, chemotherapy remains a mainstay in TNBC treatment. Although TNBCs demonstrate chemosensitivity, the evolution of chemoresistance occurs over time. Drug resistance promotes TNBC relapse and is a predilection for the development of distant metastases in organs such as the lung, brain, and liver (194). TNBC's well-documented resistance to chemotherapy and aggressive phenotype provides the ideal setting to study metastatic progression. We selected the 4T1 murine mammary adenocarcinoma model for our study as it accurately portrays stage IV human TNBC (195). Moreover, it has been used to study chemotherapy-mediated metastatic progression (196, 197).

Upon primary tumor development in the 4T1 model, the DNA cross-linking agent cisplatin was administered to inhibit cancer progression. The selection of this chemotherapeutic agent was primarily due to the renewed interest in using platinum salts in the clinical management of human TNBC (198, 199). Although the cisplatin administration failed to elicit any primary tumor response, we report that it exacerbated pulmonary metastasis in the 4T1 murine model of spontaneous metastasis. These observations suggest the possibility of a chemotherapy-induced enrichment of tumor cell populations favoring metastatic progression. While the adverse side

effects of chemotherapeutics have been observed for decades, the role played by chemotherapy in actively triggering metastatic progression has only recently been brought to light (178, 200, 201).

Targeting these drug-tolerant metastases initiating tumor cells was our next logic step forward. As described previously, phage display technology has been used in the isolation and targeting of several molecular targets involved in carcinogenesis. While drugs targeting tumor cells and other stromal components of the TME have been identified using this methodology, the recognition of molecules for selective targeting of drug-tolerant TNBC metastatic tumor cells is yet to be performed. We report the isolation of nine novel peptides by phage display (using a combined 7-mer and 8-mer phage-displayed peptide libraries), which revealed high selectivity and binding efficiency towards tumor cells in the pulmonary metastases of the 4T1 murine adenocarcinoma model. Between each round of bio-panning, the BLMP clones were sequenced, and nine different homing peptides were identified. *In vivo* enrichment and *in vitro* preference towards the cisplatin-resistant 4T1.2 cells, demonstrated by BLMP7 (motif: CLRHSSKIC), prompted its selection for further analysis. BLMP8 (motif: CRAGVGRGC) was also a candidate, owing to its homing to both 4T1 and B16F10 melanoma cells that form lung metastases.

To further validate the binding affinity and to substantiate our proposed hypothesis, phage-displayed BLMP7 and BLMP8 were intravenously injected into mice. The immunofluorescence assay on formalin-fixed paraffin-embedded tissue sections of these mice revealed a pulmonary metastases-specific tropism exhibited by both BLMP7 and BLMP8. The homing of BLMP7 and BLMP8 was also observed in the liver. This can be explained by non-specific entrapment of phage within the reticuloendothelial system of the liver (202, 203). Phage homing specificity was further corroborated by the absence of BLMP7 and BLMP8 localization in control organs such as the brain, kidney, and pancreas. Interestingly, in addition to the pulmonary metastases, phage-displayed BLMP8 also exhibited tropism to primary 4T1 tumors.

In the cisplatin-treated mice cohort, BLMP7 and BLMP8 localization patterns were similar to that of the vehicle-treated cohort. Thus, this suggests that BLMP7 and BLMP8 homing to metastases occur irrespective of chemotherapy *in vivo*. Interestingly, localization of BLMP7 and BLMP8 phage in the kidneys of cisplatin-treated mice was observed. We believe that cisplatin-induced nephrotoxicity is partly responsible for the accumulation of phage in the kidneys. To gain more insight into this unusual phenomenon, we analyzed the homing patterns of BLMP7 and BLMP8 in healthy disease-free C57BL/6 mice. With the exception of liver entrapment, neither BLMP7 nor BLMP8 demonstrated localization to kidneys or other control organs.

To explore the possibility of BLMP homing to the metastases of other cancer types, the localization of both BLMP7 and BLMP8 was further probed in the murine B16F10 melanoma model of experimental metastasis. This model was selected due to lung colonization of the implanted B16F10 melanoma cells (186, 187). Phage displaying BLMP8 demonstrated a high binding efficiency to murine B16F10 cells *in vitro*. Like in the 4T1 murine model, BLMP8 demonstrated a chemotherapy-independent homing to the pulmonary metastases of the B16F10 murine model. However, BLMP7 showed no localization. Thus, this led us to conclude that BLMP8 exhibits cross-tumor type reactivity and homes to pulmonary metastases regardless of cancer subtype. In contrast, BLMP7 demonstrates binding only to TNBC cells. Despite BLMP7 and BLMP8 homing being independent of chemotherapy administration, their metastasis-specific tropism bolsters the novelty of our findings. Further, it underscores the potential of using these peptides in the development of metastases-specific therapeutics with potentially reduced off-target effects.

Analysis of BLMP7 and BLMP8 distribution revealed localization along the invasive edge of pulmonary metastases. This pattern was also demonstrated by BLMP8 in primary tumors. In many cancers, including TNBC, metastasis is facilitated by the transitioning of tumor cells

from a non-motile, epithelial phenotype into a migratory, mesenchymal-like phenotype via EMT (28, 29). An EMT hallmark is the loss of epithelial cadherin (E-cadherin) expression and the concomitant up-regulation of neural cadherin (N-cadherin) (204). This so-called “cadherin switch” is associated with increased migratory behavior and inferior disease prognosis (33). A major consequence of N-cadherin up-regulation is the loss of stable epithelial cell-cell adhesive junctions, apicobasal cell polarity, and epithelial tissue structure, thereby facilitating the dissemination of cancer cells from the primary tumor site. Thus, N-cadherin acquisition is a critical step in metastatic progression (205).

An immunofluorescence assay was performed on formalin-fixed paraffin-embedded tissue sections of mice injected with phage-displayed BLMP7 and BLMP8 inserts. When phage co-localization with epithelial and mesenchymal cadherins was investigated, it was observed that both phage-displayed peptides homed to tumor cells with up-regulated N-cadherin expression. No phage was seen to bind E-cadherin-positive tumor cells in pulmonary metastases. An identical co-localization pattern was observed for phage-displayed BLMP8 in the primary tumors of the 4T1 spontaneous metastasis model, as well as for the pulmonary metastases in the B16F10 experimental metastasis model. These findings were further corroborated in cell culture, where it was observed that phage-displayed BLMP7 and BLMP8 bound better to 4T1.2 murine adenocarcinoma cells with reduced E-cadherin expression. Further, it was noticed both BLMP clones bound to the cell line (TNBC) MDA-MB-231 model, described as a representative of the mesenchymal phenotype of cancer cells (206). These results suggest that BLMP7 and BLMP8 have an affinity for tumor cells exhibiting mesenchymal-like characteristics. Although there are several markers that have to be considered while defining the mesenchymal status of a cancer cell, we segregated cells based on the level of E-cadherin expression (207). Reduced E-cadherin expression is frequently correlated with increased invasion, making it an ideal marker for the identification of metastatic tumor cells (208).

Although localized primary tumors are the source of malignancy burden, it is the metastases that attribute to over 90% of all cancer-associated morbidity and mortality (19). This is the case even in TNBC (20, 209). Our *in vivo* phage-peptide library bio-panning has yielded two metastasis specific peptides demonstrating a unique affinity towards tumor cells with mesenchymal-like features. These findings prompted us to explore the therapeutic potential of these peptides by translating them into agents targeting mesenchymal-like tumor cells, thus curtailing tumor growth and progression. Previous studies have established a strategy of tumor cell ablation via ‘hunter-killer’ peptides (142, 169, 189). Based on this strategy, we successfully coupled our pulmonary metastases homing peptides with an apoptosis-inducing (KLAKLAK)₂ moiety (188).

Hunter-killer peptide versions of both BLMP7 and BLMP8 termed HK-BLMP7 and HK-BLMP8 were synthesized as all D-amino acid peptides to minimize proteolytic cleavage. We first validated biotin-labeled HK-BLMP7 and HK-BLMP8 internalization into mesenchymal-like tumor cells. As expected, both HK-BLMP7 and HK-BLMP8 bound to tumor cells with reduced E-cadherin expression outside the phage context. We next used these novel hunter-killer peptides to reduce tumor cell viability in cell culture. Both HK-BLMP7 and HK-BLMP8 induced concentration-dependent apoptosis. However, only HK-BLMP8 induced apoptosis specifically of tumor cells. Investigation of HK-BLMP8’s mechanism of action revealed that it induced programmed cell death via cleaved caspase-3 activation.

Given our results in cell culture, we proceeded to test HK-BLMP8 *in vivo*, using the 4T1 murine model of spontaneous metastasis. The goal of this study was to; a) determine the working dose at which HK-BLMP8 might limit pulmonary metastatic nodule formation and, b) explore if the reduction in pulmonary metastatic burden might affect overall survival. Using HK-BLMP8, we observed a two-fold reduction in pulmonary metastatic burden. However, the statistical significance of this result is yet to be determined in repeated experiments with larger

animal numbers. Peptide administration did not elicit any primary tumor response, nor did it improve overall survival. The absence of primary tumor response corroborates HK-BLMP8's higher affinity for pulmonary metastases. It should be noted that we administered HK-BLMP8 at a low dose (10mg/kg), to minimize off-target adverse effects on mouse health. The lack of survival improvement could also be due to mice succumbing to metastatic burden at distant sites other than the lungs.

The physiochemical properties of peptides due to electric charge may partly explain the proclivity of the BLMP clones towards tumor cells. Both BLMP7 and BLMP8 have a net positive charge. Therefore, their attraction and binding could be in part due to the negative charge of the tumor cell surface (210, 211). However, peptide homing is also mediated by differentially-expressed receptors (179, 212, 213). Thus, we hypothesize that the BLMP clones might bear a resemblance to the cancer-related ligands, owing to their specificity for tumor cells. To explore this hypothesis, multiple sequence alignment and BLAST analysis were conducted. Through this analysis, we were able to, a) identify promising cancer-specific ligands the BLMP clones were homologous with, b) narrow down the cognate cancer putative receptors, and c) investigate if these receptors mediated EMT activation since the BLMP clones homed to tumor cells with mesenchymal features.

Multiple sequence alignment and BLAST analysis of BLMP7 and BLMP8 revealed their resemblance to cancer-related proteins responsible for mediating chemoresistance and metastatic progression. For BLMP7, BLAST analysis identified Mucin5B (MUC5B) to match BLMP7 with a 66% amino acid similarity. The mucin family of proteins is often implicated in the progression of human carcinomas and hematological malignancies (214). MUC5B is a secreted mucin containing tandem repeat structures composed of prolines, threonines, and serines (214). Aberrant MUC5B expression is mediated by injured alveolar epithelial cells in both idiopathic pulmonary fibrosis (IPF) and lung adenocarcinomas (215, 216). Further, several IPF events such as fibroblast

recruitment and proliferation, the formation of myofibroblastic foci due to EMT, ECM accumulation, and lung remodeling are even observed in cancers (217). MUC5B regulates the IPF phenotype by binding to the promoter region of NF- κ B and subsequently activating downstream signaling (216). The significance of NF- κ B as a prognostic marker and its role in EMT and metastasis has been well-elucidated in breast cancer (218, 219).

Blast Analysis of BLMP8, revealed a 100% amino acid identity with murine latent transforming growth factor-beta binding protein 4 (LTBP4). LTBP4 serves as a TGF β chaperone and also maintains TGF β R stability (220). Further, some studies also suggest that LTBP4 is a crucial regulator of the TGF β /TGF β R signaling axis (221). Moreover, altered LTP4 expression has been observed in the malignant tissue of both murine and human mammary carcinomas (222). Overexpression of TGF β triggers dysregulated TGF β /TGF β R downstream signaling, which is often associated with chemoresistance, EMT induction, and metastatic progression (223, 224). TGF β signaling pathway is a recognized mediator of breast cancer-associated chemoresistance, EMT induction, and metastatic progression (223, 224).

Chapter 6: Conclusions and Future Directions

In this study, we have successfully identified two novel peptides, BLMP7 and BLMP8 through *in vivo* phage-displayed peptide library screening against pulmonary metastases of the 4T1 murine model of spontaneous metastasis in the context of chemotherapy. To this end, no other study has reported metastases-specific peptides. Our data show a high enrichment of the selected peptides over several bio-panning rounds and selective binding to murine and human tumor cell lines exhibiting mesenchymal-like features *in vivo* and *in vitro*. The evolution of novel therapeutics targeting tumor cells with enhanced invasive and migratory potential is a promising step in the clinical management and treatment of metastatic disease. Future analysis underlying binding experiments for these peptides could be useful in the isolation of their cognate receptors. Identification of these metastatic cell surface receptors will help gain more insight into their downstream signaling mechanism counterparts and mechanisms.

Theranostic compounds are a promising class of radioactive contrasting agents. Over the past decade, these agents have been instrumental in improving disease outcomes owing to their ability to accurately facilitate whole-body and intraoperative imaging (225). The metastases-specific tropism by the BLMP clones prompted us to explore the potential of developing these peptides into malignancy-probing theranostic agents. In collaboration with Dr. Ali Azhdarinia (MDACC, Houston), we are conjugating the BLMP clones to radiolabeled domains using bifunctional DOTA and NODAGA chelators (226). We hope to delve deeper and gain more insight into the mechanisms underlying cancer progression through near-infrared fluorescence imaging with these compounds.

Targeted hunter-killer peptides represent a promising class of novel anti-cancer agents. Their therapeutic benefit can be optimized by adjusting properties such as domain length, residue placement, peptide hydrophobicity, and hydrophobic moment (227). Beyond this, future hunter-killer peptides might be designed to promote cell ablation using different cytotoxic domains. Our results provide a glimpse at a potential anti-metastasis therapy combining two levels of

specificity: ‘homing’ to targeted cells and selective apoptosis of such cells upon internalization. HK-BLMP8 is a novel pulmonary metastases-ablating peptide that demonstrates modest benefit when employed *in vivo*. Through the conduction of detailed efficacy studies and the adjustment of peptide properties mentioned above, we hope to potentiate this hunter-killer peptide candidate's overall activity. We believe that using this hunter-killer peptide synergistically with classical chemotherapy agents will not only push the boundaries of existing translational medicine but will potentially revolutionize cancer therapy as it exists (228, 229).

Chapter 7: Bibliography

1. Schnitt, S. J. 2010. Classification and prognosis of invasive breast cancer: from morphology to molecular taxonomy. *Mod Pathol* 23 Suppl 2: S60-64.
2. Sotiriou, C., and L. Pusztai. 2009. Gene-expression signatures in breast cancer. *N Engl J Med* 360: 790-800.
3. Siegel, R. L., K. D. Miller, and A. Jemal. 2020. Cancer statistics, 2020. *CA Cancer J Clin* 70: 7-30.
4. DeSantis, C. E., J. Ma, M. M. Gaudet, L. A. Newman, K. D. Miller, A. Goding Sauer, A. Jemal, and R. L. Siegel. 2019. Breast cancer statistics, 2019. *CA Cancer J Clin* 69: 438-451.
5. Onitilo, A. A., J. M. Engel, R. T. Greenlee, and B. N. Mukesh. 2009. Breast cancer subtypes based on ER/PR and Her2 expression: comparison of clinicopathologic features and survival. *Clin Med Res* 7: 4-13.
6. Li, J., A. M. Gonzalez-Angulo, P. K. Allen, T. K. Yu, W. A. Woodward, N. T. Ueno, A. Lucci, S. Krishnamurthy, Y. Gong, M. L. Bondy, W. Yang, J. S. Willey, M. Cristofanilli, V. Valero, and T. A. Buchholz. 2011. Triple-negative subtype predicts poor overall survival and high locoregional relapse in inflammatory breast cancer. *Oncologist* 16: 1675-1683.
7. van Golen, K. L., L. W. Bao, Q. Pan, F. R. Miller, Z. F. Wu, and S. D. Merajver. 2002. Mitogen activated protein kinase pathway is involved in RhoC GTPase induced motility, invasion and angiogenesis in inflammatory breast cancer. *Clin Exp Metastasis* 19: 301-311.
8. van Golen, K. L. 2003. Inflammatory breast cancer: relationship between growth factor signaling and motility in aggressive cancers. *Breast Cancer Res* 5: 174-179.
9. Baum, M., A. U. Budzar, J. Cuzick, J. Forbes, J. H. Houghton, J. G. Klijn, T. Sahmoud, and A. T. Group. 2002. Anastrozole alone or in combination with tamoxifen versus

- tamoxifen alone for adjuvant treatment of postmenopausal women with early breast cancer: first results of the ATAC randomised trial. *Lancet* 359: 2131-2139.
10. van 't Veer, L. J., H. Dai, M. J. van de Vijver, Y. D. He, A. A. M. Hart, M. Mao, H. L. Peterse, K. van der Kooy, M. J. Marton, A. T. Witteveen, G. J. Schreiber, R. M. Kerkhoven, C. Roberts, P. S. Linsley, R. Bernards, and S. H. Friend. 2002. Gene expression profiling predicts clinical outcome of breast cancer. *Nature* 415: 530-536.
 11. Engel, J., R. Eckel, J. Kerr, M. Schmidt, G. Furstenberger, R. Richter, H. Sauer, H. J. Senn, and D. Holz. 2003. The process of metastatisation for breast cancer. *Eur J Cancer* 39: 1794-1806.
 12. Criscitiello, C., H. A. Azim, Jr., P. C. Schouten, S. C. Linn, and C. Sotiriou. 2012. Understanding the biology of triple-negative breast cancer. *Ann Oncol* 23 Suppl 6: vi13-18.
 13. Lehmann, B. D., J. A. Bauer, X. Chen, M. E. Sanders, A. B. Chakravarthy, Y. Shyr, and J. A. Pietenpol. 2011. Identification of human triple-negative breast cancer subtypes and preclinical models for selection of targeted therapies. *J Clin Invest* 121: 2750-2767.
 14. Suttman, H., M. Retz, F. Paulsen, J. Harder, U. Zwergel, J. Kamradt, B. Wullich, G. Unteregger, M. Stockle, and J. Lehmann. 2008. Antimicrobial peptides of the Cecropin-family show potent antitumor activity against bladder cancer cells. *BMC Urol* 8: 5.
 15. Foulkes, W. D., I. M. Stefansson, P. O. Chappuis, L. R. Begin, J. R. Goffin, N. Wong, M. Trudel, and L. A. Akslen. 2003. Germline BRCA1 mutations and a basal epithelial phenotype in breast cancer. *J Natl Cancer Inst* 95: 1482-1485.
 16. Miki, Y., J. Swensen, D. Shattuck-Eidens, P. A. Futreal, K. Harshman, S. Tavtigian, Q. Liu, C. Cochran, L. M. Bennett, W. Ding, and et al. 1994. A strong candidate for the breast and ovarian cancer susceptibility gene BRCA1. *Science* 266: 66-71.

17. Hartkopf, A. D., F. A. Taran, M. Wallwiener, C. B. Walter, B. Kramer, E. M. Grischke, and S. Y. Brucker. 2016. PD-1 and PD-L1 Immune Checkpoint Blockade to Treat Breast Cancer. *Breast Care (Basel)* 11: 385-390.
18. Nguyen, D. X., P. D. Bos, and J. Massague. 2009. Metastasis: from dissemination to organ-specific colonization. *Nat Rev Cancer* 9: 274-284.
19. Seyfried, T. N., and L. C. Huysentruyt. 2013. On the origin of cancer metastasis. *Crit Rev Oncog* 18: 43-73.
20. Al-Mahmood, S., J. Sapiezynski, O. B. Garbuzenko, and T. Minko. 2018. Metastatic and triple-negative breast cancer: challenges and treatment options. *Drug Deliv Transl Res* 8: 1483-1507.
21. Collett, K., I. M. Stefansson, J. Eide, A. Braaten, H. Wang, G. E. Eide, S. O. Thoresen, W. D. Foulkes, and L. A. Akslen. 2005. A basal epithelial phenotype is more frequent in interval breast cancers compared with screen detected tumors. *Cancer Epidemiol Biomarkers Prev* 14: 1108-1112.
22. Liedtke, C., C. Mazouni, K. R. Hess, F. Andre, A. Tordai, J. A. Mejia, W. F. Symmans, A. M. Gonzalez-Angulo, B. Hennessy, M. Green, M. Cristofanilli, G. N. Hortobagyi, and L. Pusztai. 2008. Response to neoadjuvant therapy and long-term survival in patients with triple-negative breast cancer. *J Clin Oncol* 26: 1275-1281.
23. Sorlie, T., C. M. Perou, R. Tibshirani, T. Aas, S. Geisler, H. Johnsen, T. Hastie, M. B. Eisen, M. van de Rijn, S. S. Jeffrey, T. Thorsen, H. Quist, J. C. Matese, P. O. Brown, D. Botstein, P. E. Lonning, and A. L. Borresen-Dale. 2001. Gene expression patterns of breast carcinomas distinguish tumor subclasses with clinical implications. *Proc Natl Acad Sci U S A* 98: 10869-10874.
24. Bergamaschi, A., Y. H. Kim, P. Wang, T. Sorlie, T. Hernandez-Boussard, P. E. Lonning, R. Tibshirani, A. L. Borresen-Dale, and J. R. Pollack. 2006. Distinct patterns of DNA copy

- number alteration are associated with different clinicopathological features and gene-expression subtypes of breast cancer. *Genes Chromosomes Cancer* 45: 1033-1040.
25. Larue, L., and A. Bellacosa. 2005. Epithelial–mesenchymal transition in development and cancer: role of phosphatidylinositol 3' kinase/AKT pathways. *Oncogene* 24: 7443-7454.
 26. Fristrom, D. 1988. The cellular basis of epithelial morphogenesis. A review. *Tissue Cell* 20: 645-690.
 27. Heerboth, S., G. Housman, M. Leary, M. Longacre, S. Byler, K. Lapinska, A. Willbanks, and S. Sarkar. 2015. EMT and tumor metastasis. *Clin Transl Med* 4: 6.
 28. Kalluri, R., and R. A. Weinberg. 2009. The basics of epithelial-mesenchymal transition. *J Clin Invest* 119: 1420-1428.
 29. Kalluri, R. 2009. EMT: when epithelial cells decide to become mesenchymal-like cells. *J Clin Invest* 119: 1417-1419.
 30. Dykxhoorn, D. M., Y. Wu, H. Xie, F. Yu, A. Lal, F. Petrocca, D. Martinvalet, E. Song, B. Lim, and J. Lieberman. 2009. miR-200 enhances mouse breast cancer cell colonization to form distant metastases. *PLoS One* 4: e7181.
 31. van der Pluijm, G. 2011. Epithelial plasticity, cancer stem cells and bone metastasis formation. *Bone* 48: 37-43.
 32. Brooks, M. D., M. L. Burness, and M. S. Wicha. 2015. Therapeutic Implications of Cellular Heterogeneity and Plasticity in Breast Cancer. *Cell Stem Cell* 17: 260-271.
 33. Hazan, R. B., R. Qiao, R. Keren, I. Badano, and K. Suyama. 2004. Cadherin switch in tumor progression. *Ann N Y Acad Sci* 1014: 155-163.
 34. Lamouille, S., J. Xu, and R. Derynck. 2014. Molecular mechanisms of epithelial-mesenchymal transition. *Nat Rev Mol Cell Biol* 15: 178-196.

35. Voulgari, A., and A. Pintzas. 2009. Epithelial-mesenchymal transition in cancer metastasis: mechanisms, markers and strategies to overcome drug resistance in the clinic. *Biochim Biophys Acta* 1796: 75-90.
36. Liu, T., X. Zhang, M. Shang, Y. Zhang, B. Xia, M. Niu, Y. Liu, and D. Pang. 2013. Dysregulated expression of Slug, vimentin, and E-cadherin correlates with poor clinical outcome in patients with basal-like breast cancer. *J Surg Oncol* 107: 188-194.
37. Soini, Y., H. Tuhkanen, R. Sironen, I. Virtanen, V. Kataja, P. Auvinen, A. Mannermaa, and V. M. Kosma. 2011. Transcription factors zeb1, twist and snail in breast carcinoma. *BMC Cancer* 11: 73.
38. Jeong, H., Y. J. Ryu, J. An, Y. Lee, and A. Kim. 2012. Epithelial-mesenchymal transition in breast cancer correlates with high histological grade and triple-negative phenotype. *Histopathology* 60: E87-95.
39. van Maaren, M. C., L. de Munck, G. H. de Bock, J. J. Jobsen, T. van Dalen, S. C. Linn, P. Poortmans, L. J. A. Strobbe, and S. Siesling. 2016. 10 year survival after breast-conserving surgery plus radiotherapy compared with mastectomy in early breast cancer in the Netherlands: a population-based study. *Lancet Oncol* 17: 1158-1170.
40. Freedman, G. M., P. R. Anderson, T. Li, and N. Nicolaou. 2009. Locoregional recurrence of triple-negative breast cancer after breast-conserving surgery and radiation. *Cancer* 115: 946-951.
41. O'Reilly, E. A., L. Gubbins, S. Sharma, R. Tully, M. H. Guang, K. Weiner-Gorzel, J. McCaffrey, M. Harrison, F. Furlong, M. Kell, and A. McCann. 2015. The fate of chemoresistance in triple negative breast cancer (TNBC). *BBA Clin* 3: 257-275.
42. Cleator, S., W. Heller, and R. C. Coombes. 2007. Triple-negative breast cancer: therapeutic options. *Lancet Oncol* 8: 235-244.

43. Makovec, T. 2019. Cisplatin and beyond: molecular mechanisms of action and drug resistance development in cancer chemotherapy. *Radiol Oncol* 53: 148-158.
44. Bergin, A. R. T., and S. Loi. 2019. Triple-negative breast cancer: recent treatment advances. *F1000Res* 8.
45. Byrski, T., M. Foszczynska-Kloda, T. Huzarski, R. Dent, J. Gronwald, C. Cybulski, T. Debniak, B. Gorski, J. Lubinski, and S. Narod. 2009. Cisplatin chemotherapy in the treatment of BRCA1-positive metastatic breast cancer (MBC). *Journal of Clinical Oncology* 27: 1099-1099.
46. Abal, M., J. M. Andreu, and I. Barasoain. 2003. Taxanes: microtubule and centrosome targets, and cell cycle dependent mechanisms of action. *Curr Cancer Drug Targets* 3: 193-203.
47. Henderson, I. C., D. A. Berry, G. D. Demetri, C. T. Cirrincione, L. J. Goldstein, S. Martino, J. N. Ingle, M. R. Cooper, D. F. Hayes, K. H. Tkaczuk, G. Fleming, J. F. Holland, D. B. Duggan, J. T. Carpenter, E. Frei, 3rd, R. L. Schilsky, W. C. Wood, H. B. Muss, and L. Norton. 2003. Improved outcomes from adding sequential Paclitaxel but not from escalating Doxorubicin dose in an adjuvant chemotherapy regimen for patients with node-positive primary breast cancer. *J Clin Oncol* 21: 976-983.
48. Iglesias, J. 2009. nab-Paclitaxel (Abraxane®): an albumin-bound cytotoxic exploiting natural delivery mechanisms into tumors. *Breast Cancer Research : BCR* 11: S21-S21.
49. Hugh, J., J. Hanson, M. C. Cheang, T. O. Nielsen, C. M. Perou, C. Dumontet, J. Reed, M. Krajewska, I. Treilleux, M. Rupin, E. Magherini, J. Mackey, M. Martin, and C. Vogel. 2009. Breast cancer subtypes and response to docetaxel in node-positive breast cancer: use of an immunohistochemical definition in the BCIRG 001 trial. *J Clin Oncol* 27: 1168-1176.

50. Harris, L. N., G. Broadwater, N. U. Lin, A. Miron, S. J. Schnitt, D. Cowan, J. Lara, I. Bleiweiss, D. Berry, M. Ellis, D. F. Hayes, E. P. Winer, and L. Dressler. 2006. Molecular subtypes of breast cancer in relation to paclitaxel response and outcomes in women with metastatic disease: results from CALGB 9342. *Breast Cancer Res* 8: R66.
51. Szulawska, A., and M. Czyz. 2006. [Molecular mechanisms of anthracyclines action]. *Postepy Hig Med Dosw (Online)* 60: 78-100.
52. Carey, L. A., E. C. Dees, L. Sawyer, L. Gatti, D. T. Moore, F. Collichio, D. W. Ollila, C. I. Sartor, M. L. Graham, and C. M. Perou. 2007. The triple negative paradox: primary tumor chemosensitivity of breast cancer subtypes. *Clin Cancer Res* 13: 2329-2334.
53. Rouzier, R., C. M. Perou, W. F. Symmans, N. Ibrahim, M. Cristofanilli, K. Anderson, K. R. Hess, J. Stec, M. Ayers, P. Wagner, P. Morandi, C. Fan, I. Rabiul, J. S. Ross, G. N. Hortobagyi, and L. Pusztai. 2005. Breast cancer molecular subtypes respond differently to preoperative chemotherapy. *Clin Cancer Res* 11: 5678-5685.
54. Gluz, O., C. Liedtke, N. Gottschalk, L. Pusztai, U. Nitz, and N. Harbeck. 2009. Triple-negative breast cancer--current status and future directions. *Ann Oncol* 20: 1913-1927.
55. Bramati, A., S. Girelli, V. Torri, G. Farina, E. Galfrascoli, S. Piva, A. Moretti, M. C. Dazzani, P. Sburlati, and N. M. La Verde. 2014. Efficacy of biological agents in metastatic triple-negative breast cancer. *Cancer Treat Rev* 40: 605-613.
56. Kroman, N., M. B. Jensen, J. Wohlfahrt, H. T. Mouridsen, P. K. Andersen, and M. Melbye. 2000. Factors influencing the effect of age on prognosis in breast cancer: population based study. *BMJ* 320: 474-478.
57. Joensuu, H., P.-L. Kellokumpu-Lehtinen, R. Huovinen, A. Jukkola-Vuorinen, M. Tanner, R. Kokko, J. Ahlgren, P. Auvinen, P. Bono, and H. Lindman. 2010. Abstract S4-1: FinXX Final 5-Year Analysis: Results of the Randomised, Open-Label, Phase III Trial in Medium-to-High Risk Early Breast Cancer. *Cancer Research* 70: S4-1-S4-1.

58. Verma, S., L. Provencher, and R. Dent. 2011. Emerging trends in the treatment of triple-negative breast cancer in Canada: a survey. *Curr Oncol* 18: 180-190.
59. Bianchini, G., J. M. Balko, I. A. Mayer, M. E. Sanders, and L. Gianni. 2016. Triple-negative breast cancer: challenges and opportunities of a heterogeneous disease. *Nat Rev Clin Oncol* 13: 674-690.
60. Morales, J., L. Li, F. J. Fattah, Y. Dong, E. A. Bey, M. Patel, J. Gao, and D. A. Boothman. 2014. Review of poly (ADP-ribose) polymerase (PARP) mechanisms of action and rationale for targeting in cancer and other diseases. *Crit Rev Eukaryot Gene Expr* 24: 15-28.
61. Farmer, H., N. McCabe, C. J. Lord, A. N. Tutt, D. A. Johnson, T. B. Richardson, M. Santarosa, K. J. Dillon, I. Hickson, C. Knights, N. M. Martin, S. P. Jackson, G. C. Smith, and A. Ashworth. 2005. Targeting the DNA repair defect in BRCA mutant cells as a therapeutic strategy. *Nature* 434: 917-921.
62. Fong, P. C., D. S. Boss, T. A. Yap, A. Tutt, P. Wu, M. Mergui-Roelvink, P. Mortimer, H. Swaisland, A. Lau, M. J. O'Connor, A. Ashworth, J. Carmichael, S. B. Kaye, J. H. Schellens, and J. S. de Bono. 2009. Inhibition of poly(ADP-ribose) polymerase in tumors from BRCA mutation carriers. *N Engl J Med* 361: 123-134.
63. Tutt, A., M. Robson, J. E. Garber, S. M. Domchek, M. W. Audeh, J. N. Weitzel, M. Friedlander, B. Arun, N. Loman, R. K. Schmutzler, A. Wardley, G. Mitchell, H. Earl, M. Wickens, and J. Carmichael. 2010. Oral poly(ADP-ribose) polymerase inhibitor olaparib in patients with BRCA1 or BRCA2 mutations and advanced breast cancer: a proof-of-concept trial. *Lancet* 376: 235-244.
64. O'Shaughnessy, J., C. Osborne, J. Pippen, M. Yoffe, D. Patt, G. Monaghan, C. Rocha, V. Ossovskaya, B. Sherman, and C. Bradley. 2009. Efficacy of BSI-201, a poly (ADP-ribose) polymerase-1 (PARP1) inhibitor, in combination with gemcitabine/carboplatin (G/C) in

- patients with metastatic triple-negative breast cancer (TNBC): Results of a randomized phase II trial. *Journal of Clinical Oncology* 27: 3-3.
65. O'Shaughnessy, J., C. Osborne, J. E. Pippen, M. Yoffe, D. Patt, C. Rocha, I. C. Koo, B. M. Sherman, and C. Bradley. 2011. Iniparib plus chemotherapy in metastatic triple-negative breast cancer. *N Engl J Med* 364: 205-214.
 66. Meric-Bernstam, F., and A. M. Gonzalez-Angulo. 2009. Targeting the mTOR Signaling Network for Cancer Therapy. *Journal of Clinical Oncology* 27: 2278-2287.
 67. Minami, C. A., D. U. Chung, and H. R. Chang. 2011. Management options in triple-negative breast cancer. *Breast Cancer (Auckl)* 5: 175-199.
 68. Neshat, M. S., I. K. Mellingerhoff, C. Tran, B. Stiles, G. Thomas, R. Petersen, P. Frost, J. J. Gibbons, H. Wu, and C. L. Sawyers. 2001. Enhanced sensitivity of PTEN-deficient tumors to inhibition of FRAP/mTOR. *Proceedings of the National Academy of Sciences* 98: 10314-10319.
 69. Beuvink, I., A. Boulay, S. Fumagalli, F. Zilbermann, S. Ruetz, T. O'Reilly, F. Natt, J. Hall, H. A. Lane, and G. Thomas. 2005. The mTOR inhibitor RAD001 sensitizes tumor cells to DNA-damaged induced apoptosis through inhibition of p21 translation. *Cell* 120: 747-759.
 70. Schmid, P., J. Abraham, S. Chan, D. Wheatley, A. M. Brunt, G. Nemsadze, R. D. Baird, Y. H. Park, P. S. Hall, T. Perren, R. C. Stein, L. Mangel, J. M. Ferrero, M. Phillips, J. Conibear, J. Cortes, A. Foxley, E. C. de Bruin, R. McEwen, D. Stetson, B. Dougherty, S. J. Sarker, A. Prendergast, M. McLaughlin-Callan, M. Burgess, C. Lawrence, H. Cartwright, K. Mousa, and N. C. Turner. 2020. Capivasertib Plus Paclitaxel Versus Placebo Plus Paclitaxel As First-Line Therapy for Metastatic Triple-Negative Breast Cancer: The PAKT Trial. *J Clin Oncol* 38: 423-433.

71. Stagg, J., and B. Allard. 2013. Immunotherapeutic approaches in triple-negative breast cancer: latest research and clinical prospects. *Ther Adv Med Oncol* 5: 169-181.
72. Thompson, E., J. M. Taube, H. Elwood, R. Sharma, A. Meeker, H. N. Warzecha, P. Argani, A. Cimino-Mathews, and L. A. Emens. 2016. The immune microenvironment of breast ductal carcinoma in situ. *Mod Pathol* 29: 249-258.
73. Cimino-Mathews, A., E. Thompson, J. M. Taube, X. Ye, Y. Lu, A. Meeker, H. Xu, R. Sharma, K. Lecksell, T. C. Cornish, N. Cuka, P. Argani, and L. A. Emens. 2016. PD-L1 (B7-H1) expression and the immune tumor microenvironment in primary and metastatic breast carcinomas. *Hum Pathol* 47: 52-63.
74. Adams, S., P. Schmid, H. S. Rugo, E. P. Winer, D. Loirat, A. Awada, D. W. Cescon, H. Iwata, M. Campone, R. Nanda, R. Hui, G. Curigliano, D. Toppmeyer, J. O'Shaughnessy, S. Loi, S. Paluch-Shimon, D. Card, J. Zhao, V. Karantza, and J. Cortes. 2017. Phase 2 study of pembrolizumab (pembro) monotherapy for previously treated metastatic triple-negative breast cancer (mTNBC): KEYNOTE-086 cohort A. *Journal of Clinical Oncology* 35: 1008-1008.
75. Nanda, R., L. Q. Chow, E. C. Dees, R. Berger, S. Gupta, R. Geva, L. Pusztai, K. Pathiraja, G. Aktan, J. D. Cheng, V. Karantza, and L. Buisseret. 2016. Pembrolizumab in Patients With Advanced Triple-Negative Breast Cancer: Phase Ib KEYNOTE-012 Study. *J Clin Oncol* 34: 2460-2467.
76. Adams, S., P. Schmid, H. S. Rugo, E. P. Winer, D. Loirat, A. Awada, D. W. Cescon, H. Iwata, M. Campone, R. Nanda, R. Hui, G. Curigliano, D. Toppmeyer, J. O'Shaughnessy, S. Loi, S. Paluch-Shimon, A. R. Tan, D. Card, J. Zhao, V. Karantza, and J. Cortes. 2019. Pembrolizumab monotherapy for previously treated metastatic triple-negative breast cancer: cohort A of the phase II KEYNOTE-086 study. *Ann Oncol* 30: 397-404.

77. Emens, L. A., C. Cruz, J. P. Eder, F. Braiteh, C. Chung, S. M. Tolaney, I. Kuter, R. Nanda, P. A. Cassier, J. P. Delord, M. S. Gordon, E. ElGabry, C. W. Chang, I. Sarkar, W. Grossman, C. O'Hear, M. Fasso, L. Molinero, and P. Schmid. 2019. Long-term Clinical Outcomes and Biomarker Analyses of Atezolizumab Therapy for Patients With Metastatic Triple-Negative Breast Cancer: A Phase 1 Study. *JAMA Oncol* 5: 74-82.
78. Schmid, P., S. Adams, H. S. Rugo, A. Schneeweiss, C. H. Barrios, H. Iwata, V. Diéras, R. Hegg, S.-A. Im, G. Shaw Wright, V. Henschel, L. Molinero, S. Y. Chui, R. Funke, A. Husain, E. P. Winer, S. Loi, and L. A. Emens. 2018. Atezolizumab and Nab-Paclitaxel in Advanced Triple-Negative Breast Cancer. *New England Journal of Medicine* 379: 2108-2121.
79. Davis, N. M., M. Sokolosky, K. Stadelman, S. L. Abrams, M. Libra, S. Candido, F. Nicoletti, J. Polesel, R. Maestro, A. D'Assoro, L. Drobot, D. Rakus, A. Gizak, P. Laidler, J. Dulińska-Litewka, J. Basecke, S. Mijatovic, D. Maksimovic-Ivanic, G. Montalto, M. Cervello, T. L. Fitzgerald, Z. N. Demidenko, A. M. Martelli, L. Cocco, L. S. Steelman, and J. A. McCubrey. 2014. Deregulation of the EGFR/PI3K/PTEN/Akt/mTORC1 pathway in breast cancer: possibilities for therapeutic intervention. *Oncotarget* 5.
80. Wang, W. M., Z. L. Zhao, S. R. Ma, G. T. Yu, B. Liu, L. Zhang, W. F. Zhang, A. B. Kulkarni, Z. J. Sun, and Y. F. Zhao. 2015. Epidermal growth factor receptor inhibition reduces angiogenesis via hypoxia-inducible factor-1alpha and Notch1 in head neck squamous cell carcinoma. *PLoS One* 10: e0119723.
81. Patel, D., R. Bassi, A. Hooper, M. Prewett, D. J. Hicklin, and X. Kang. 2009. Anti-epidermal growth factor receptor monoclonal antibody cetuximab inhibits EGFR/HER-2 heterodimerization and activation. *Int J Oncol* 34: 25-32.
82. Srivastava, R. M., S. C. Lee, P. A. Andrade Filho, C. A. Lord, H.-B. Jie, H. C. Davidson, A. López-Albaitero, S. P. Gibson, W. E. Gooding, S. Ferrone, and R. L. Ferris. 2013.

- Cetuximab-Activated Natural Killer and Dendritic Cells Collaborate to Trigger Tumor Antigen-Specific T-cell Immunity in Head and Neck Cancer Patients. *Clinical Cancer Research* 19: 1858-1872.
83. Dechant, M., W. Weisner, S. Berger, M. Peipp, T. Beyer, T. Schneider-Merck, J. J. Lammerts van Bueren, W. K. Bleeker, P. W. H. I. Parren, J. G. J. van de Winkel, and T. Valerius. 2008. Complement-Dependent Tumor Cell Lysis Triggered by Combinations of Epidermal Growth Factor Receptor Antibodies. *Cancer Research* 68: 4998-5003.
 84. Prewett, M. C., A. T. Hooper, R. Bassi, L. M. Ellis, H. W. Waksal, and D. J. Hicklin. 2002. Enhanced Antitumor Activity of Anti-epidermal Growth Factor Receptor Monoclonal Antibody IMC-C225 in Combination with Irinotecan (CPT-11) against Human Colorectal Tumor Xenografts. *Clinical Cancer Research* 8: 994-1003.
 85. Baselga, J., L. Norton, H. Masui, A. Pandiella, K. Coplan, W. H. Miller, Jr., and J. Mendelsohn. 1993. Antitumor effects of doxorubicin in combination with anti-epidermal growth factor receptor monoclonal antibodies. *J Natl Cancer Inst* 85: 1327-1333.
 86. Baselga, J., P. Gomez, R. Greil, S. Braga, M. A. Climent, A. M. Wardley, B. Kaufman, S. M. Stemmer, A. Pego, A. Chan, J. C. Goeminne, M. P. Graas, M. J. Kennedy, E. M. Ciruelos Gil, A. Schneeweiss, A. Zubel, J. Groos, H. Melezinkova, and A. Awada. 2013. Randomized phase II study of the anti-epidermal growth factor receptor monoclonal antibody cetuximab with cisplatin versus cisplatin alone in patients with metastatic triple-negative breast cancer. *J Clin Oncol* 31: 2586-2592.
 87. Liu, T., R. Yacoub, L. D. Taliaferro-Smith, S. Y. Sun, T. R. Graham, R. Dolan, C. Lobo, M. Tighiouart, L. Yang, A. Adams, and R. M. O'Regan. 2011. Combinatorial effects of lapatinib and rapamycin in triple-negative breast cancer cells. *Mol Cancer Ther* 10: 1460-1469.

88. O'Shaughnessy, J., V. Dieras, J. Glaspy, A. Brufsky, K. Miller, D. Miles, P. Koralewski, S. Phan, and S. Bhattacharya. 2009. Comparison of Subgroup Analyses of PFS from Three Phase III Studies of Bevacizumab in Combination with Chemotherapy in Patients with HER2-Negative Metastatic Breast Cancer (MBC). *Cancer Research* 69: 207-207.
89. Gray, R., S. Bhattacharya, C. Bowden, K. Miller, and R. L. Comis. 2009. Independent review of E2100: a phase III trial of bevacizumab plus paclitaxel versus paclitaxel in women with metastatic breast cancer. *J Clin Oncol* 27: 4966-4972.
90. Miles, D. W., A. Chan, L. Y. Dirix, J. Cortés, X. Pivot, P. Tomczak, T. Delozier, J. H. Sohn, L. Provencher, F. Puglisi, N. Harbeck, G. G. Steger, A. Schneeweiss, A. M. Wardley, A. Chlistalla, and G. Romieu. 2010. Phase III Study of Bevacizumab Plus Docetaxel Compared With Placebo Plus Docetaxel for the First-Line Treatment of Human Epidermal Growth Factor Receptor 2–Negative Metastatic Breast Cancer. *Journal of Clinical Oncology* 28: 3239-3247.
91. Untch, M., S. Loibl, J. Bischoff, H. Eidtmann, M. Kaufmann, J. U. Blohmer, J. Hilfrich, D. Strumberg, P. A. Fasching, R. Kreienberg, H. Tesch, C. Hanusch, B. Gerber, M. Rezai, C. Jackisch, J. Huober, T. Kuhn, V. Nekljudova, G. von Minckwitz, G. German Breast, and G. Arbeitsgemeinschaft Gynakologische Onkologie-Breast Study. 2012. Lapatinib versus trastuzumab in combination with neoadjuvant anthracycline-taxane-based chemotherapy (GeparQuinto, GBG 44): a randomised phase 3 trial. *Lancet Oncol* 13: 135-144.
92. Crown, J., J. O'Shaughnessy, and G. Gullo. 2012. Emerging targeted therapies in triple-negative breast cancer. *Ann Oncol* 23 Suppl 6: vi56-65.
93. Robey, R. W., K. M. Pluchino, M. D. Hall, A. T. Fojo, S. E. Bates, and M. M. Gottesman. 2018. Revisiting the role of ABC transporters in multidrug-resistant cancer. *Nat Rev Cancer* 18: 452-464.

94. Aniogo, E. C., B. Plackal Adimuriyil George, and H. Abrahamse. 2019. The role of photodynamic therapy on multidrug resistant breast cancer. *Cancer Cell International* 19: 91.
95. Schwarz, B., K. Weise, O. Bach, and K. Bach. 1976. [Structural and functional conception of in-patient and ambulatory psychiatric care in Leipzig]. *Psychiatr Neurol Med Psychol (Leipz)* 28: 307-313.
96. Giaccone, G., and H. M. Pinedo. 1996. Drug Resistance. *Oncologist* 1: 82-87.
97. Fedier, A., V. A. Schwarz, H. Walt, R. D. Carpin, U. Haller, and D. Fink. 2001. Resistance to topoisomerase poisons due to loss of DNA mismatch repair. *Int J Cancer* 93: 571-576.
98. Foroni, C., M. Brogini, D. Generali, and G. Damia. 2012. Epithelial-mesenchymal transition and breast cancer: role, molecular mechanisms and clinical impact. *Cancer Treat Rev* 38: 689-697.
99. Kajita, M., K. N. McClinic, and P. A. Wade. 2004. Aberrant expression of the transcription factors snail and slug alters the response to genotoxic stress. *Mol Cell Biol* 24: 7559-7566.
100. Li, Q. Q., J. D. Xu, W. J. Wang, X. X. Cao, Q. Chen, F. Tang, Z. Q. Chen, X. P. Liu, and Z. D. Xu. 2009. Twist1-mediated adriamycin-induced epithelial-mesenchymal transition relates to multidrug resistance and invasive potential in breast cancer cells. *Clin Cancer Res* 15: 2657-2665.
101. Saxena, M., M. A. Stephens, H. Pathak, and A. Rangarajan. 2011. Transcription factors that mediate epithelial-mesenchymal transition lead to multidrug resistance by upregulating ABC transporters. *Cell Death Dis* 2: e179.
102. Li, J., and B. P. Zhou. 2011. Activation of beta-catenin and Akt pathways by Twist are critical for the maintenance of EMT associated cancer stem cell-like characters. *BMC Cancer* 11: 49.

103. Bhola, N. E., J. M. Balko, T. C. Dugger, M. G. Kuba, V. Sanchez, M. Sanders, J. Stanford, R. S. Cook, and C. L. Arteaga. 2013. TGF-beta inhibition enhances chemotherapy action against triple-negative breast cancer. *J Clin Invest* 123: 1348-1358.
104. Mani, S. A., W. Guo, M. J. Liao, E. N. Eaton, A. Ayyanan, A. Y. Zhou, M. Brooks, F. Reinhard, C. C. Zhang, M. Shipitsin, L. L. Campbell, K. Polyak, C. Brisken, J. Yang, and R. A. Weinberg. 2008. The epithelial-mesenchymal transition generates cells with properties of stem cells. *Cell* 133: 704-715.
105. Samanta, D., D. M. Gilkes, P. Chaturvedi, L. Xiang, and G. L. Semenza. 2014. Hypoxia-inducible factors are required for chemotherapy resistance of breast cancer stem cells. *Proc Natl Acad Sci U S A* 111: E5429-5438.
106. Lee, S. J., H. P. Kim, Y. Jin, A. M. Choi, and S. W. Ryter. 2011. Beclin 1 deficiency is associated with increased hypoxia-induced angiogenesis. *Autophagy* 7: 829-839.
107. Gerweck, L. E., S. Vijayappa, and S. Kozin. 2006. Tumor pH controls the in vivo efficacy of weak acid and base chemotherapeutics. *Mol Cancer Ther* 5: 1275-1279.
108. Chouaib, S., M. Z. Noman, K. Kosmatopoulos, and M. A. Curran. 2017. Hypoxic stress: obstacles and opportunities for innovative immunotherapy of cancer. *Oncogene* 36: 439-445.
109. Cosse, J. P., and C. Michiels. 2008. Tumour hypoxia affects the responsiveness of cancer cells to chemotherapy and promotes cancer progression. *Anticancer Agents Med Chem* 8: 790-797.
110. Huang, P., D.-j. Ouyang, S. Chang, M.-y. Li, L. Li, Q.-y. Li, R. Zeng, Q.-y. Zou, J. Su, P. Zhao, L. Pei, and W.-j. Yi. 2018. Chemotherapy-driven increases in the CDKN1A/PTN/PTPRZ1 axis promote chemoresistance by activating the NF-κB pathway in breast cancer cells. *Cell Communication and Signaling* 16: 92.
111. D'Ignazio, L., and S. Rocha. 2016. Hypoxia Induced NF-kappaB. *Cells* 5.

112. Ueng, S. H., S. C. Chen, Y. S. Chang, S. Hsueh, Y. C. Lin, H. P. Chien, Y. F. Lo, S. C. Shen, and C. Hsueh. 2012. Phosphorylated mTOR expression correlates with poor outcome in early-stage triple negative breast carcinomas. *Int J Clin Exp Pathol* 5: 806-813.
113. Steelman, L. S., P. M. Navolanic, M. L. Sokolosky, J. R. Taylor, B. D. Lehmann, W. H. Chappell, S. L. Abrams, E. W. Wong, K. M. Stadelman, D. M. Terrian, N. R. Leslie, A. M. Martelli, F. Stivala, M. Libra, R. A. Franklin, and J. A. McCubrey. 2008. Suppression of PTEN function increases breast cancer chemotherapeutic drug resistance while conferring sensitivity to mTOR inhibitors. *Oncogene* 27: 4086-4095.
114. Li, L., and A. H. Ross. 2007. Why is PTEN an important tumor suppressor? *J Cell Biochem* 102: 1368-1374.
115. Guanizo, A. C., C. D. Fernando, D. J. Garama, and D. J. Gough. 2018. STAT3: a multifaceted oncoprotein. *Growth Factors* 36: 1-14.
116. Hartman, Z. C., G. M. Poage, P. den Hollander, A. Tsimelzon, J. Hill, N. Panupinthu, Y. Zhang, A. Mazumdar, S. G. Hilsenbeck, G. B. Mills, and P. H. Brown. 2013. Growth of triple-negative breast cancer cells relies upon coordinate autocrine expression of the proinflammatory cytokines IL-6 and IL-8. *Cancer Res* 73: 3470-3480.
117. Sirkisoon, S. R., R. L. Carpenter, T. Rimkus, A. Anderson, A. Harrison, A. M. Lange, G. Jin, K. Watabe, and H. W. Lo. 2018. Interaction between STAT3 and GLI1/tGLI1 oncogenic transcription factors promotes the aggressiveness of triple-negative breast cancers and HER2-enriched breast cancer. *Oncogene* 37: 2502-2514.
118. Wang, K., X. Zhu, K. Zhang, Y. Yin, Y. Chen, and T. Zhang. 2018. Interleukin-6 contributes to chemoresistance in MDA-MB-231 cells via targeting HIF-1 α . *J Biochem Mol Toxicol* 32: e22039.

119. Asiedu, M. K., J. N. Ingle, M. D. Behrens, D. C. Radisky, and K. L. Knutson. 2011. TGFbeta/TNF(alpha)-mediated epithelial-mesenchymal transition generates breast cancer stem cells with a claudin-low phenotype. *Cancer Res* 71: 4707-4719.
120. Xu, X., L. Zhang, X. He, P. Zhang, C. Sun, X. Xu, Y. Lu, and F. Li. 2018. TGF-beta plays a vital role in triple-negative breast cancer (TNBC) drug-resistance through regulating stemness, EMT and apoptosis. *Biochem Biophys Res Commun* 502: 160-165.
121. Ng, L. F., P. Kaur, N. Bunnag, J. Suresh, I. C. H. Sung, Q. H. Tan, J. Gruber, and N. S. Tolwinski. 2019. WNT Signaling in Disease. *Cells* 8.
122. Dey, N., B. G. Barwick, C. S. Moreno, M. Ordanic-Kodani, Z. Chen, G. Oprea-Ilie, W. Tang, C. Catzavelos, K. F. Kerstann, G. W. Sledge, Jr., M. Abramovitz, M. Bouzyk, P. De, and B. R. Leyland-Jones. 2013. Wnt signaling in triple negative breast cancer is associated with metastasis. *BMC Cancer* 13: 537.
123. Xu, J., J. R. Prosperi, N. Choudhury, O. I. Olopade, and K. H. Goss. 2015. beta-Catenin is required for the tumorigenic behavior of triple-negative breast cancer cells. *PLoS One* 10: e0117097.
124. Shen, M., C. Dong, X. Ruan, W. Yan, M. Cao, D. Pizzo, X. Wu, L. Yang, L. Liu, X. Ren, and S. E. Wang. 2019. Chemotherapy-Induced Extracellular Vesicle miRNAs Promote Breast Cancer Stemness by Targeting ONECUT2. *Cancer Res* 79: 3608-3621.
125. Pohl, S. G., N. Brook, M. Agostino, F. Arfuso, A. P. Kumar, and A. Dharmarajan. 2017. Wnt signaling in triple-negative breast cancer. *Oncogenesis* 6: e310.
126. Park, H. S., M. H. Jang, E. J. Kim, H. J. Kim, H. J. Lee, Y. J. Kim, J. H. Kim, E. Kang, S. W. Kim, I. A. Kim, and S. Y. Park. 2014. High EGFR gene copy number predicts poor outcome in triple-negative breast cancer. *Mod Pathol* 27: 1212-1222.

127. Zhang, M., X. Zhang, S. Zhao, Y. Wang, W. Di, G. Zhao, M. Yang, and Q. Zhang. 2014. Prognostic value of survivin and EGFR protein expression in triple-negative breast cancer (TNBC) patients. *Target Oncol* 9: 349-357.
128. Meyer zu Schwabedissen, H. E., M. Grube, A. Dreisbach, G. Jedlitschky, K. Meissner, K. Linnemann, C. Fusch, C. A. Ritter, U. Volker, and H. K. Kroemer. 2006. Epidermal growth factor-mediated activation of the map kinase cascade results in altered expression and function of ABCG2 (BCRP). *Drug Metab Dispos* 34: 524-533.
129. Farabaugh, S. M., D. N. Boone, and A. V. Lee. 2015. Role of IGF1R in Breast Cancer Subtypes, Stemness, and Lineage Differentiation. *Front Endocrinol (Lausanne)* 6: 59.
130. Yuan, J., Z. Yin, K. Tao, G. Wang, and J. Gao. 2018. Function of insulin-like growth factor 1 receptor in cancer resistance to chemotherapy. *Oncol Lett* 15: 41-47.
131. Mohammed, M. K., C. Shao, J. Wang, Q. Wei, X. Wang, Z. Collier, S. Tang, H. Liu, F. Zhang, J. Huang, D. Guo, M. Lu, F. Liu, J. Liu, C. Ma, L. L. Shi, A. Athiviraham, T. C. He, and M. J. Lee. 2016. Wnt/beta-catenin signaling plays an ever-expanding role in stem cell self-renewal, tumorigenesis and cancer chemoresistance. *Genes Dis* 3: 11-40.
132. Sawyers, C. 2004. Targeted cancer therapy. *Nature* 432: 294-297.
133. Scodeller, P., and E. K. Asciutto. 2020. Targeting Tumors Using Peptides. *Molecules* 25.
134. Boohaker, R. J., M. W. Lee, P. Vishnubhotla, J. M. Perez, and A. R. Khaled. 2012. The use of therapeutic peptides to target and to kill cancer cells. *Curr Med Chem* 19: 3794-3804.
135. Hayashi, M. A., F. Ducancel, and K. Konno. 2012. Natural Peptides with Potential Applications in Drug Development, Diagnosis, and/or Biotechnology. *Int J Pept* 2012: 757838.
136. Smith, G. P. 1985. Filamentous fusion phage: novel expression vectors that display cloned antigens on the virion surface. *Science* 228: 1315-1317.

137. O'Neil, K. T., R. H. Hoess, S. A. Jackson, N. S. Ramachandran, S. A. Mousa, and W. F. DeGrado. 1992. Identification of novel peptide antagonists for GPIIb/IIIa from a conformationally constrained phage peptide library. *Proteins* 14: 509-515.
138. Kim, S., D. Kim, H. H. Jung, I. H. Lee, J. I. Kim, J. Y. Suh, and S. Jon. 2012. Bio-inspired design and potential biomedical applications of a novel class of high-affinity peptides. *Angew Chem Int Ed Engl* 51: 1890-1894.
139. Silva, V. L., D. Ferreira, F. L. Nobrega, I. M. Martins, L. D. Kluskens, and L. R. Rodrigues. 2016. Selection of Novel Peptides Homing the 4T1 CELL Line: Exploring Alternative Targets for Triple Negative Breast Cancer. *PLoS One* 11: e0161290.
140. Pasqualini, R., and E. Ruoslahti. 1996. Organ targeting in vivo using phage display peptide libraries. *Nature* 380: 364-366.
141. Odermatt, A., A. Audige, C. Frick, B. Vogt, B. M. Frey, F. J. Frey, and L. Mazzucchelli. 2001. Identification of receptor ligands by screening phage-display peptide libraries ex vivo on microdissected kidney tubules. *J Am Soc Nephrol* 12: 308-316.
142. Arap, W., M. G. Kolonin, M. Trepel, J. Lahdenranta, M. Cardo-Vila, R. J. Giordano, P. J. Mintz, P. U. Ardel, V. J. Yao, C. I. Vidal, L. Chen, A. Flamm, H. Valtanen, L. M. Weavind, M. E. Hicks, R. E. Pollock, G. H. Botz, C. D. Bucana, E. Koivunen, D. Cahill, P. Troncoso, K. A. Baggerly, R. D. Pentz, K. A. Do, C. J. Logothetis, and R. Pasqualini. 2002. Steps toward mapping the human vasculature by phage display. *Nat Med* 8: 121-127.
143. Ruoslahti, E., and M. D. Pierschbacher. 1987. New perspectives in cell adhesion: RGD and integrins. *Science* 238: 491-497.
144. Pasqualini, R., E. Koivunen, and E. Ruoslahti. 1997. Alpha v integrins as receptors for tumor targeting by circulating ligands. *Nat Biotechnol* 15: 542-546.

145. Arap, W., R. Pasqualini, and E. Ruoslahti. 1998. Cancer treatment by targeted drug delivery to tumor vasculature in a mouse model. *Science* 279: 377-380.
146. Pasqualini, R., E. Koivunen, R. Kain, J. Lahdenranta, M. Sakamoto, A. Stryhn, R. A. Ashmun, L. H. Shapiro, W. Arap, and E. Ruoslahti. 2000. Aminopeptidase N is a receptor for tumor-homing peptides and a target for inhibiting angiogenesis. *Cancer Res* 60: 722-727.
147. Wierzbicka-Patynowski, I., and J. E. Schwarzbauer. 2003. The ins and outs of fibronectin matrix assembly. *J Cell Sci* 116: 3269-3276.
148. Kim, H., Y. Lee, I. H. Lee, S. Kim, D. Kim, P. E. Saw, J. Lee, M. Choi, Y. C. Kim, and S. Jon. 2014. Synthesis and therapeutic evaluation of an aptide-docetaxel conjugate targeting tumor-associated fibronectin. *J Control Release* 178: 118-124.
149. Saw, P. E., S. Kim, I. H. Lee, J. Park, M. Yu, J. Lee, J. I. Kim, and S. Jon. 2013. Aptide-conjugated liposome targeting tumor-associated fibronectin for glioma therapy. *J Mater Chem B* 1: 4723-4726.
150. Lingasamy, P., A. Tobi, K. Kurm, S. Kopanchuk, A. Sudakov, M. Salumae, T. Ratsep, T. Asser, R. Bjerkvig, and T. Teesalu. 2020. Tumor-penetrating peptide for systemic targeting of Tenascin-C. *Sci Rep* 10: 5809.
151. Yeow, Y. L., V. R. Kotamraju, X. Wang, M. Chopra, N. Azme, J. Wu, T. D. Schoep, D. S. Delaney, K. Feindel, J. Li, K. M. Kennedy, W. M. Allen, B. F. Kennedy, I. Larma, D. D. Sampson, L. M. Mahakian, B. Z. Fite, H. Zhang, T. Friman, A. P. Mann, F. A. Aziz, M. P. Kumarasinghe, M. Johansson, H. C. Ee, G. Yeoh, L. Mou, K. W. Ferrara, H. Billiran, R. Ganss, E. Ruoslahti, and J. Hamzah. 2019. Immune-mediated ECM depletion improves tumour perfusion and payload delivery. *EMBO Mol Med* 11: e10923.

152. Koivunen, E., W. Arap, H. Valtanen, A. Rainisalo, O. P. Medina, P. Heikkila, C. Kantor, C. G. Gahmberg, T. Salo, Y. T. Konttinen, T. Sorsa, E. Ruoslahti, and R. Pasqualini. 1999. Tumor targeting with a selective gelatinase inhibitor. *Nat Biotechnol* 17: 768-774.
153. Liu, T., C. Han, S. Wang, P. Fang, Z. Ma, L. Xu, and R. Yin. 2019. Cancer-associated fibroblasts: an emerging target of anti-cancer immunotherapy. *Journal of Hematology & Oncology* 12: 86.
154. Brinton, L. T., D. K. Bauknight, S. S. Dasa, and K. A. Kelly. 2016. PHASTpep: Analysis Software for Discovery of Cell-Selective Peptides via Phage Display and Next-Generation Sequencing. *PLoS One* 11: e0155244.
155. Goodson, R. J., M. V. Doyle, S. E. Kaufman, and S. Rosenberg. 1994. High-affinity urokinase receptor antagonists identified with bacteriophage peptide display. *Proc Natl Acad Sci U S A* 91: 7129-7133.
156. Chanmee, T., P. Ontong, K. Konno, and N. Itano. 2014. Tumor-associated macrophages as major players in the tumor microenvironment. *Cancers (Basel)* 6: 1670-1690.
157. Guo, C., A. Buranych, D. Sarkar, P. B. Fisher, and X. Y. Wang. 2013. The role of tumor-associated macrophages in tumor vascularization. *Vasc Cell* 5: 20.
158. Cieslewicz, M., J. Tang, J. L. Yu, H. Cao, M. Zavaljevski, K. Motoyama, A. Lieber, E. W. Raines, and S. H. Pun. 2013. Targeted delivery of proapoptotic peptides to tumor-associated macrophages improves survival. *Proc Natl Acad Sci U S A* 110: 15919-15924.
159. Scodeller, P., L. Simon-Gracia, S. Kopanchuk, A. Tobi, K. Kilk, P. Saalik, K. Kurm, M. L. Squadrito, V. R. Kotamraju, A. Rinken, M. De Palma, E. Ruoslahti, and T. Teesalu. 2017. Precision Targeting of Tumor Macrophages with a CD206 Binding Peptide. *Sci Rep* 7: 14655.
160. Saw, P. E., and E.-W. Song. 2019. Phage display screening of therapeutic peptide for cancer targeting and therapy. *Protein & Cell* 10: 787-807.

161. Li, Z., R. Zhao, X. Wu, Y. Sun, M. Yao, J. Li, Y. Xu, and J. Gu. 2005. Identification and characterization of a novel peptide ligand of epidermal growth factor receptor for targeted delivery of therapeutics. *FASEB J* 19: 1978-1985.
162. Hamzeh-Mivehroud, M., A. Mahmoudpour, and S. Dastmalchi. 2012. Identification of new peptide ligands for epidermal growth factor receptor using phage display and computationally modeling their mode of binding. *Chem Biol Drug Des* 79: 246-259.
163. Ghosh, S., C. A. Sullivan, M. P. Zerkowski, A. M. Molinaro, D. L. Rimm, R. L. Camp, and G. G. Chung. 2008. High levels of vascular endothelial growth factor and its receptors (VEGFR-1, VEGFR-2, neuropilin-1) are associated with worse outcome in breast cancer. *Hum Pathol* 39: 1835-1843.
164. Wulfig, P., C. Kersting, H. Buerger, B. Mattsson, R. Mesters, C. Gustmann, B. Hinrichs, J. Tio, W. Bocker, and L. Kiesel. 2005. Expression patterns of angiogenic and lymphangiogenic factors in ductal breast carcinoma in situ. *Br J Cancer* 92: 1720-1728.
165. Duff, S. E., M. Jeziorska, D. D. Rosa, S. Kumar, N. Haboubi, D. Sherlock, S. T. O'Dwyer, and G. C. Jayson. 2006. Vascular endothelial growth factors and receptors in colorectal cancer: implications for anti-angiogenic therapy. *Eur J Cancer* 42: 112-117.
166. Qin, X., Y. Wan, M. Li, X. Xue, S. Wu, C. Zhang, Y. You, W. Wang, C. Jiang, Y. Liu, W. Zhu, Y. Ran, Z. Zhang, W. Han, and Y. Zhang. 2007. Identification of a novel peptide ligand of human vascular endothelial growth factor receptor 3 for targeted tumour diagnosis and therapy. *J Biochem* 142: 79-85.
167. Giordano, R. J., M. Cardo-Vila, J. Lahdenranta, R. Pasqualini, and W. Arap. 2001. Biopanning and rapid analysis of selective interactive ligands. *Nat Med* 7: 1249-1253.
168. Johnstone, C. N., A. Chand, T. L. Putoczki, and M. Ernst. 2015. Emerging roles for IL-11 signaling in cancer development and progression: Focus on breast cancer. *Cytokine Growth Factor Rev* 26: 489-498.

169. Zurita, A. J., P. Troncoso, M. Cardo-Vila, C. J. Logothetis, R. Pasqualini, and W. Arap. 2004. Combinatorial screenings in patients: the interleukin-11 receptor alpha as a candidate target in the progression of human prostate cancer. *Cancer Res* 64: 435-439.
170. Hartmann, L. C., G. L. Keeney, W. L. Lingle, T. J. Christianson, B. Varghese, D. Hillman, A. L. Oberg, and P. S. Low. 2007. Folate receptor overexpression is associated with poor outcome in breast cancer. *Int J Cancer* 121: 938-942.
171. Xing, L., Y. Xu, K. Sun, H. Wang, F. Zhang, Z. Zhou, J. Zhang, F. Zhang, B. Caliskan, Z. Qiu, and M. Wang. 2018. Identification of a peptide for folate receptor alpha by phage display and its tumor targeting activity in ovary cancer xenograft. *Sci Rep* 8: 8426.
172. Farooqi, A. A., and Z. H. Siddik. 2015. Platelet-derived growth factor (PDGF) signalling in cancer: rapidly emerging signalling landscape. *Cell Biochem Funct* 33: 257-265.
173. Askoxylakis, V., A. Marr, A. Altmann, A. Markert, W. Mier, J. Debus, P. E. Huber, and U. Haberkorn. 2013. Peptide-based targeting of the platelet-derived growth factor receptor beta. *Mol Imaging Biol* 15: 212-221.
174. Javadpour, M. M., M. M. Juban, W. C. Lo, S. M. Bishop, J. B. Albery, S. M. Cowell, C. L. Becker, and M. L. McLaughlin. 1996. De novo antimicrobial peptides with low mammalian cell toxicity. *J Med Chem* 39: 3107-3113.
175. Law, B., L. Quinti, Y. Choi, R. Weissleder, and C. H. Tung. 2006. A mitochondrial targeted fusion peptide exhibits remarkable cytotoxicity. *Mol Cancer Ther* 5: 1944-1949.
176. Kim, H. Y., S. Kim, H. Youn, J. K. Chung, D. H. Shin, and K. Lee. 2011. The cell penetrating ability of the proapoptotic peptide, KLAKLAKKLAKLAK fused to the N-terminal protein transduction domain of translationally controlled tumor protein, MIIYRDLISH. *Biomaterials* 32: 5262-5268.

177. Daquinag, A. C., C. Tseng, Y. Zhang, F. Amaya-Manzanares, F. Florez, A. Dadbin, T. Zhang, and M. G. Kolonin. 2016. Targeted Proapoptotic Peptides Depleting Adipose Stromal Cells Inhibit Tumor Growth. *Mol Ther* 24: 34-40.
178. Chabner, B. A. 2018. Does Chemotherapy Induce Metastases? *Oncologist* 23: 273-274.
179. Kolonin, M. G., J. Sun, K. A. Do, C. I. Vidal, Y. Ji, K. A. Baggerly, R. Pasqualini, and W. Arap. 2006. Synchronous selection of homing peptides for multiple tissues by in vivo phage display. *FASEB J* 20: 979-981.
180. Kim, S. W., J. Roh, and C. S. Park. 2016. Immunohistochemistry for Pathologists: Protocols, Pitfalls, and Tips. *J Pathol Transl Med* 50: 411-418.
181. Yang, S., J. J. Zhang, and X. Y. Huang. 2012. Mouse models for tumor metastasis. *Methods Mol Biol* 928: 221-228.
182. Bailey-Downs, L. C., J. E. Thorpe, B. C. Disch, A. Bastian, P. J. Hauser, T. Farasyn, W. L. Berry, R. E. Hurst, and M. A. Ihnat. 2014. Development and Characterization of a Preclinical Model of Breast Cancer Lung Micrometastatic to Macrometastatic Progression. *PLOS ONE* 9: e98624.
183. Paschall, A. V., and K. Liu. 2016. An Orthotopic Mouse Model of Spontaneous Breast Cancer Metastasis. *J Vis Exp*.
184. Gomez-Cuadrado, L., N. Tracey, R. Ma, B. Qian, and V. G. Brunton. 2017. Mouse models of metastasis: progress and prospects. *Dis Model Mech* 10: 1061-1074.
185. Kolonin, M., R. Pasqualini, and W. Arap. 2001. Molecular addresses in blood vessels as targets for therapy. *Curr Opin Chem Biol* 5: 308-313.
186. Fidler, I. J., and G. L. Nicolson. 1976. Organ selectivity for implantation survival and growth of B16 melanoma variant tumor lines. *J Natl Cancer Inst* 57: 1199-1202.
187. Overwijk, W. W., and N. P. Restifo. 2001. B16 as a mouse model for human melanoma. *Curr Protoc Immunol* Chapter 20: Unit 20 21.

188. Ellerby, H. M., W. Arap, L. M. Ellerby, R. Kain, R. Andrusiak, G. D. Rio, S. Krajewski, C. R. Lombardo, R. Rao, E. Ruoslahti, D. E. Bredesen, and R. Pasqualini. 1999. Anti-cancer activity of targeted pro-apoptotic peptides. *Nat Med* 5: 1032-1038.
189. Ellerby, H. M., D. E. Bredesen, S. Fujimura, and V. John. 2008. Hunter-killer peptide (HKP) for targeted therapy. *J Med Chem* 51: 5887-5892.
190. Daquinag, A. C., C. Tseng, A. Salameh, Y. Zhang, F. Amaya-Manzanares, A. Dadbin, F. Florez, Y. Xu, Q. Tong, and M. G. Kolonin. 2015. Depletion of white adipocyte progenitors induces beige adipocyte differentiation and suppresses obesity development. *Cell Death Differ* 22: 351-363.
191. Kolonin, M. G., P. K. Saha, L. Chan, R. Pasqualini, and W. Arap. 2004. Reversal of obesity by targeted ablation of adipose tissue. *Nat Med* 10: 625-632.
192. Ibragimova, M. K., M. M. Tsyganov, and N. V. Litviakov. 2017. Natural and Chemotherapy-Induced Clonal Evolution of Tumors. *Biochemistry (Mosc)* 82: 413-425.
193. Marusyk, A., and K. Polyak. 2010. Tumor heterogeneity: causes and consequences. *Biochim Biophys Acta* 1805: 105-117.
194. Tseng, L. M., N. C. Hsu, S. C. Chen, Y. S. Lu, C. H. Lin, D. Y. Chang, H. Li, Y. C. Lin, H. K. Chang, T. C. Chao, F. Ouyang, and M. F. Hou. 2013. Distant metastasis in triple-negative breast cancer. *Neoplasia* 60: 290-294.
195. Tao, K., M. Fang, J. Alroy, and G. G. Sahagian. 2008. Imagable 4T1 model for the study of late stage breast cancer. *BMC Cancer* 8: 228.
196. Bao, L., A. Haque, K. Jackson, S. Hazari, K. Moroz, R. Jetly, and S. Dash. 2011. Increased expression of P-glycoprotein is associated with doxorubicin chemoresistance in the metastatic 4T1 breast cancer model. *Am J Pathol* 178: 838-852.
197. Samanta, D., Y. Park, X. Ni, H. Li, C. A. Zahnow, E. Gabrielson, F. Pan, and G. L. Semenza. 2018. Chemotherapy induces enrichment of

- CD47⁺/CD73⁺/PDL1⁺ immune evasive triple-negative breast cancer cells. *Proceedings of the National Academy of Sciences* 115: E1239-E1248.
198. Isakoff, S. J. 2010. Triple-negative breast cancer: role of specific chemotherapy agents. *Cancer J* 16: 53-61.
 199. Wahba, H. A., and H. A. El-Hadaad. 2015. Current approaches in treatment of triple-negative breast cancer. *Cancer Biol Med* 12: 106-116.
 200. Karagiannis, G. S., J. S. Condeelis, and M. H. Oktay. 2018. Chemotherapy-induced metastasis: mechanisms and translational opportunities. *Clin Exp Metastasis* 35: 269-284.
 201. Volk-Draper, L., K. Hall, C. Griggs, S. Rajput, P. Kohio, D. DeNardo, and S. Ran. 2014. Paclitaxel therapy promotes breast cancer metastasis in a TLR4-dependent manner. *Cancer Res* 74: 5421-5434.
 202. Dabrowska, K. 2019. Phage therapy: What factors shape phage pharmacokinetics and bioavailability? Systematic and critical review. *Med Res Rev* 39: 2000-2025.
 203. Huh, H., S. Wong, J. St Jean, and R. Slavcev. 2019. Bacteriophage interactions with mammalian tissue: Therapeutic applications. *Adv Drug Deliv Rev* 145: 4-17.
 204. Gheldof, A., and G. Berx. 2013. Cadherins and epithelial-to-mesenchymal transition. *Prog Mol Biol Transl Sci* 116: 317-336.
 205. Wu, Y., and B. P. Zhou. 2008. New insights of epithelial-mesenchymal transition in cancer metastasis. *Acta Biochim Biophys Sin (Shanghai)* 40: 643-650.
 206. Gregoire, J. M., L. Fleury, C. Salazar-Cardozo, F. Alby, V. Masson, P. B. Arimondo, and F. Ausseil. 2016. Identification of epigenetic factors regulating the mesenchyme to epithelium transition by RNA interference screening in breast cancer cells. *BMC Cancer* 16: 700.

207. Basu, D., K. T. Montone, L. P. Wang, P. A. Gimotty, R. Hammond, J. A. Diehl, A. K. Rustgi, J. T. Lee, K. Rasanen, G. S. Weinstein, and M. Herlyn. 2011. Detecting and targeting mesenchymal-like subpopulations within squamous cell carcinomas. *Cell Cycle* 10: 2008-2016.
208. Jeanes, A., C. J. Gottardi, and A. S. Yap. 2008. Cadherins and cancer: how does cadherin dysfunction promote tumor progression? *Oncogene* 27: 6920-6929.
209. Anders, C., and L. A. Carey. 2008. Understanding and treating triple-negative breast cancer. *Oncology (Williston Park)* 22: 1233-1239; discussion 1239-1240, 1243.
210. Abercrombie, M., and E. J. Ambrose. 1962. The surface properties of cancer cells: a review. *Cancer Res* 22: 525-548.
211. 1963. Surface Properties of Cancer Cells. *Br Med J* 2: 264-265.
212. Joyce, J. A., P. Laakkonen, M. Bernasconi, G. Bergers, E. Ruoslahti, and D. Hanahan. 2003. Stage-specific vascular markers revealed by phage display in a mouse model of pancreatic islet tumorigenesis. *Cancer Cell* 4: 393-403.
213. Sergeeva, A., M. G. Kolonin, J. J. Molldrem, R. Pasqualini, and W. Arap. 2006. Display technologies: application for the discovery of drug and gene delivery agents. *Advanced drug delivery reviews* 58: 1622-1654.
214. Kufe, D. W. 2009. Mucins in cancer: function, prognosis and therapy. *Nat Rev Cancer* 9: 874-885.
215. Hu, X., X. Sui, L. Li, X. Huang, R. Rong, X. Su, Q. Shi, L. Mo, X. Shu, Y. Kuang, Q. Tao, and C. He. 2013. Protocadherin 17 acts as a tumour suppressor inducing tumour cell apoptosis and autophagy, and is frequently methylated in gastric and colorectal cancers. *J Pathol* 229: 62-73.
216. Yang, I. V., T. E. Fingerlin, C. M. Evans, M. I. Schwarz, and D. A. Schwartz. 2015. MUC5B and Idiopathic Pulmonary Fibrosis. *Ann Am Thorac Soc* 12 Suppl 2: S193-199.

217. Vancheri, C. 2013. Common pathways in idiopathic pulmonary fibrosis and cancer. *Eur Respir Rev* 22: 265-272.
218. Pires, B. R., A. L. Mencalha, G. M. Ferreira, W. F. de Souza, J. A. Morgado-Diaz, A. M. Maia, S. Correa, and E. S. Abdelhay. 2017. NF-kappaB Is Involved in the Regulation of EMT Genes in Breast Cancer Cells. *PLoS One* 12: e0169622.
219. Huber, M. A., N. Azoitei, B. Baumann, S. Grunert, A. Sommer, H. Pehamberger, N. Kraut, H. Beug, and T. Wirth. 2004. NF-kappaB is essential for epithelial-mesenchymal transition and metastasis in a model of breast cancer progression. *J Clin Invest* 114: 569-581.
220. Su, C. T., J. W. Huang, C. K. Chiang, E. C. Lawrence, K. L. Levine, B. Dabovic, C. Jung, E. C. Davis, S. Madan-Khetarpal, and Z. Urban. 2015. Latent transforming growth factor binding protein 4 regulates transforming growth factor beta receptor stability. *Hum Mol Genet* 24: 4024-4036.
221. Robertson, I. B., M. Horiguchi, L. Zilberberg, B. Dabovic, K. Hadjiolova, and D. B. Rifkin. 2015. Latent TGF-beta-binding proteins. *Matrix Biol* 47: 44-53.
222. Kretschmer, C., A. Conradi, W. Kemmner, and A. Sterner-Kock. 2011. Latent transforming growth factor binding protein 4 (LTBP4) is downregulated in mouse and human DCIS and mammary carcinomas. *Cell Oncol (Dordr)* 34: 419-434.
223. Drabsch, Y., and P. ten Dijke. 2011. TGF-beta signaling in breast cancer cell invasion and bone metastasis. *J Mammary Gland Biol Neoplasia* 16: 97-108.
224. Chiechi, A., D. L. Waning, K. R. Stayrook, J. T. Buijs, T. A. Guise, and K. S. Mohammad. 2013. Role of TGF-beta in breast cancer bone metastases. *Adv Biosci Biotechnol* 4: 15-30.
225. Ma, Z., H. Wan, W. Wang, X. Zhang, T. Uno, Q. Yang, J. Yue, H. Gao, Y. Zhong, Y. Tian, Q. Sun, Y. Liang, and H. Dai. 2019. A theranostic agent for cancer therapy and imaging in the second near-infrared window. *Nano Research* 12: 273-279.

226. Ghosh, S. C., K. L. Pinkston, H. Robinson, B. R. Harvey, N. Wilganowski, K. Gore, E. M. Sevick-Muraca, and A. Azhdarinia. 2015. Comparison of DOTA and NODAGA as chelators for (64)Cu-labeled immunoconjugates. *Nucl Med Biol* 42: 177-183.
227. Wade, D., A. Boman, B. Wahlin, C. M. Drain, D. Andreu, H. G. Boman, and R. B. Merrifield. 1990. All-D amino acid-containing channel-forming antibiotic peptides. *Proc Natl Acad Sci U S A* 87: 4761-4765.
228. Bedi, D., J. W. Gillespie, V. A. Petrenko, Jr., A. Ebner, M. Leitner, P. Hinterdorfer, and V. A. Petrenko. 2013. Targeted delivery of siRNA into breast cancer cells via phage fusion proteins. *Mol Pharm* 10: 551-559.
229. Gray, B. P., S. Li, and K. C. Brown. 2013. From phage display to nanoparticle delivery: functionalizing liposomes with multivalent peptides improves targeting to a cancer biomarker. *Bioconjug Chem* 24: 85-96.

VITA

Shraddha Subramanian was born in Hyderabad, India. She is the daughter of Girija Subramanian and Subramanian Sankaran. She received her Bachelor of Engineering degree in Biotechnology from PES Institute of Technology in Bangalore, India in June 2017. In August of 2017, she entered The University of Texas MD Anderson Cancer Center UTHealth Graduate School of Biomedical Sciences, with the goal of attaining the degree of Master of Science in Biomedical Sciences.

Permanent Address:

3002 Sobha Jasmine

Bellandur, Sarjapur Outer Ring Road

Bengaluru-560103

Karnataka, India.